DNA NANOTECHNOLOGY ENABLED MOLECULAR MECHANISMS AND APPLICATIONS

by

Feiran Li

A Dissertation

Submitted to the Faculty of Purdue University

In Partial Fulfillment of the Requirements for the degree of

Doctor of Philosophy

School of Mechanical Engineering

West Lafayette, Indiana

May 2020

THE PURDUE UNIVERSITY GRADUATE SCHOOL

STATEMENT OF COMMITTEE APPROVAL

Dr. Jong Hyun Choi, Chair

School of Mechanical Engineering

Dr. Chengde Mao

Department of Chemistry

Dr. Bumsoo Han

School of Mechanical Engineering

Dr. Cagri A. Savran

School of Mechanical Engineering

Approved by:

Dr. Nicole Key

Associate Head for Graduate Studies

To my parents

ACKNOWLEDGMENTS

I would like to thank my PhD advisor Prof. Jong Hyun Choi for his stable financial support and his guidance to my research. His knowledge and passion for research helped to overcome one after another barrier in my research life for all these years. With the research opportunities provided by him, I am gradually improved and finally could be considered as an independent researcher. I am sure all these experiences will be my strength and confidence which can guide me in my future career. I would like to thank all my committee members for their kind advice and help in my research throughout my PhD study. I would also like to thank the Office of Navel Research and National Science Foundation for their finiancial support.

For the most time in my PhD study, I communicated with my labmates for both life and research topics. As both friends and colleagues, my labmates have provided lots of help to me. I would like to thank my fellow labmates Dr. Tae-gon Cha, Dr. Hanyu Zhang, Dr. Haorong Chen, Dr. Jing Pan, Ruixin Li, Yancheng Du, Jaehoon Ji and Hengming Qiu for their help.

Furthermore, I would like to thank Prof. Chengde Mao and his students Dr. Jinwen Yu and Dr. Longfei Liu for their knowledge and help in building up my DNA nanotechnology knowledge and experiments. I would like to thank Prof. Bumsoo Han and his students Dr. Altug Ozcelikkale, Hyeran Moon and Michael Bradney for their facilities and advice in my cell experiments and protein experiments. I would also like to thank Dr. Igor L. Medintz of U.S. Naval Research Laboratory for his support in chemical samples and guidance in article writing.

Last but not least, I would like to thank my parents for their support. They have been encouraging me and believing in me no matter what kind of situations I am in. They understand the decisions I have made and try their best to support me. Without them, I definitely cannot reach this step as a PhD.

TABLE OF CONTENTS

LIST OF FIGURES

ABBREVIATIONS

ORG	Origami
MT	Microtubule
KIN	Kinesin
AuNP	Gold nanoparticle
CNT	Carbon nanotube
SWCNT	Single-walled carbon nanotube
QD	Quantum dot
PL	Photoluminescence
MW	Molecular weight
EDTA	Ethylenediaminetetraacetic acid
PIPES	Piperazine-N,N'-bis(2-ethanesulfonic acid)
TAE	A buffer with 40 mM Tris, 20 mM acetic acid and 1 mM EDTA
TAEM	A buffer with 40 mM Tris, 20 mM acetic acid, 1 mM EDTA and 12.5 mM Mg^{2+}
BRB80	A buffer with 80 mM PIPES, 1 mM $MgCl_2$, and 1 mM EGTA

ABSTRACT

DNA is well known for its function as a genetic information carrier. Based on its base pairing property, DNA can retain and reproduce the information. In recent decades, the base complementarity has been explored beyond its original function and takes DNA engineering to a new stage. With the recognition of specific bases in a DNA sequence, programmability and accessibility can be achieved for a DNA-made nanostructure. In addition, numerous reactive chemical groups may be linked to DNA strands which makes DNA nanotechnology more important. With these unique strength, DNA nanotechnology can serve as a powerful tool for molecular biology research including nanostructure construction and signal processing. DNA engineering can bring new characterization and control methods for various other scientific areas. In order to achieve better control of DNA, one must study the mechanisms and dynamics behind DNA nanotechnology.

This thesis investigates DNA nanotechnology, exploring the interactions of engineered DNA molecules with small molecules, proteins, nanoparticles, and cells. As a signal molecule, DNA is engineered in a logic gate for cargo pickup and release as well as in a dynamic walker device for controlled drug release for cancer cell treatment. In these DNA-based nanosystems, we develop novel logic gate mechanisms and study biomolecular reaction kinetics. In addition, DNA is also used to modulate surface gliding microtubules *in vitro* where individual microtubules are re-directed locally. With a fundamental understanding of DNA signaling systems, we propose to program activity of synthetic cells. Here, liposomes are constructed from phospholipids with transmembrane pores made of DNA origami. DNA signals are recognized and processed with transmembrane pores on synthetic cells. Programmable cell aggregation was demonstrated as a proof-of-principle. We envision that this thesis will provide a deeper understanding of DNA nanotechnology for both fundamental mechanisms and engineering applications. New powerful platforms for molecular and cellular biology systems could be developed and possibly help study dynamics and kinetics in physiology and medicine.

1 INTRODUCTION

Nanotechnology has been studied since the last century where numerous scientists have contributed to this field. It bloomed so fast in the past few decades that an extensive amount of new materials and characterization methods have been developed. As nanotechnology develops further, its application in biology and medicine has become more and more important. Scientists can access and manipulate those tiny biological components which can only be studied ensemble before. Thus bio-nanotechnology which uses those biomaterials from life as its fundamental materials become popular, like proteins and DNA. Deoxyribonucleic acid, DNA, as one of the most important biomaterials has attracted great attention from researchers. Instead of using it as a genetic information carrier, DNA is used as an engineering material for building nanostructures and communicating between different systems. Protein is another big portion of bio-materials. While its function is highly dependent on a protein's sequence and structure, diverse studies can be done on proteins. Among all these proteins, motor protein is a type of essential proteins in vivo which controls the intracellular transport. This makes the motor proteins related to numerous diseases and necessary to be studied. Furthermore, cellular control is also an important topic to be studies. However, given the complexity of the real cell system, it is extremely difficult to understand all the details of them. Thus, the tool, artificial cell was developed in order to study the problem. As the same lipid bilayer as real cell, artificial cell has a much simpler inner environment. This thesis presents the engineering of DNA signals including its generation, process, and interaction with other DNA molecules, proteins, nanoparticles, and artificial cell. These studies explore the possibilities to extend the use of DNA as a signal to control artificial cell behavior.

This chapter introduces the recent progress in DNA nanotechnology, motor proteins, and artificial cell research, as well as the interaction between these materials. Our research effort in using DNA signals for artificial cell control is summarized in the scope of this study. The organization of the entire thesis is also presented.

1.1 DNA Nanotechnology

DNA is the most important material that carries genetic information. It is a high molecular weight (MW) molecule composed of two nucleotide chains which can realize self-replicating by using each chain as a template. This ability comes from the Watson-Crick complementary principle in DNA structure. There are 4 types of nitrogenous bases in a DNA molecule, purine adenine (A), purine guanine (G), pyrimidine cytosine (C) and pyrimidine thymine (T). Among these 4 bases, A pairs with T and G pairs with C, each pair of bases forms hydrogen bond which lowers free energy of the molecule and stabilizes DNA double helix structure. With the base-pairing property, the assemble and disassemble of DNA strands could be controlled. Since each single base pair is unique, the precision of control could be as high as nanometer level. Thus DNA has been widely used in nanotechnology research.[1,2] It could be used as an engineering material to be assembled into larger-scale structures which could be 2D or even 3D. Furthermore, the whole functional structure could also interact with other molecules to achieve more applications including molecular probing, material deposition, drug delivery and more. This makes DNA a promising tool for nanotechnology research. Within DNA nanotechnology, DNA origami, DNA walker and DNAzyme are all important nanostructures.

1.1.1 DNA origami

The idea of assembling DNA strands together was first published in the 1980s by Seeman et al.[3] Like Figure 1.1a shows, four DNA strands could form a junction structure by partially binding to another strand. This nucleic acid junction structure shows a very different aspect of DNA structures other than the double-stranded DNA structure which scientists have known for a long time. This work also triggers the research of DNA structures. Multiple short DNA strand based structures have been developed during this time period.[4-6] In 2006, Rothemund introduced a scaffold and staple method which dramatically increase the complexity and size of the DNA-based structures.[7] The structures made from one long single strand (scaffold) and hundreds of shorter strands (staples) is now known as DNA origami. This long single strand is from the bacteriophage M13mp18 and short strands are synthesized. Since each base of the origami is known, the whole structure can be easily accessed, and this programmability makes the placements and modifications of molecules on DNA origami as precise as nanometer level. The size of an origami is around 90 nm x 60 nm and can be assembled within 2 hours (Figure 1.1b). The robust and simple fabrication makes DNA

origami a perfect tool for extensive DNA based studies. Not only the rectangle shape of DNA origami, other shapes can also be designed and made by this method. Figure 1.1c shows some DNA origami structures including star, smile face, and triangles. These structures also use the same scaffold M13mp18 while their staple strands are different from each other. Moreover, a large amount of modifications could be done on the DNA strands which could produce versatile nanostructures with different molecules. Like Figure 1.1d, proteins can be attached onto DNA origami through biotin modification and they are shown as small dots under AFM scanning.[8] Other than protein modifications, DNA origami could also be modified with small molecules and nanoparticles.

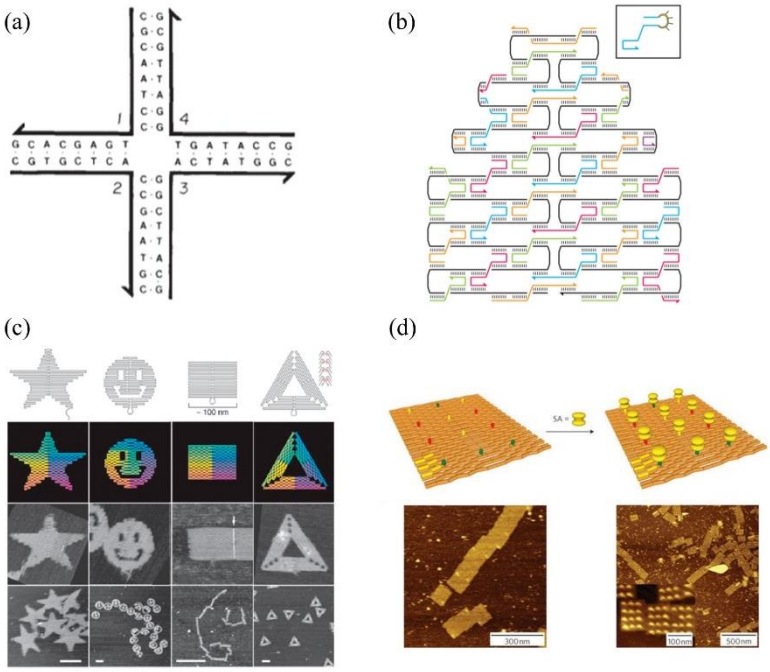

Figure 1.1. (a) A nucleic acid junction composed of four DNA strands. Each label means one DNA strand.[3] (b) Design of a DNA origami. The long black strand indicates the scaffold strand M13mp18 bacteriophage. The colored strands are the short staple strands. They are complementary to part of the scaffold strand and stabilize the origami structure.[7] (c) Different shapes of DNA origami. Origamis can be folded into not only rectangle shape but also other shapes. The first two rows show the scheme of the design and the following two rows are the actual structure of origamis under AFM. The scale bar is 1 um in the third column, while in other images, the scale bars are 100 nm.[7] (d) DNA origami with biotinylated DNA strands on it. Biotins are modified to the positions indicated by red, green and yellow bars. Streptavidin can recognize the biotin molecules and bind to them. The AFM images show the difference before and after streptavidin binding. The yellow dots in AFM images indicates the higher height in this area which means one streptavidin is attached at that position. Scale bars are listed in the figures.[8]

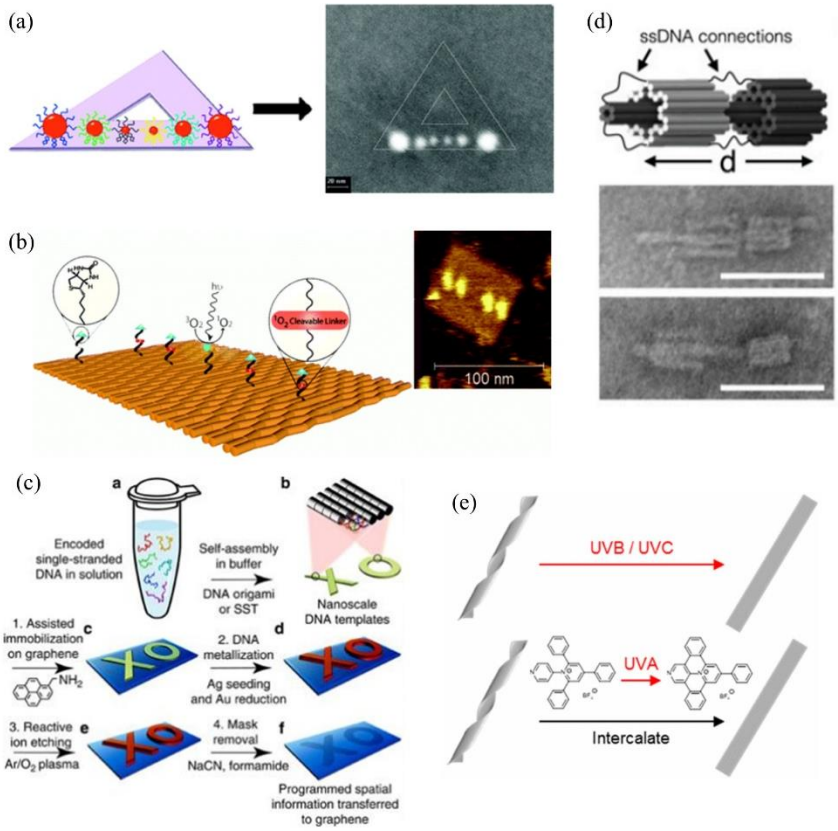

Figure 1.2. (a) 6 gold nanoparticles (AuNP) are covered by different DNA strands (shown in various colors). These 6 AuNPs are grafted onto the DNA origami at their designed positions as the SEM image shows. The scale bar is 20 nm.[9] (b) Distance sensitive enzymatic reactions on DNA origami. The green ball is singlet oxygen photosensitizer (IPS) and the red part is a singlet oxygen cleavable (SOC) linker. Blue triangles are biotin and DNA strands are in black. The distance between two adjacent DNA strands is 18 nm. The yellow dots in the AFM image are streptavidin molecules which bind to biotin molecules are origami. The cleavage of SOC linker will depend on the distance between the linker and IPS, longer distance will reduce the chance of the cleavage.[10] (c) Lithography using DNA origami. The procedure of using DNA origami as a tool for lithography is indicated in a-f steps. After synthesis, the DNA origami will be immobilized onto 1-pyrenemethylamine graphene substrate by direction deposition. The origami will then be coated with Ag and Au sequentially to protect the covered area during lithography. Then Ar/O2 plasma will be used to remove the unprotected region. Finally, origami will be removed, and spatial information will be kept on graphene.[11] (d) 3D DNA origami slider. The slider is composed of two stiff components and connected by some single strand DNAs (ssDNA). The distance between two components can be controlled by the length of ssDNA. If the ssDNA is short, the components are closer (middle image). Otherwise, the two components are separated farther (bottom image). The scale bars in TEM image are 50 nm.[12] (e) Conformation change of DNA origami by interacting with light and chemical signals. The original conformation of long DNA origami tiles is twisted as the figure shows. When the structure is exposed to UVB/ UVC or exposed to UVA after mixing with triarylpyridinium, the twisted DNA tiles are released and become flat.[13]

The programmability and various structure of DNA origami makes it an ideal tool for applications requiring precise positioning and dynamic structural change. To make the DNA origami effective for designed functions, the programmability of the origami needs to be confirmed. Ding et al.[9] used the DNA origami as a platform for positioning gold nanoparticles (AuNPs). AuNPs are modified with 6 different DNA strands as Figure 1.2a shows. With complementary strands on the origami, AuNPs can only bind to their target positions. This precise control of particles onto DNA origami makes it possible to study some distance-sensitive chemical reactions. Helmig et al.[10] placed a singlet oxygen photosensitizer (IPS) at the center of the origami and placed several singlet oxygen cleavable (SOC) linkers nearby (Figure 1.2b). The singlet oxygen generated by IPS can catalyze the cleavage of SOC linkers if the two chemicals are close. This platform could be used to study the effective distance of chemical reactions especially enzymatic reactions not only limited to the singlet oxygen reaction.

Other than using DNA origami as a platform, the whole DNA origami could also be considered as an element. Since origami can be assembled into the desired shape, it can be used for lithography. In Figure 1.2c, the 'XO' shaped DNA origami is placed onto a graphene surface.[11] With metallization and etching, the shape information of the DNA origami will be left on the surface. As the shape of DNA origami is quite important, methods to control origami shape are also developed. Chen et al.[13] used UV irradiation to flat the twisted DNA origami tiles (Figure 1.2e). Since there is a difference between the helicity of relaxed DNA and typical used DNA strands, thus there is internal stress in the origami to make the whole structure twisted. UV irradiation can cause slight defects on origami to relive those stress and to flat the origami structure. Not only 2D structures, 3D origami has also been developed and attracted lots of attention. The mechanical system produced by DNA origami (Figure 1.2d) shows an interesting direction for future study.[12] Overall, with various DNA origami structures and programmability of DNA strands, DNA origami is a promising tool and platform in nanotechnology studies.

1.1.2 DNA logic gate

DNA logic gate is a concept that uses DNA strands to imitate digital logic gates. An output will be given corresponding to the input values. In DNA logic gate system, the inputs and outputs

become DNA strands or other chemical signals. By adding or removing DNA signals from the system, the final product could be controlled.

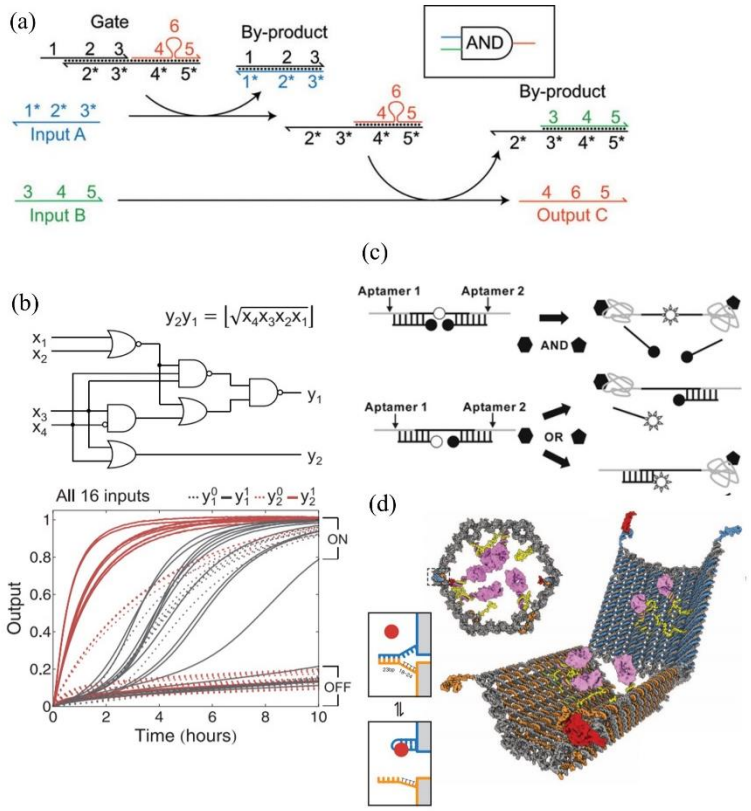

Figure 1.3. (a) AND gate made by DNA strands. Each labeled line indicates a DNA strand. The number on the strand means one segment of DNA and the number with a star means a fully complementary strand to the same number labeled DNA strand. In this design, with both input A and input B added, output C could be produced. So this could be converted to a AND logic gate.[14] (b) A DNA logic gate design to do the square root calculation. x1- x4 indicates the 4 input DNA strands and y1, y2 are the outputs. The bottom figure shows the output of 16 different inputs varying from 0000 to 1111. Each logic gate in the figure is associated with a logic gate strand.[15] (c) DNA aptamer-based DNA logic gate. A long DNA strand which can recognize two different aptamer ligands with two segments of its sequences individually. Two shorter DNA strands are bound to the long strand at the beginning. Once the aptamer ligand is added into the mixture, one or both shorter strands will be released from the long strand since ligands bind to those nucleotides. With the detachment of quencher and fluorophore on DNA strands, the system will also generate light signals.[16] (d) The design for a logic-gated nanorobot with payload inside. Both 3D view and side view are shown in the figure. The extended red, blue, orange strands are the locks are the robot that will hybridize together to lock the robot. When an aptamer is added into the system, it will recognize DNA strands and break the hybridization. Thus the robot will be opened and the payloads inside could be exposed.[17]

A fully DNA-based logic gate is based on DNA strand displacement. It is a mechanism that in two pre-hybridized DNA strands, one of them is replaced by another DNA strand. This process is controlled by the thermodynamic free energy of the system. For two DNA strands, there are hydrogen bonds between base pairs. Thus, with more complementary bases, there will be more hydrogen bonds between DNA strands. To break a double-strand DNA (dsDNA) into two separate DNA strands, extra is needed to add into the system to disrupt the hydrogen bonds. So the dsDNA will be more stable (lower free energy) if there are more complementary bases between the two DNA strands. Since a thermodynamic system tends to change towards the lower free energy side, if the free energy can decrease after the new hybridization, the strand displacement could happen. This speed of this process can be controlled by temperature, strand design, and toehold length.[14,18,19]

With the strand displacement mechanism, DNA logic gate could be designed (Figure 1.3a).[14] The whole logic gate system consists of gate strands and two input strands. Only with both input A and input B added, the desired output strand will be created. Thus, this logic gate could be considered as an 'AND' gate. In addition, with the strand displacement cascade, a more complex DNA logic gate system can also be designed. Qian et al.[15] designed a logic gate system to calculate the square root of an input (Figure 1.3b). The input varies from 0000 to 1111 with four different DNA strands as input. '0' means no input strand added, and '1' means adding a strand. Furthermore, DNA logic gate system has been extended to have more components involved, not limited to DNA strands. Yoshida et al.[16] introduced aptamer ligand into the system (Figure 1.3c). The aptamer ligands can bind to DNA strands to replace another hybridized DNA strand. The fluorophores on the DNA strands could be used to indicate if the DNA logic gate works or not. With all these properties, DNA logic gate could be used for detection of a DNA/ RNA strand, ions, chemicals or pH. Douglas et al.[17] built a DNA-based nanorobot with payload molecules inside (Figure 1.3d). The lock of the nanorobot is controlled by a DNA logic gate system. Only if the target aptamer exists in the solution, the dsDNA strand will unzip to open the robot and expose the payload inside.

1.1.3 DNA walker

DNA walker is a type of DNA based nanomachine[20] like Figure 1.4a shows, with adding DNA strands as fuel, the tweezer structure can switch between 'OPEN' and 'CLOSE' states. A DNA walker is developed from this type of nanomachine where the walker is inspired by protein motors like kinesin, myosin, and dynein. These protein motors move along a track in the cell to transport cargos. Figure 1.4b shows a schematic of a kinesin walking on a microtubule.[21] To imitate these protein motors, DNA strands are designed in the same way to achieve the conversion of chemical energy to mechanical work.

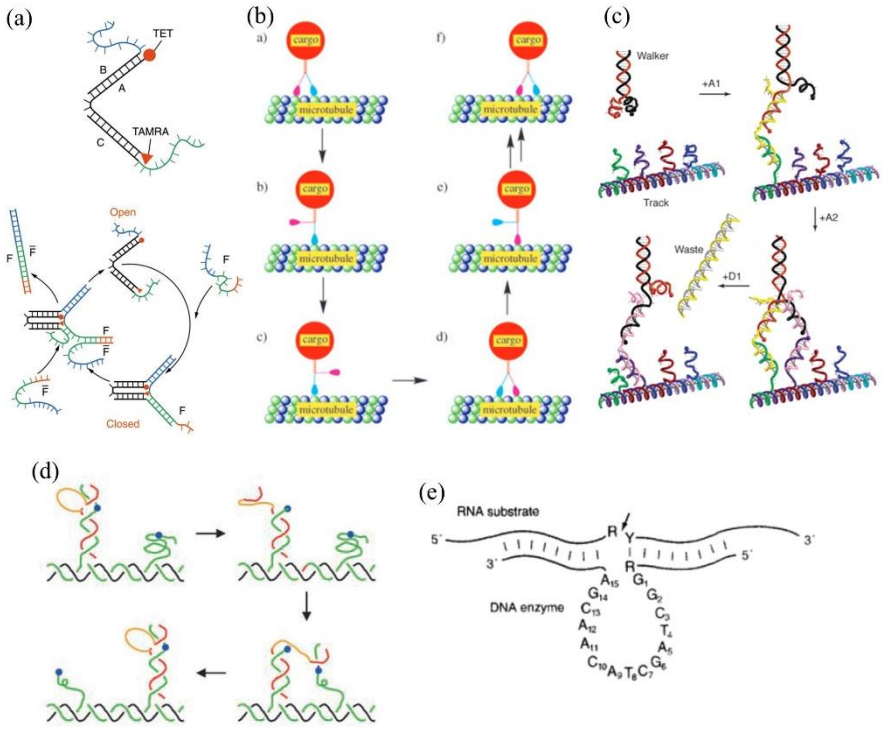

Figure 1.4. (a) DNA based tweezers are switching between 'OPEN' and 'CLOSE' forms by adding additional DNA strands into the system. The state of the tweezer can be confirmed by the fluorophores modified on it.[20] (b) A kinesin molecule carrying a cargo walks along the microtubule track.[21] (c) DNA walker walking powered by strand displacement. The two legs of DNA walkers are initially bound to the track by adding two complementary strands. One leg of the walker is released from the track and it can then bind to another DNA strand to make a step on the track.[22] (d) Brunt-bridge method-based DNA walker. The green and black strands are the track, red strand is the walker and orange part is the catalytic core. Blue dot means the cutting point of the fuel strand on track. Once walker strand binds to one fuel strand, the fuel strand will be cleaved and a free energy gradient will be created. Thus DNA walker will bind to the next fuel strand and proceed.[23] (e) A 10-23 DNAzyme. 10-23 means the enzyme is derived from the 23rd clone obtained after the 10th round of in vitro selection. The arrow pointed position will be cleaved if the DNAzyme is present.[24]

Typically, there are four components of a DNA walker, which are walking legs, walking track, cargo and fuel. Oligonucleotides strand is always used as the walking leg while walking track could either be oligonucleotides formed nanostructure or another substrate which can be modified by DNA like carbon nanotube and glass slide. There are many options for cargos including small molecules and nanoparticles. Fuel is usually an additional DNA strand or the cleavage mechanism that provide chemical energy to the system. There are two common mechanisms for DNA walker which are strand displacement and brunt-bridge. Strand displacement is as discussed in chapter

1.1.2, where the strand displacement cascade can create an energy gradient for the walker. Shin et al.[22] designed a strand displacement-based DNA walker as Figure 1.4c shows. Four strands formed a track and served as stops for the walker. A partially complementary dsDNA strand was considered as the walker. The walker can either bind to the stop strand or be released from the stop depending on which fuel strand was added. By adding fuel strands sequentially, the walker could move forward on the track. Brunt-bridge method uses DNAzyme to cleave the fuel strand and thus generate a free energy difference to initiate the walking (Figure 1.4d).[23] Deoxyribozymes (DNAzyme) is a type of DNA oligonucleotides which can perform specific chemical reactions. For most DNAzymes, they can serve as ribonucleases which can catalyze the cleavage of RNA strands (Figure 1.4e).[24]

With the motility of DNA walker, it can be used for cargo transport and sorting (Figure 1.5ab).[25,26] Based on the proximity of walker strand and fuel strand during the walking process, DNA walker system can also be used for molecular synthesis (Figure 1.5c). He et al.[27] designed a molecular synthesis system based on DNA walker. As the DNA walker proceeds, its amine group at the top will react with the N-hydroxysuccinimidyl (NHS) group on the fuel strands on the track. This work presented a novel application for DNA walker. In addition, the released DNA strand could be considered as a DNA signal to communicate with other system which may lead to other possible applications.

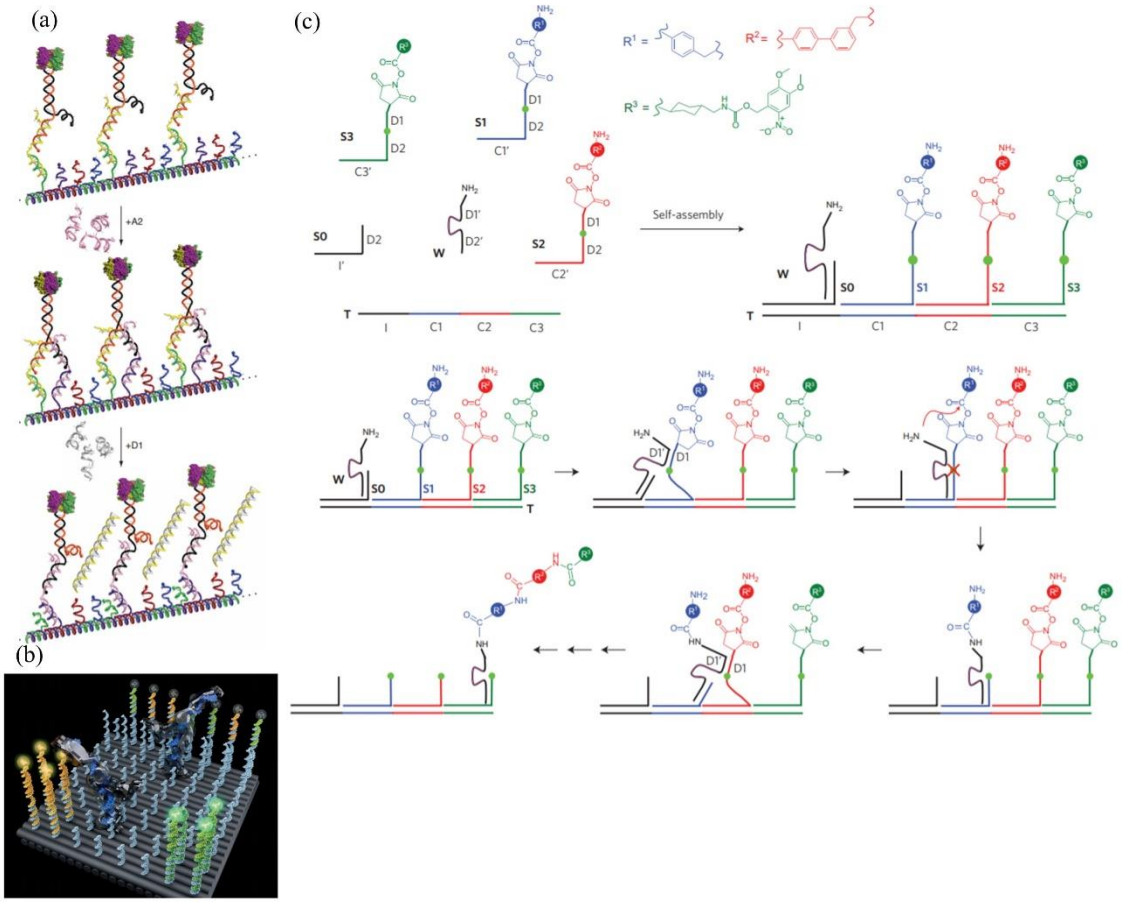

Figure 1.5. (a) DNA walker transport a streptavidin molecule as its cargo.[25] (b) DNA walker sorting different cargos to their designed destinations on a DNA origami.[26] (c) Molecular synthesis on a DNA walker. Three molecules with reactive N-hydroxysuccinimidyl (NHS) groups are placed on three consecutive stops on the track. The walker contains an amine group on its top. When the walker moves forward, the NHS group and amine group are close enough and the moiety R1, R2, R3 will be linked to the walker.[27]

1.2 Motor Protein System

1.2.1 Types of motor proteins

Motor proteins are a class of molecular proteins which can move along the cytoplasm of a cell. They can convert chemical energy into mechanical work by hydrolysis of ATP. They play an import role in intracellular transport which is essential for molecules exchange inside a cell. Based on their substrate and moving direction, there are three basic types of motor proteins: myosin, kinesin, and dynein.

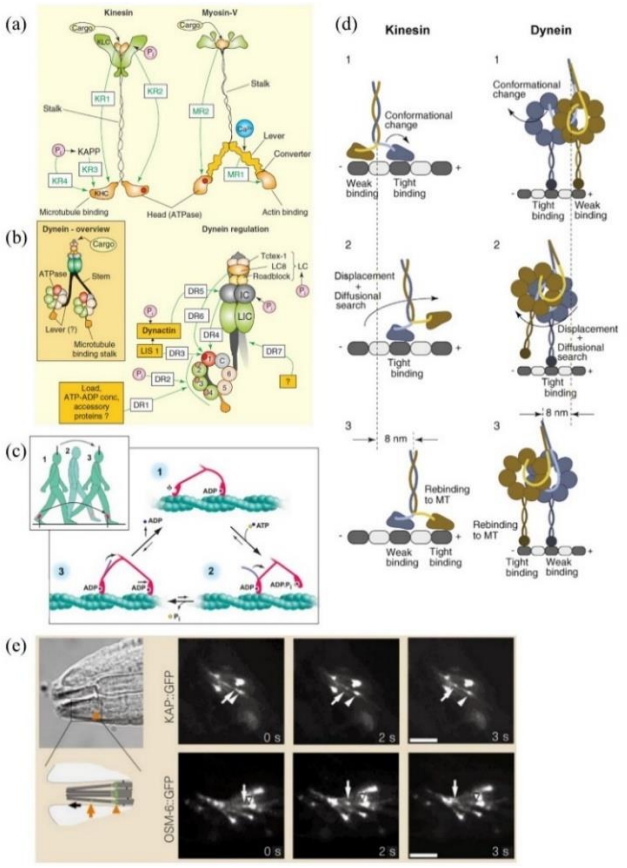

Figure 1.6. (a) Structure of kinesin and myosin. Both myosin and kinesin are composed of head, stalk (neck) and tail parts. Kinesin head binds to the microtubule and myosin head binds to the actin. Both heads in myosin and kinesin contains ATPase which will hydrolyze ATP to gain chemical energy. The stalk connects head and tail part. The tails in both proteins bind to cargos.[28] (b) Structure of dynein. Dynein is composed of two stalks, two motor heads, two stems and light chains connecting to the cargo. Dynein uses stalks to connect with microtubules. Its motor heads are composed of 7 accessory domains.[28] (c) Walking mechanism of myosin. ATP binds to the lagging head of the myosin. Then ATP will be hydrolyzed to ADP and Pi to make the head step to the front. The Pi will then be released and the whole reaction cycled over and over again to make myosin proceed.[29] (d) Walking mechanism of kinesin and dynein. Both motor proteins are moving forward step by step and their step length on the microtubule are both 8 nm. The walking procedure needs the hydrolysis of ATP when they make a step forward.[30] (e) Visualization of intraflagellar transportation. Kinesin and OSM-6 (a cargo molecule) are labeled by green fluorescent protein (GFP). The figure shows the transportation of kinesins and OSM-6 inside cilia.[31]

Myosin is one type of motor protein which moves along actin filaments. A myosin molecule is composed of three domains, head, neck, and tail like Figure 1.6a shows.[28] Its head domain is responsible for binding onto an actin filament and hydrolyzing ATP to provide energy to move forward (Figure 1.6c).[29] Its neck domain serves as a linker between head and tail domains. The tail

domain is mainly for interacting with cargo molecules. Majority of myosins will move towards the plus (+) end of actin while some myosins will do it reversely.

Kinesin and dynein (Figure 1.6ab) are both working with microtubules where kinesins are moving towards the plus (+) end of microtubules and dyneins are moving towards the minus (-) end (Figure 1.6d).[30] While kinesin and myosin have similar structures, dynein is quite different from these two proteins in structure. Dynein (~1.5 MDa) is a much larger protein compared to kinesin (~150 kDa) and myosin (~500 kDa) and it also requires various accessory proteins to realize its function.

The speed of these motor proteins varies dramatically based on the motor type and environment conditions. One motor protein can be as slow as ~10 nm/s while a different type of protein can move faster than 1000 nm/s. Even for the same motor protein, its speed is still different between in vitro and in vivo situation as well as other environmental factors like temperature and pH.

1.2.2 In vivo cargo transport

Since motor proteins are critical to intracellular transport, thus in vivo studies become a very important way to understand their kinetics. Drugs which may have effects on motor proteins can be studied by recording the different performance of the proteins before and after treatment of the drug. The role of proteins in this motility system could also be tested with gene editing methods to suppress or express some proteins. For these purposes, the visualization of cargo transport by motor proteins in vivo is necessary. Orozco et al.[31] imaged the cargo transport of kinesins inside cilia (Figure 1.6e). Both the kinesin and the cargo (OSM-6, a type of protein) are labeled with green fluorescent protein (GFP). Thus the in vivo transport can be directly visualized by fluorescence imaging. In addition, not only the visualization study, with the importance of motor proteins in vivo, they are also used as drug targets for different diseases.[32,33]

1.2.3 In vitro studies

To further understand motor proteins, isolating the change of experiment conditions would be the best method. Thus in vitro study shows its importance. To visualize the walking of motor proteins on a substrate, the microtubules/ actin filaments could be deposited onto the surface first and then load motor proteins onto them. Like Figure 1.7a shows, Svoboda et al.[34] used an optical tweezer

system to place the kinesin with a cargo onto the immobilized microtubule. With the modifications on the motor proteins, it is also possible to characterize the force exerted by the motor, motor walking velocity and step size. Myosin could also be studied with a similar experimental setup.[35]

There is one other in vitro method to study motor protein behavior which is named motility assay. This method immobilizes motor proteins onto a surface and puts their substrates (microtubules, actins) on the top as Figure 1.7b shows.[36,37] Thus instead of observing moving motor proteins, this method will mainly be analyzing the moving microtubules and actin filaments. With this platform, drugs which will affect motor proteins in vivo can be studied in vitro now. Gearhart et al.[38] used a microtubule motility assay to study the inhibition effect of three chemicals chlorpyrifos, chlorpyrifos-oxon and diisopropylfluorophosphate on the kinesins and microtubules (Figure 1.7c). They found these drugs can directly affect kinesin and the microtubule gliding, as well as kinesin-based cargo transport, will be disrupted.

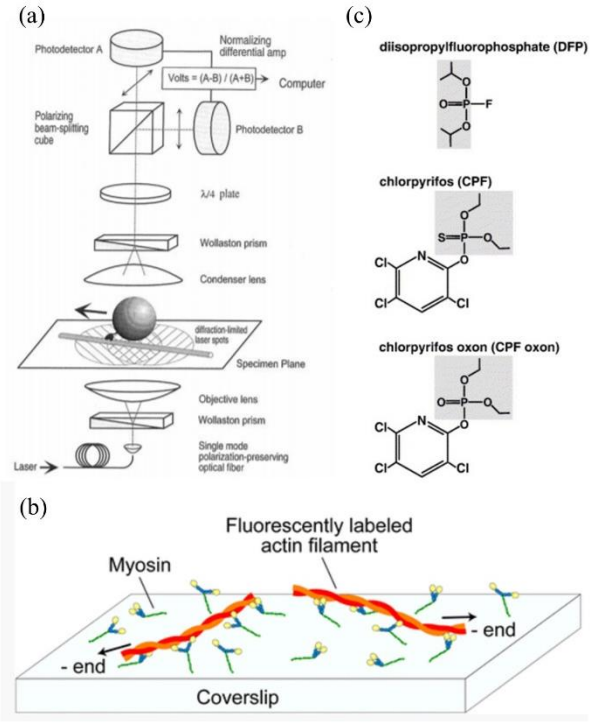

Figure 1.7. (a) Optical trapping setup to study kinesin moving on a microtubule.[34] (b) Schematic of actin motility assay. Myosins are deposited on the coverslip and fluorescently labeled actin filaments are then attached to the myosins.[36] (c) Structures of the chemicals that can inhibit kinesin-dependent microtubule motility.[38]

1.3 Interaction between DNA and Motor Protein

1.3.1 Motor protein system control with DNA

To study the interaction between motor protein and DNA strands, the most direct method is to conjugate DNA onto kinesins through chemical reactions. Miyazono et al.[39] directly conjugated DNA strands onto the motor domain of kinesins (Figure 1.8a). The DNA strands connect two motor heads together and the strands also served as the function of neck and tail part in normal kinesins. This DNA-kinesin conjugation can also walk on a microtubule and its speed is around 1/2 of the intact kinesin moving on a microtubule. Similar motor protein-DNA conjugation has also been done by Hariadi et al. (Figure 1.8b), where they conjugated DNA strands onto a myosin protein on its tail.[40] The myosins were then placed onto a DNA nanotube with a designed distance. The fluorescent actin filament was attached on myosin heads and glided. Since the distance between two myosins are controlled due to programmability of DNA, the effect of myosin distance could be studied by the system.

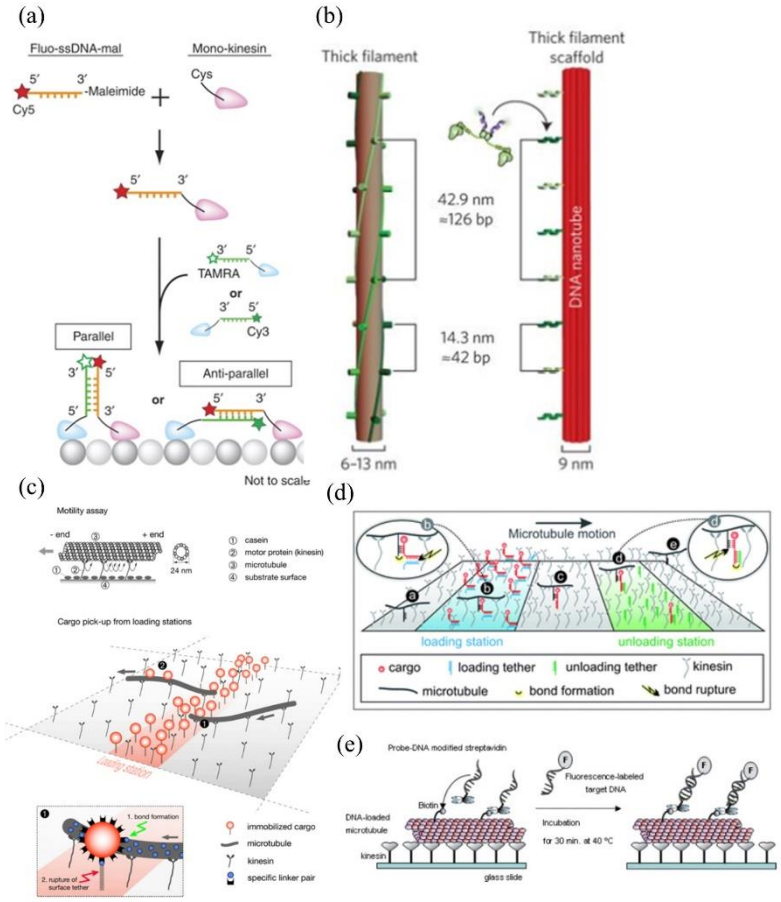

Figure 1.8. (a) Assembly of kinesin-DNA. DNA and kinesin motor domain are conjugated together. Two kinesin motor domains are assembled together by the hybridization of complementary DNA strands.[39] (b) DNA nanotube with myosin positioned on it. Actin filaments could be transported by the myosins on the DNA nanotube.[40] (c) A microtubule picks up cargos from loading area by a linking mechanism. Multiple cargos could be picked up by the same microtubule.[41] (d) Microtubules pick up and drop cargos at designed areas with the help of DNA strands. Particles are immobilized onto the surface by double DNA strands. A DNA strand is also attached on the microtubule which can hybridize with the DNA strands connecting cargos.[42] (e) Detection and transport of DNA strands which are fully complementary to the DNA strands attached on the microtubules.[43]

1.3.2 DNA-assisted cargo transport

In motility assay, microtubules can serve as molecular shuttles to transport cargos just like what motor proteins can do. Since microtubules can be ~10 μm in vitro, multiple cargos could be transported at the same time (Figure 1.8c).[41] To further improve the capability of molecular shuttles, DNA modifications could be applied to them. With the specific sequence recognition

property of DNA strands, molecular shuttles can selectively load and unload different types of cargos (Figure 1.8de).[42,43] Schmidt et al.[42] designed a microtubule motility assay based cargo transport system with the help of DNA strands. Two areas are modified on the surface where one is loading zone and another one is unloading zone. With two different DNA strands on the two areas and the DNA strand on the microtubule, the cargo could be picked up by the microtubule first in loading area first and then dropped into unloading area because of the free energy difference. They also used this mechanism to show some cool images on the surface. Furthermore, with the help of DNA strands, it is also possible for microtubules to sort a mixture of cargos to their individual destination.

1.3.3 DNA-assisted microtubule gliding

Other than cargo transport, DNA strands can also be involved in motility assays to change their gliding kinetics. DNA can interconnect microtubules together to achieve swarming behavior of microtubules. Keya et al.[44] conjugated DNA strands onto the microtubules (Figure 1.9a). With the hybridization of DNA strands, microtubules will gradually bind together and do collective motion. This motion can also be controlled 'ON' and 'OFF' by adding extra DNA strands to let DNA on microtubules hybridize and de-hybridize. It can also change the surface charge density of microtubules to affect their gliding behavior under electrical field. As Figure 1.9b shows, the microtubules with DNA strands on them will behave differently under electrical field, and thus can be separated from the unmodified microtubules.[45]

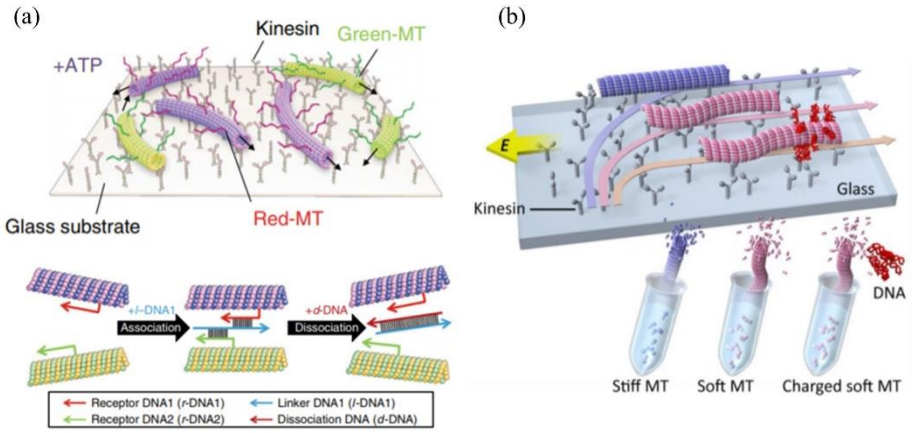

Figure 1.9. (a) Association and dissociation of microtubules by DNA strands. Two different DNA strands are conjugated onto two fluorescent-labeled microtubules. Once a template DNA strand is added, both microtubules will bind to the template. The microtubule will dissociate when a DNA strand fully complementary to the temple is added.[44] (b) Redirection of microtubules gliding under the electrical field. Microtubules with DNA attached will behave differently compared to bare microtubules. Thus the microtubules can be separated by the electrical field.[45]

1.4 Artificial Cells

Since the biological environment is very complicated, it is difficult to understand the behavior of a cell as there are so many components inside. To simplify the cellular environment to specifically study the interested factors and eliminate variations of other factors, artificial cells are needed.[46] The idea of artificial cell was first proposed by Dr. Thomas Ming Swi Chang in 1957.[47] Artificial cell is a substitute of the actual cell created by scientists. Different cell functions can be achieved in the artificial cell by adding components from a real biological cell (Figure 1.10a). Thus it becomes a perfect tool to study cell behavior as all factors could be under control with this setup. In addition, based on its similarity to biological cells, artificial cell could also be used in drug delivery or medical imaging. More importantly, since these synthetic cells can be created with functions different from real cells, the artificial cell research could also be considered as upgrading biological cells by inserting desired functions. All these factors make artificial cell attract lots of attention from scientists.

1.4.1 Lipids and liposomes

Artificial cell can be prepared by different methods including the top-down method and bottom-up method (Figure 1.10b). Based on the complexity of the target system for study, one of these

two methods can be chosen. Top-down method starts from a real cell and reduces its components by editing the genes inside. Bottom-up method starts from an empty cell whose membrane is made by polymers, proteins, lipids or mixtures of these and gradually encapsulates needed cell components into the cell. Among these materials, the lipid bilayer is the actual form of membrane for biologic cell, thus lipids have been studied extensively.

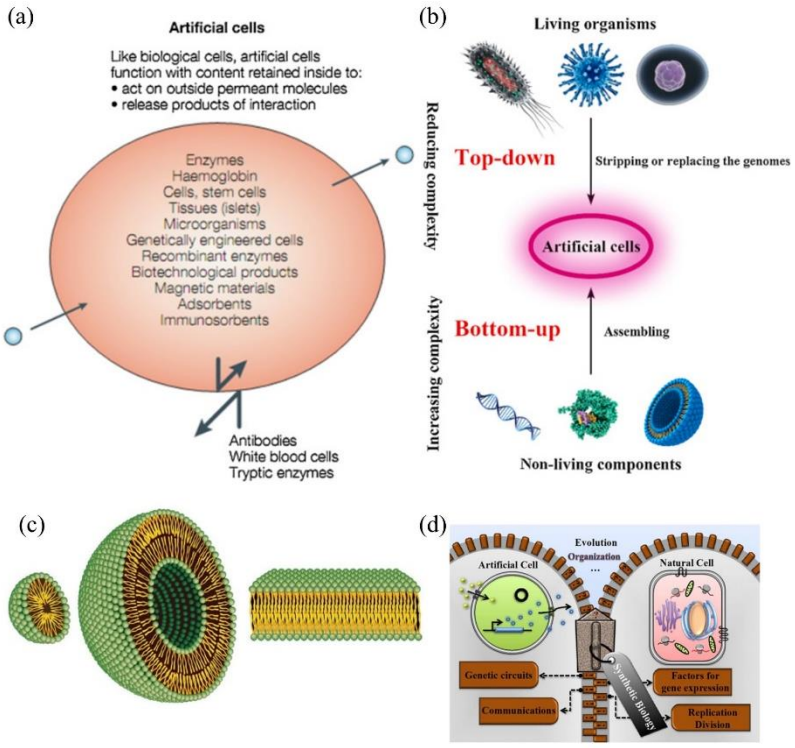

Figure 1.10. (a) Typical artificial cell structure.[48] (b) Approaches to construct an artificial cell. Top-down method is to reduce the complexity of living organisms like viruses, bacteria, and cells. Bottom-up method is to assemble building block materials like DNA, proteins, and lipids into a cell structure.[48] (c) Structure of micelle, liposome and lipid bilayer.[49] (d) Structure comparison of liposomes and natural cells.[50]

Typically, a lipid molecule contains a polar head and a long non-polar tail. The polar head is the hydrophilic part and the tail is hydrophobic part based on their chemical structures. This structure leads to a phenomenon that when the lipids are in aqueous solution, they tend to hide their tails. They need to expose their polar head towards the aqueous solution, so the lipids will gather together and form certain aggregations. Either micelle or liposome (with lipid bilayer) could form while liposome is more favorable because the lipid tails are usually too large to fit in a micelle (Figure 1.10c).[49] A liposome is formed with lipid bilayers the same as a biological cell. This

structure can encapsulate larger volumes inside compared to micelle. This capability makes the liposome a good candidate for the artificial cell. Like Figure 1.10d shows, liposome-based artificial cells have the similar membrane structure to the cell.[50] In addition, liposomes can also be coated by proteins, polysaccharides to add its functions and make it better to achieve actual cell function.[51]

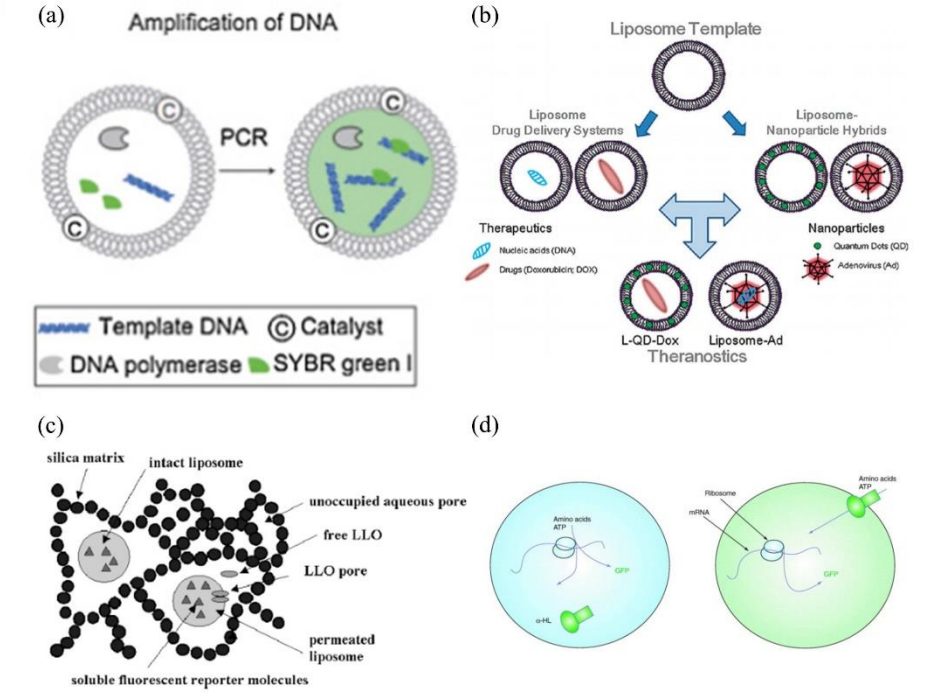

Figure 1.11. (a) Polymerase chain reaction (PCR) inside a liposome. Components for PCR reaction are encapsulated into a liposome and DNA strands start to duplicate inside the liposome.[52] (b) A theranostic system made by liposome. The liposomes are loaded with DNA, doxorubicin drug, quantum dot or adenovirus which make this system able to realize both therapeutic and imaging functions.[53] (c) Structure of a liposome doped silica nanocomposite for listeriolysin O (LLO) detection. The liposomes are captured inside a 3D silica matrix.[54] (d) Translation happening in an artificial cell. GFP and alpha-HL are synthesized based on the amino acids and ATP inside the liposome. As more and more alpha-HL inside the liposome, they will bind to the membrane and create a channel for more ATP and amino acids entering. Thus more alpha-HL and GFP can be synthesized.[55]

A variety of applications can be done by these liposomes including bio-reactor, drug delivery, bio-sensor and biological cell modeling (Figure 1.11).[53,55] Kurihara et al.[52] built a liposome as a bio-reactor for polymerase chain reaction (PCR) as Figure 1.11a shows. They encapsulated DNA polymerase, DNA template, nucleotides, catalyst and SYBR green I inside the liposome. By controlling the environment suitable for PCR, DNA strands are duplicated and fluorescence intensity increased dramatically since SYBR green I binds to the dsDNA products. For the sensing

purpose, a liposome-based listeriolysin O (LLO) sensing system was designed by Zhao et al. (Figure 1.11c).[54] The liposomes are doped inside a 3D silica matrix. Since LLO is a pore-forming hemolysin which can create pores on cell membrane, so once an LLO interacts with a liposome, the fluorophores originally encapsulated inside the liposome will leak into the matrix. Thus LLO existence can be detected.

1.4.2 Synthetic cells with motor protein system

As discussed in Chapter 1.2, the function of motor proteins inside a cell is very important. Since the environment in a biological cell is too complicated and the surface-based motility assay is a little far from actual cell study. Thus artificial cells may be an appropriate tool for motor protein study with their similar but simpler cellular environment compared to a real cell. In addition, since protein motors are necessary components in a biological cell, the study of interaction of motor proteins and liposome could also contribute to the development of artificial cell towards the actual biological cell as well.

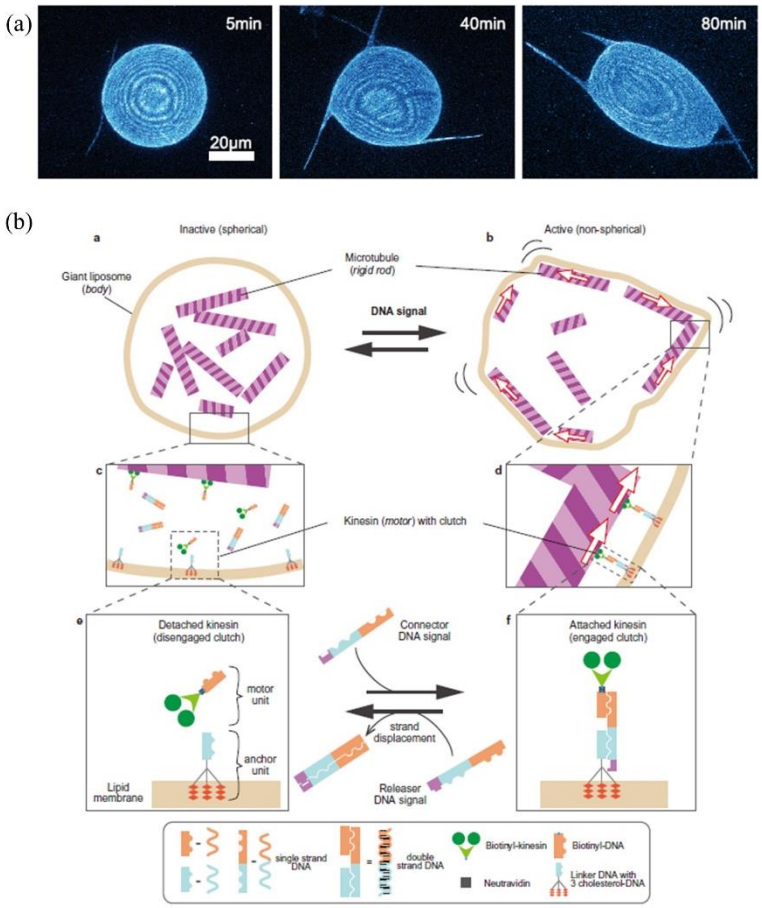

Figure 1.12. (a) Versatile structures of liposome with microtubules encapsulated inside. The round structure is the liposome while the long tube structures are the microtubule bundles.[56] (b) Liposome structure change with motor protein systems and DNA signals. Microtubules and kinesins are encapsulated into a liposome and kinesins are attached on the surface through DNA strands. By adding DNA signals into the liposome, the kinesins will be captured and released from the liposome surface, and thus microtubules will be transported or freely dispersed inside the liposome. The structure of liposome varies based on the microtubules.[57]

Keber et al.[56] encapsulated microtubules and motor proteins into the liposomes (Figure 1.12a). The active transport of microtubules is topologically constrained by a liposome outside. With this design, they studied the structures and dynamics of liposomes which mimic the living organisms with active matters inside. Sato et al.[57] developed this design further and investigate the liposome structure change with DNA signals (Figure 1.12b). Other than motor proteins and microtubules, DNA strands are also encapsulated into the liposome to graft kinesins on the surface. Their DNA strands contain a photo-responsive domain which makes the structure of liposomes can be controlled by UV irradiation.

1.4.3 Artificial cells with transmembrane pores

Transmembrane channels are very important inside a cell since they connect inner cell environment with outer biological condition and they also select if certain molecules could have access to the inner cell. With this function, successful control of cell transmembrane channels could become a strong advantage for controlling cell behavior. Since large protein complexes are the common material for these channels, the study, and control of these bio-molecules are limited. Thus, instead of using proteins, DNA molecules are used to construct transmembrane channels. As mentioned in chapter 1.1, DNA can be assembled into 2D structure and further into 3D. In addition, DNA could also be easily chemical modified and affected by external signals including light, pH, and enzymes. These abilities make DNA a perfect candidate for the transmembrane channel as it can be built into similar shape and added more control possibilities.

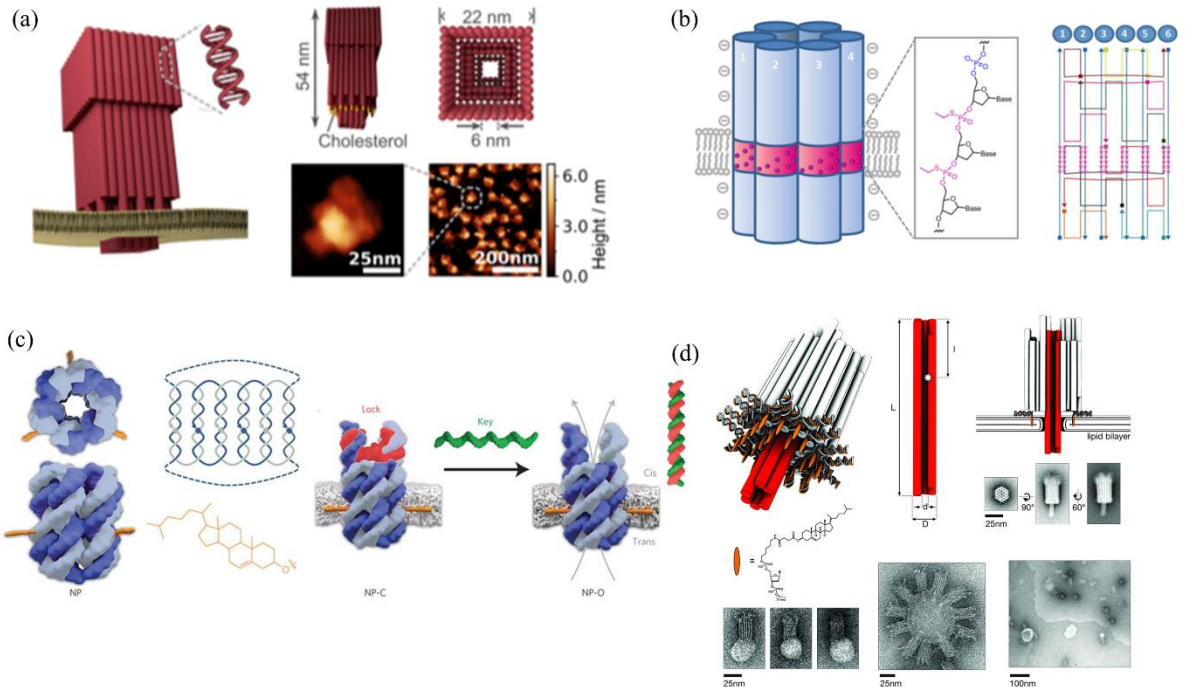

Figure 1.13. (a) DNA origami with cholesterol moieties attached at the bottom. The 3-D DNA origami structure can be inserted into the lipid bilayer with the cholesterol part. The channel size of the DNA origami is around 6 nm x 6 nm square.[58] (b) A DNA-based liposome channel formed with 6 DNA strands only. A hydrophobic moiety is attached to the DNA backbone of the bases, while those bases are at the center of the DNA pore. With this modification, DNA pore can be inserted into lipid bilayer.[59] (c) Improved DNA pore work from (b). An additional DNA (red) strand can be added into the structure of DNA pore where it will block the inlet of the pore to make it as the close state. When the key strand (green) comes in, the block can be removed, and the DNA pore will have its function back.[60] (d) A similar DNA origami pore work as (a). Cholesterol molecules are modified on the bottom of the origami to have DNA origami pore inserting into the liposome. Size of this channel is around 2 nm in diameter.[61]

Several researchers have done studies on DNA origami pore for artificial cell (Figure 1.13). With hydrophobic chain attached on DNA strands or modified with a cholesterol moiety, DNA can be inserted into liposome bilayer as the similar structure of a lipid molecule. Thus, the tube-shaped DNA origami can also be inserted into liposome bilayer. Typical size of these origami pores 10nm x 10nm or less. The assembly varies from a full DNA origami (~200 DNA strands) to 6 DNA strands.[60,62] The existence of DNA origami on liposome has been verified by fluorescence imaging and transmembrane current measurement.[58,59] The function of these origami pores currently focuses on the influx and outflux of small molecules. Simmel et al.[61,63] have published several

papers on origami pore study where his group has designed this synthetic DNA origami pore and achieve molecular transport through the pore. However, study of this type of origami pore on liposome is still at its early stage as the current research mainly focuses on the most fundamental capabilities of the DNA pore. The effort to take a step further would be needed.

1.5 Motivation

Study of cellular environment is a very important topic as it is directly related to life. However, with its extreme complexity, simplification of this system is necessary in order to study. As one of the most popular and promising methods, artificial cell research shows its great importance. In order to achieve the similar cell functions inside a human-built lipid bilayer, the components of an artificial cell should be as close as possible to a real cell while they can be controlled by external signals. Transmembrane protein channel as gate of cell helps maintain the inner environment of cell. If a similar channel structure could also be implemented onto an artificial cell, the simulation of the real cell could take a big step forward. As one of the promising candidates for synthetic transmembrane channel, DNA origami pore research is still on its early stage, so there are lots of things need to be done on this topic and that motivates me to work on this project.

1.6 Scope of the Study

This thesis focuses on the interaction between motor protein systems and DNA nanotechnology. We study the manipulation of DNA signals using a DNA logic gate system on a DNA origami platform. The DNA logic gate is investigated through the capture and release of molecular cargos on the origami. The cargos include small molecules, proteins, and nanoparticles. We also study the light-triggered capture and release.

Cancer cell treatment by a DNA walker based system will also be discussed. The kinetics of DNA walker is analyzed by fluorescence imaging. Cell viability is used to evaluate the effect of DNA walker system treatment on breast cancer cells.

Microtubule motility assay is used to study the interaction between motor protein and DNA. DNA strands are conjugated onto nanoparticles and are used for redirection of microtubule gliding on

the surface. Models are built to study this process, as well as to compare with the crossflow based microtubule direction change. Their interactions and kinetics within a liposome will also be discussed.

1.7 Organization

This thesis discusses experimental efforts in using DNA nanotechnology method to study motor proteins. Chapter 2 provides the general experimental setups and sample preparation methods. The design and investigation of DNA logic gate system on a DNA origami are presented in Chapter 3. Breast cancer cell treatment using a DNA walker system is discussed in Chapter 4. Microtubule motility assay evaluation and its direction change by the DNA-particle system as well as the modeling work are described in Chapter 5. The integration of DNA signals into artificial cell for reversible liposome aggregation and release, and DNA origami pore study are discussed in Chapter 6. Concluding remarks and future work are presented in Chapter 7.

2 METHODS

2.1 Materials

All the DNA strands used are purchased from Integrated DNA Technologies Inc. If not specified, all the chemicals are purchased from Sigma-Aldrich.

2.2 Preparation of DNA Decorated Nanoparticles

2.2.1 DNA-assisted quantum dot growth

Aqueous synthesis of QD nanocrystals with excellent quantum yield and photo-stability has been reported previously.[64-66] We modified those synthesis routes to generate DNAzyme functionalized CdTe/CdS nanocrystal QDs. The QDs helps to locate DNA on carbon nanotube for DNA walking measurement. CdTe core with 2 nm diameter was first synthesized using NaHTe and $CdCl_2$ as precursors and mercaptopropionic acid (MPA) as capping ligand. The synthesized core was subsequently purified by using 3 M NaCl and methanol as non-solvent and centrifuged at 15,000 g for 10 min. CdS shell was grown epitaxially over the CdTe core by heating a mixture of the core solution, $CdCl_2$-MPA, and phosphorothiolated DNAzyme strands. CdTe/CdS QDs with ~3.5 nm diameter and emission peak centered at 610 nm will form after 40 min heating time. The synthesized QDs were purified using a 30 K column filtration (Amicon) for 4 times to remove the excess CdS and DNA.

2.2.2 DNA conjugation with polystyrene particles

Polystyrene particle has more uniform size distribution and brighter fluorescence, thus it is used for DNA grafting for guided microtubule gliding. To prepare the sample, 2% polystyrene particle solution was diluted in 70 μl 2-(N-morpholino)ethanesulfonic acid (MES) buffer (pH 6.0). Approximately 20 μL of 100 μM amine-modified single-stranded (ss) DNA was added to the particle solution, and the mixture was incubated for 15 mins. Then, 5 μL 100 μM 1-ethyl-3-(3-dimethylaminopropyl)carbodiimide (EDC) was added into the mixture and the solution was sonicated for 1 min. After sonication, the mixture was incubated in dark for 2 hours to let carboxyl groups on particles and amine group on DNA react. Lastly, the solution was centrifuged for 30 mins at 20,000 g, which was repeated for 3 times. Each time the supernatant was discarded, and

the precipitate was re-dissolved in 200 μL 1x PBS buffer. After centrifugation, purified particles with ssDNA were obtained.

2.3 Preparation of Carbon Nanotubes based DNA Walker System

Carbon nanotube-based DNA walker consists of two parts, one is fuel strand coated carbon nanotube, another is quantum dot associated DNA walker.

Dispersion of CNTs decorated with fuel strands

The procedure for dispersing DNA-functionalized carbon nanotubes in aqueous solution was reported elsewhere.[67,68] Briefly, an aqueous sample of HiPco CNTs dispersed by sodium cholate was subject to a surfactant replacement via a 2-stage dialysis. The first dialysis was performed to replace cholate with fuel strands for CNT suspension, while the second dialysis removed unbound DNA strands. The CNT and DNA concentrations were determined by the absorbance measurements using a Perkin-Elmer Lambda 950 UV/visible/near-IR spectrophotometer.

Conjugation of QD-modified DNAzyme and fuel strands on CNT track

The solution of CdTe/CdS QD-capped DNAzymes was mixed with the solution of dispersed fuel strand-decorated CNTs at a ratio of approximately 10:1.

2.4 Microtubule Polymerization

In this work, microtubule is polymerized by us with purchased tubulin. Fluorescent HiLyte 647 labelled and biotin labelled tubulins were mixed 1/1 ratio and then dissolved in the polymerization buffer (80 mM piperazine-N,Nrabis(2-ethanesulfonic acid) (PIPES), 2 mM $MgCl_2$, 1 mM ethylene glycol-bis(β-aminoethyl ether)-N,N,N',N'-tetraacetic acid (EGTA), 1 mM guanosine triphosphate (GTP), and 6% glycerol) to make a 5 mg/ml tubulin solution. The solution was then incubated in 37°C water bath for 30 mins. Unused tubulin solution can be snap freezing in liquid nitrogen and stored at -80°C. After incubation, tubulins were polymerized into microtubules. Polymerized microtubules were diluted in the tubulin buffer (80 mM PIPES, 1 mM $MgCl_2$, and 1 mM EGTA, BRB80) with 10 μM paclitaxel to stabilize polymerized microtubules.

2.5 In vitro Microtubule Gliding Assay

Gliding assay is performed with the polymerized microtubule and purchased kinesin on the glass surface. To do that, first, 10 μgml^{-1} kinesin solution was flowed into the fabricated microfluidic channel and incubated for 10 mins to let kinesins adsorb on the coverslip. Then, kinesin solution was washed away with BRB80 buffer, and the channel was filled with 5 mg/ml casein solution for another 10 mins. After this, the microtubule solution together with the anti-fade solution (20 mM glucose, 200 μgml^{-1} glucose oxidase, 50 μgml^{-1} catalase, and 0.5% beta-mercaptoethanol) was added into the channel. Microtubules were grafted by kinesins on the surface in 5 mins. Unbound microtubules were washed away by supplying the BRB80 buffer with anti-fade solution. Approximately 1 mM ATP in buffer with anti-fade solution was then flowed into the channel to trigger microtubule gliding. Since the kinesins only have the motor domain, the expected speed for gliding assay is ~1 μm/min which is much slower compared to those full-length kinesins.

2.6 Liposome Preparation

Liposome preparation uses the inverted emulsion method.[69,70] Lipid solution dissolved in chloroform were purchased from Avanti Polar Lipids Inc. 1,2- dimyristoyl-sn-glycerol-3-phosphocholine (DMPC) and 1,2-Dioleoyl-sn-Glycero-3-Phosphoethanolamine-N-(Biotinyl) (18:1 Biotinyl PE) were mixed 1:1 ratio to make a 100 μL solution. The 10 mg/ml lipid solution was added into a glass vial and vacuum dried for 20 minutes to form a thin layer of lipid on the glass vial. Then 300 μL liquid paraffin was added to dissolve the lipids. The new solution was sonicated at 50 °C for 3 hours to have lipid disperse uniformly in the sonicated solution. To make liposome only with nothing encapsulated, 20 μL DI water was added and the mixture was vortexed for 15 s. After vortex, the solution became blurred. The mixture was then poured onto 300 μL water and centrifuged for 15 minutes at 8,000 g. The liposome will be in the precipitates.

2.7 Characterization Methods

2.7.1 AFM Imaging

All AFM imaging was performed on dried sample unless otherwise stated. The sample (*e.g.* Origami solution) was first diluted to 1 nM by 1xTAE buffer with 12.5 mM Mg^{2+} (TAEM) buffer. Approximately 10 μL of the diluted solution was then deposited on a freshly cleaved mica. After

incubation for 5 – 10 minutes, the solution was blown away with compressed air. The mica surface was further rinsed with about 50 μL DI water and blown dry with compressed air. The AFM imaging was performed with a SCANASYST-AIR probe.

To perform liquid AFM, the sample will be characterized in TAEM buffer. To prepare the sample, 10 μL of 1 nM origami sample in TAEM was first deposited on a freshly cleaved mica. After incubation for 5 – 10 minutes, another 30 μL TAEM buffer was added onto the mica surface. The sample was then scanned with a SCANASYST-FLUID+ probe.

2.7.2 Spectral Characterization

Absorption is a great way to quantitatively determine how much a certain molecule existing in solution. To accurately measure the amount of solute, absorption of the solvent has to be measured first as the baseline. Usually, 100 μL buffer was added into both cuvettes and placed in the holder inside the Perkin Elmer Lambda 950 spectrophotometer with desired wavelength range selected. After collected the baseline, buffer in sample cuvette was replaced with real sample. With running the measurement again, the absorbance spectra of the sample could be collected and the concentration of solute can be calculated.

2.7.3 Ensemble Fluorescence Measurement

Horiba FL-1039/40 Fluorometer was used to perform ensemble fluorescence measurements. Sample was loaded into cuvette and placed inside the machine. With desired excitation wavelength, emission wavelength range and slit size chosen, emission of the sample can be measured. With fixed excitation and emission wavelength set, change of fluorescence as time goes could be detected.

2.7.4 Fluorescence Microscopy

Different from fluorometer, fluorescence microscopy can be used for single-molecule fluorescence imaging. The sample was flowed into an assembled microfluidic channel. The channel was then put on the stage of the fluorescence microscopy. The EMCCD camera was needed to be cooled to -90 °C before use. With choosing the appropriate laser line (405 nm, 561nm, 658nm available), filter set and exposure time, the samples could be imaged.

2.7.5 Gel Electrophoresis

2.7.5.1 PAGE

To prepare 15% native PAGE experiment, approximately 1.875 mL 40% acrylamide, 0.5 mL 10x TBE, and 2.625 mL DI H_2O were mixed well first. Then, 20 μL 25% (w/v) ammonium persulfate (APS) and 10 μL tetramethylethylenediamine (TEMED) were added into the solution. The gel was cast by a gel casting system (Bio-Rad) immediately and ready to use. Different percentage PAGE gel can be prepared in the same way, while more concentrated gel will be used for shorter DNA strands.

2.7.5.2 Agarose gel

Like PAGE gel, agarose gel is also used to separate DNA strands. While the difference is agarose gel has larger pores inside which means it has better effect to separate huge DNA structure. To prepare a 1.5% agarose solution, approximately 600 mg agarose was added to 40 mL 0.5x TBE buffer. The solution was then heated to boil to dissolve all agarose. After the solution cooled down, before the polymerization of agarose, 2 μL 10 mg/mL ethidium bromide was added to the solution and mixed well. Ethidium bromide can be used to stain DNA and visualize them under UV light. The solution was then left in room temperature to finish polymerization.

2.7.5.3 SDS-PAGE

SDS-PAGE used in this work was 10% separating gel and 10% stacking gel which were used to load and separate protein samples. To prepare the separating gel, 1.52 mL H_2O, 1.02 mL 40% acrylamide, 1.04 mL 1.5 M Tris (pH 8.8), 40 μL 10% (w/v) SDS were mixed well first. Then, 40 μL 10% (w/v) APS and 4 μL TEMED were added into the solution. Then a separating layer was cast by a gel casting system.

To prepare the stacking gel, 0.98 mL H_2O, 0.5 mL 40% acrylamide, 0.5 mL 0.5 M Tris-HCl (pH 6.8), 20 μL 10% (w/v) SDS were mixed well. Then, 20 μL 10% (w/v) APS and 2 μL TEMED were added into the solution. On top of a freshly prepared separating layer, a stacking layer was cast, and the gel was ready to use.

2.8 Microfluidic Channel Assembly

Microfluidic channel was the platform used in this work to study DNA walker, microtubules and liposomes. It can be easily assembled and has multiple surface modifications which makes it a good tool for single-molecule study. In general, to prepare a microfluidic channel, a coverslip, and a glass slide are needed. The coverslip was immersed in piranha solution (sulfuric acid: peroxide = 3:1) for 1 hour to remove organic residues from the surface. It was then rinsed with deionized water and stored at room temperature. For the glass slide, two holes were drilled as inlet and outlet ports. A bonded-port connector and a one-piece fitting (LabSmith) were adhered to each hole to connect with tubing. With these preparations done, the glass slide and the coverslip were adhered together by a double-sided tape with a channel pattern cut off to make the channel ready to use. The channel pattern on the double-sided tape was created by a cutting machine (Silhouette Curio).

3 DNA LOGIC GATE FOR CAPTURE AND RELEASE OF ANALYTES

3.1 Introduction

As discussed in chapter 1, DNA can interact with functional molecules, proteins, and nanoparticles while some of them can inspire great interest of researchers. In order to understand their properties and harness their functionalities, sorting and isolating them is important. Thus, capturing and releasing, as the two crucial steps for sorting, are needed. Various strategies for molecular capture and release have been proposed to ensure high specificity and fidelity (Figure 3.1).[71-73] With its strict base-pairing property, DNA is perhaps the most promising tool for such purposes. Additionally, oligonucleotides could be easily modified with a wide variety of chemical groups just as introduced in chapter 1. These chemical groups can render DNA molecules responsive to external signals such as light, cations, and pH.[74,75]

To successfully process molecular capture and release, a stable base surface is needed. This base surface should have high precision which can deal with molecules in nanometer level and high specificity which can recognize different molecules. Given the heterogeneity, DNA origami structures are highly addressable, serving as virtual nanoscale breadboards where analytes can be arranged precisely, and their bioorganic molecular reactions may be controlled. All these properties make DNA origami a perfect candidate for studying molecular capture and release. For example, one similar work has been done by Voigt et al. showing the strength of using DNA origami. They demonstrated that streptavidin may be placed site-specifically on DNA origami using biotinylated strands and that such a platform can be used to study single-molecule chemical reactions.[8] While diverse small molecules, proteins, and nanocrystals have been captured on DNA origami structures for widespread purposes, the release processes demonstrated to date have predominantly relied on simple strand displacement mechanisms.[76-78] Therefore, novel strategies for programmable analyte release upon external signals will complement the impressive addressability available, while providing access to new applications.

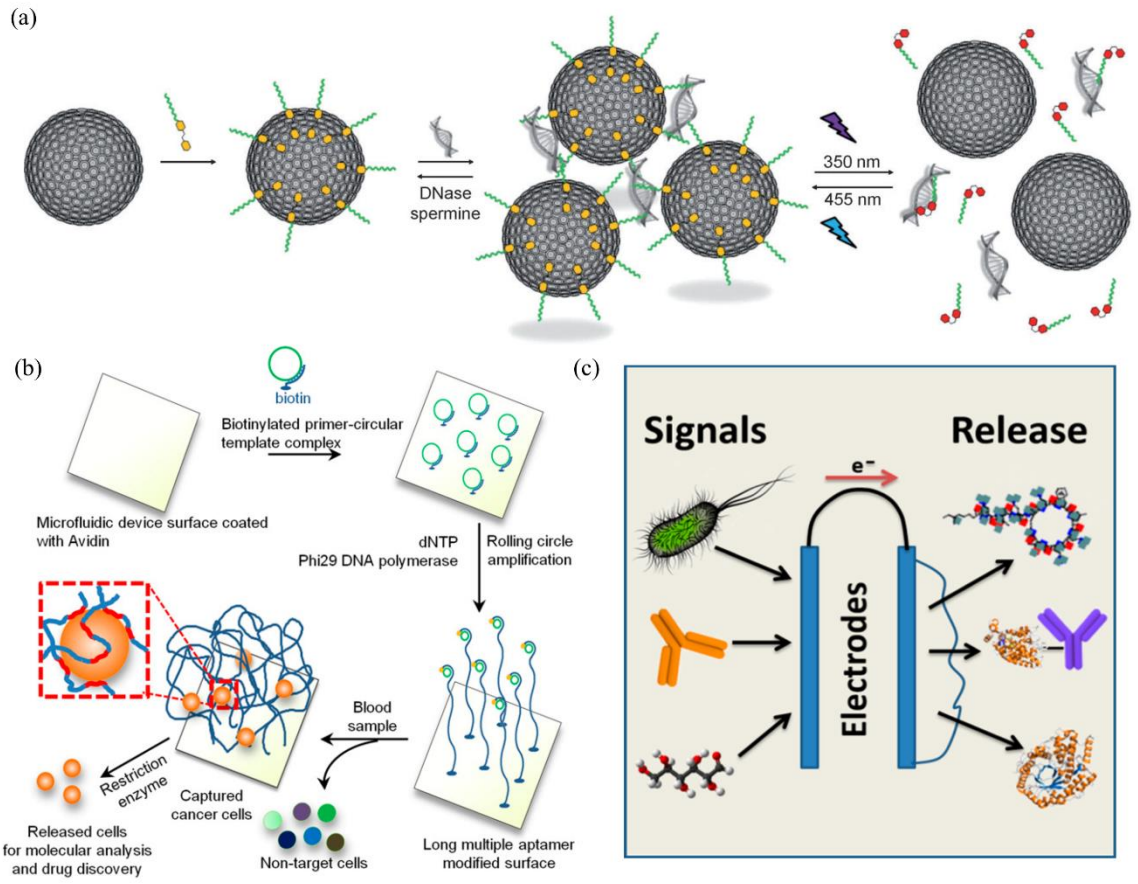

Figure 3.1. (a) Light responsive DNA capture and release. Azobenzene-spermine can bind to cyclodextrin (CD) vesicle by trans azobenzene group and bind to DNA through a positively charged spermine unit. Once UV shines, azobenzene will convert to cis form and released from CD vesicle and visible light can convert it back. Thus, capture and release of DNA strands can be achieved by shining UV and visible light.[71] (b) DNA aptamer is immobilized onto microfluidic channel surface to capture target cells, while the non-target cells cannot be captured due to lack of affinity.[73] (c) Bioelectronic sensing. With different types of inputs coming in including bacteria, proteins or small molecules, corresponding output is generated with the use of sensing electrode.[72]

Here, we demonstrate a DNAzyme-mediated logic gate system that can be used for programmable molecular capture and release on DNA origami. Input of DNA logic gates use specially designed DNA strands to mimic the Boolean logic calculation (i.e. 1 or 0 meaning having DNA strands or not).[79-81] The output of the DNA logic gate process could be in the forms of DNA strands or fluorescence, via strand displacement mechanisms.[82,83] In this work, a defined DNAzyme-based logic gate mechanism was used[84,85] to release the captured molecular targets of small functional

molecules, proteins, and nanocrystals on DNA origami. The output generated by DNA logic gate is consisting of a DNAzyme which cleaves its substrate with sequence specificity, thereby analytes on DNA origami will be its target and released. The logic gate process is triggered, when and only when two distinct DNA inputs (i.e. initiators) are present. In addition, the release can also be controlled by external light irradiation by inserting a photocleavable spacer into the logic gate complex (LGC).

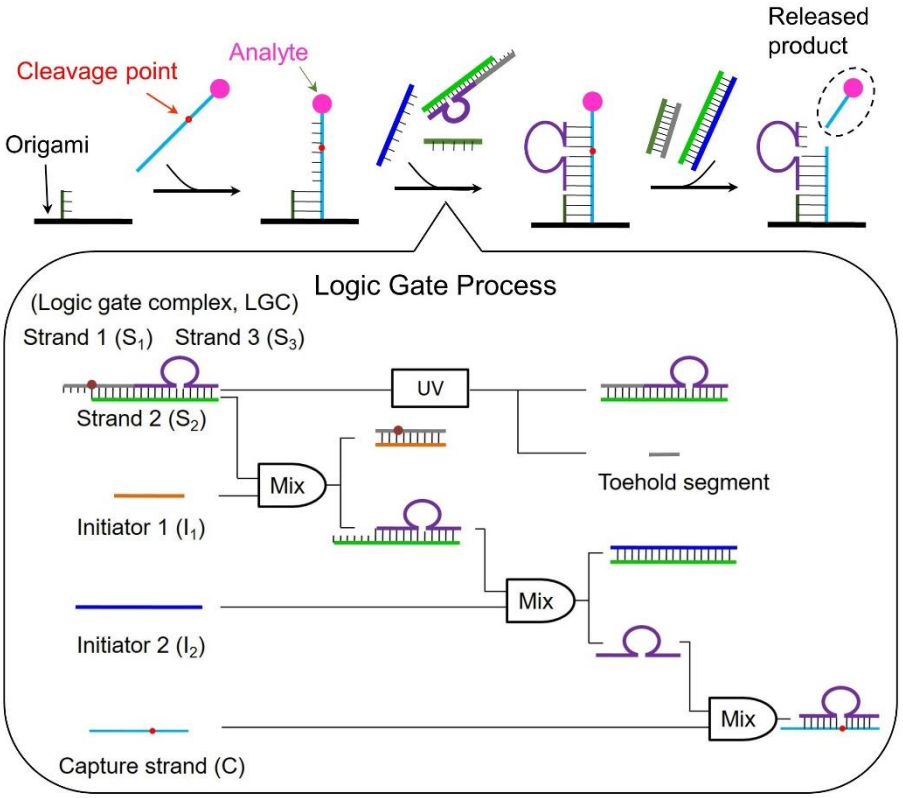

Figure 3.2. Programmable DNA logic gate mediated capture and release. In this work, analytes include the choices of ruthenium dye, thrombin, and AuNP.

3.2 Scheme

Figure 3.2 shows the schematic of the logic gate programmed molecular capture and release processes. Here, a DNA capture arm (cyan) with a prearranged cleavage point (red) is used for capturing free analyte in solution and the DNAzyme strand (purple, 10-23 DNAzyme, the 23rd clone of the 10th round in-vitro selection)[86] is used for cleaving target molecule as a controlled release. The capture arm will be tethered with a staple extension on the DNA origami, and the

analyte captured on it will be ruthenium bipyridinephenanthroline (or Ru dye),[87] thrombin, and gold nanoparticles (AuNPs). They are presented as the model systems in this study.

The DNA logic gate mechanism is based on toehold-mediated strand displacement. LGC strands (S_1, S_2, and S_3, preformed complex) are in the same solution with the analyte (a pink, filled circle in Figure 3.2). Once the analyte is captured onto the origami platform, initiators 1 (orange) and 2 (blue) will be added separately. The initiator 1 (I1) is fully complementary with S_1 (grey). I1 first base-pairs with the single-stranded toehold segment of S_1 (the extra bases left unbound in LGC) and then hybridize fully, thereby dissociating S_1 from the complex. Initiator 2 (I2) will then react with the product of this step (strands 2 and 3, or S_2/S_3), via a similar toehold-mediated strand displacement process, producing the final product S_3 (purple). S_3 (DNAzyme) has two recognition arms that bind to capture arm (cyan) on DNA origami and a catalytic core which cleaves the prearranged site (rArU, shown as a red dot) in the presence of divalent metal cations such as Mg^{2+} via a cation-assisted deprotonation process.[88] The analyte will be released from origami after this cleavage.

This DNAzyme-mediated logic gate system can capture one or more analytes with high specificity and release them from origami through the LGC reaction cascade. Not only interacting with DNA signals, but this analyte release process could also be programmed using photo-irradiation as an external signal. By incorporating a photocleavable moiety into the toehold segment of S_1 (brown dot in Figure 3.2), UV irradiation as an external signal could be introduced into the system which can cleaves this moiety. Without the extra toehold overhang needed for triggering the logic gate process on S_1, the logic gate process is not triggered by the initiators, and thus, the release is prohibited.

3.3 Experimental Methods

3.3.1 Materials

Gold nanoparticles (AuNPs) of 10 nm in diameter were purchased from BBI Solutions. PAGE and SDS-PAGE buffer and reagents were obtained from Bio-Rad. Thrombin was obtained from

Haematologic Technologies Inc. PD 10 desalting columns were acquired from GE Healthcare Life Sciences.

3.3.2 DNA logic gate design

PAGE is used to confirm the effectiveness of the DNA logic gate. Initiator 1, initiator 2, LGC and all their combinations were tested. LGC was prepared by mixing S_1, S_2, and S_3 first and centrifuged 6 times at 5,000 rpm for 3 minutes in a 30 kD centrifugal filter (EMD Millipore) to remove excess single strand. Sample was incubated at room temperature for 1 hour before loading on 15% PAGE. About 120V was applied onto the gel to separate the DNA strands inside.

For the UV-trigged logic gate experiment, instead of using S1, the photocleavable strand S1* was mixed with S2 and S3 to prepare LGC. Before loading sample, other than incubation at room temperature, UV irradiation was also introduced to the sample using a UV lamp (UVP, model# UVGL-25, λ~254 nm) for about 15 minutes. The DNA samples were placed approximately 5 cm away UV lamp.

All DNA logic gate strands are designed by NUPACK.[89]

Logic gate strand sequence (left to right: 5' – 3')

Logic gate A

Strand 1: ATC TAA CAA CCA CCA CCA AAC CAT CCC ACA CAC CAC

Strand 2: ATG GTT TGG TGG TGG TTG TTA GAT GTC ACT CTG TCC GAA TCA GCA CT

Strand 3: AGT GCT GAT TCG GAC AGG CTA GCT ACA ACG AGA GTG AC

Initiator 1: GTG GTG TGT GGG ATG GTT TGG TGG TGG TTG TTA GAT

Initiator 2: AGT GCT GAT TCG GAC AGA GTG ACA TCT AAC AAC CA

Capture strand: GTC ACT CrArU GTC CGA ATC AGC ACT

Logic gate B

Strand 1: ACC GCG TCT CAT ACA TCA TCT GGC ACA TCA TCT CAC

Strand 2: GCC AGA TGA TGT ATG AGA CGC GGT GTG CAG GTG GAG AGC ATA AAG TC

Strand 3: GAC TTT ATG CTC TCC AGG CTA GCT ACA ACG ACC TGC AC

Initiator 1: GTG AGA TGA TGT GCC AGA TGA TGT ATG AGA CGC GGT

Initiator 2: GAC TTT ATG CTC TCC ACC TGC ACA CCG CGT CTC AT

Capture strand: GTG CAG GrArU GGA GAG CAT AAA GTC

Photo-cleavable logic gate strand

Logic gate A

Strand 1': ATC TAA CAA CCA CCA CCA AAC CAT /iSpPC/CC CAC ACA CCA C

Capture strand for Ru-dye

/5AmMC6/GTG CAG GrArU GGA GAG CAT AAA GTC TTT TTT TTT TTT TTT

Capture strand for AuNP

[16,04]:TTT TTT TTT TTT TTT TTT TTT TTT GTC ACT CrArU GTC CGA ATC AGC ACT /3ThioMC3-D/

[30,24]:TAC GAG TTG AGA ATC CTG AAT TTT GTG CAG GrArU GGA GAG CAT AAA GTC /3ThioMC3-D/

Capture strand for thrombin

TTT TTT TTT TTT TTT GTC ACT CrArU GTC CGA ATC AGC ACT CAT CTC GGT TGG TGT GGT TGG

The DNA origami has been used in our group, which is designed by Haorong Chen. The detailed sequence information is listed in his thesis.[90]

3.3.3 Analyte conjugation with DNA

Ru complex conjugation with DNA

Synthesis of ruthenium bipyridine phenanthroline isothiocyanates (Ru-bpy-phen-itc) was reported elsewhere.[87] To conjugate the Ru complex with amino-modified capture strand,[91] Ru-bpy-phen-itc (offered by Dr. Igor L Medintz) was dissolved into dimethyl sulfoxide (DMSO) as a 20 mM solution. Approximately 10 μL Ru-bpy-phen-itc was mixed with 10 μL 1mM DNA dissolved in

DI water. The mixture was filled to 100 μL with sodium carbonate buffer (0.1 M, pH 8.5). It was then incubated for 6 hours at room temperature, with gentle tapping of the vial every 2 hours to make sure that the solution is well mixed. After the reaction was done, DNA-Ru sample was purified by a PD 10 desalting column. To separate products from excess Ru-bpy-phen-itc, 100 μM triethylamine acetate was used as elution buffer and each elution 750 μL buffer was used. Ruthenium labeled DNA was washed out at 3rd or 4th elution. Concentration of purified DNA-Ru was determined by absorbance measurement.

Phosphine-capping of AuNPs

AuNPs were incubated overnight with 2.5 mM bis(para-sulfonatophenyl) phenylphosphine dihydrate dipotassium salt (BSPP). The solution was then centrifuged for 15 minutes at 13,000 rpm. The precipitate was re-dispersed in 2.5 mM BSPP solution while the supernatant was discarded. The concentration of AuNPs was determined by measuring the absorption at 520 nm using a NanoDrop 1000 spectrophotometer.

AuNP functionalization

Thiol modified DNA strands were mixed with Phosphine-coated AuNPs at an approximately 200:1 concentration ratio in 0.5x Tris-borate-EDTA (TBE) buffer containing 0.1 M NaCl for 12 hours. After incubation, NaCl concentration was slowly raised to 0.3 M by pumping higher concentration NaCl into the mixture in the next 12 hours. The solution was then centrifuged for 15 minutes at 13,000 rpm. The precipitate was collected and re-dissolved in 1x TBE buffer.[92]

3.3.4 Molecular capture and release on origami

DNA origami synthesis

The scaffold strands (M13mp18, Bayou Biolabs) were mixed with 180 32-nt long staple strands in TAEM buffer. The final concentrations of the scaffold and staple strands were 10 and 100 nM respectively. The mixture was put in a thermal cycler (Bio-Rad S1000) with annealing from 75 °C to 4 °C by 0.1 °C every 6 seconds.[93] The DNA strands would self-assemble into rectangular origami tiles of 100 nm x 70 nm during the annealing process.

AuNP-origami conjugation

In order to get a clean sample while AuNP is on origami without free AuNPs in solution, purification of AuNP-origami is needed. First, DNA origami was mixed with AuNP-modified DNA strands at a concentration ratio of approximately 1:4. After overnight incubation, the product was purified by 1.5% agarose gel. The electrophoresis was performed at 60 V, 4 °C. The desired band that contains AuNP-origami was cut and extracted with Freeze 'N Squeeze column (Bio-Rad). The band was frozen for 5 minutes at -20 °C and then centrifuged for 3 minutes at 13,000 g. The purified AuNP-origami could be retracted from agarose after this process.

Thrombin-origami conjugation

Thrombin-binding aptamer (TBA) sequence (5' – GGT TGG TGT GGT TGG – 3') was demonstrated elsewhere for thrombin capture.[94] To examine the binding specificity, an equal amount of thrombin and glutathione s-transferase (GST) molecules were mixed and incubated with TBA-expressed DNA origami at a concentration ratio of 100:1 for 2 hours at room temperature. After incubation, the mixture was centrifuged in a 100 kD centrifugal filter (EMD Millipore) for 3 minutes at 5,000 g to remove the unbound proteins. Sample left in the filter column was collected. DNA logic gate strands (LGC, I_1, I_2) was used to release the captured proteins on origami. The collected protein molecules were incubated denatured at 95 °C for 4 minutes, and then loaded onto SDS-PAGE. The electrophoresis was performed at 120 V for around 1 hour and was stained by Oriole Fluorescent Gel Stain (Bio-Rad) which could be visualized under UV irradiation. Thrombin and GST will show two distinct bands on the gel given their different molecular weight.

Release of analytes (Ru-dye/thrombin/AuNP) from origami tiles

LGC and both initiators were added to analyte-conjugated origami solution to trigger the release with a concentration ratio around 10: 1. The mixture was then incubated for 2 hours at room temperature.

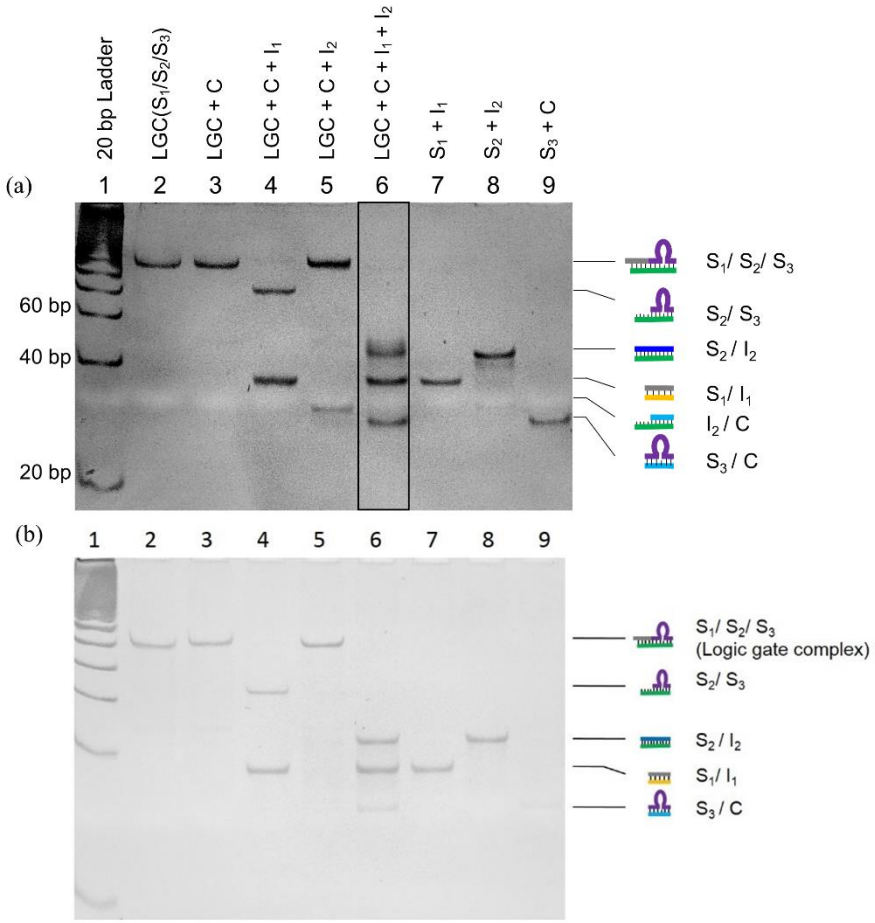

Figure 3.3. (a) 15% native PAGE analysis of the logic gate process. (b) 15% native PAGE analysis of the logic gate set B. For both images, Lane 1: 20 bp ladder. Lane 2: LGC ($S_1/S_2/S_3$). Lane 3: LGC + C. Lane 4: LGC + I_1 + C. Lane 5: LGC + I_2 + C. Lane 6: LGC + I_1 + I_2 + C. Lane 7: S_1 + I_1. Lane 8: S_2 + I_2. Lane 9: S_3 + C. LGC, capture strand (C), and both initiators are mixed to a final concentration at 0.5 μM. In lines 7-9, S_1/I_1, S_2/I_2, and S_3/C are examined as controls. Only when both initiator strands are present, the logic gate process generates the final product S_3, which subsequently hybridizes with a capture strand, shown as S_3/C band in lane 6.

3.4 Results and Discussion

3.4.1 Programmable DNA logic gate

Before we discuss the actual application of this DNA logic gate system, its function must be proved first. In this case, we use native PAGE to confirm the DNA logic gate functionality, as shown in Figure 3.3. Here, without addition of I_1 and I_2, the LGC ($S_1/S_2/S_3$) always shows a distinct band on the gel regardless of the presence of C (lanes 2 and 3), suggesting no direct interaction with

capture strand. However, if I_1 is added, LGC will release S_1 and generate S_2/S_3 (lane 4), whereas I_2 associated with C which will keep LGC intact (lane 5). As designed, either I_1 or I_2 individually could not generate the final product S_3. The final product is produced only when both initiators are present where S_3 can be released and bind to C (lane 6). Additionally, to serve as a reference, S_1/I_1 (lane 7), S_2/I_2 (lane 8), and S_3/C (lane 9) are also examined.

3.4.2 DNA controlled molecular capture and release

With the logic gate function proven, programmable capture and release on DNA origami could then be tested. First, the fluorescent Ru compound was used as optical probes to test the idea. DNA origami rectangles were prepared as shown in Figure 3.4a (approximately 70 nm x 100 nm). Single strand DNA was linked with a ruthenium compound as discussed in methods and was characterized by absorbance measurement (Figure 3.5a). The Ru dye-conjugated capture strands were then mixed with origami and incubated for 2 hours to allow hybridization. The modified spots on origami for ruthenium was shown in Figure 3.4b (yellow dots) with 6 sparsely placed staple extensions. The purpose of putting 6 ruthenium molecules on a single origami is to increase its fluorescence for easier measurement. The mixture was purified 4 times by centrifuging at 5,000 g in a 30 kD filter for 3 minutes to remove excess Ru dyes. Photoluminescence (PL) of the purified ruthenium origami sample was measured before adding any logic gate strands. Ten times more LGC and selected initiator strands were then added into the purified origami solution to fully release the ruthenium from origami tiles. This incubation took another 2 hours and the release Ru from origami is removed by the same centrifugal purification method. Finally, the origami sample was examined for PL intensity again to determine how much ruthenium is left on the origami.

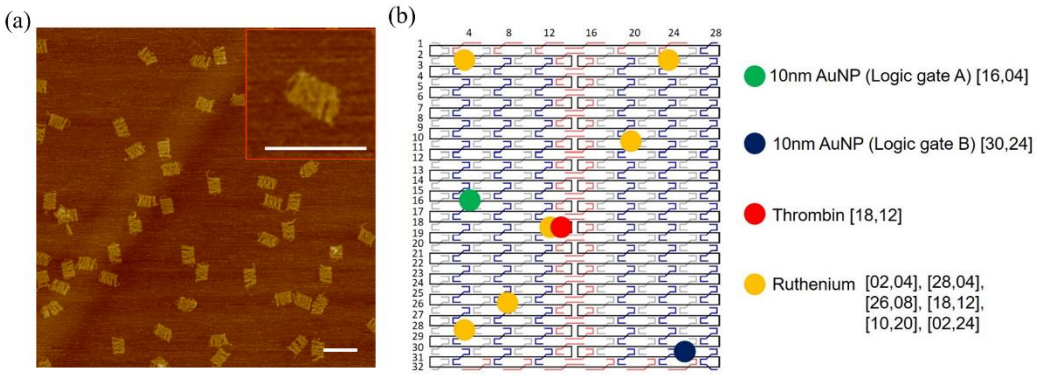

Figure 3.4. (a) DNA origami tiles AFM images, a typical size of an origami is 100 × 70 nm^2. Scale bar: 200 nm. (b) Schematic of origami scaffold (black) and staples (grey, blue, and red) modification. The staple positions for Ruthenium, thrombin, and AuNPs are denoted in orange, red, and green/navy, respectively.

Figure 3.5b shows the resulting PL spectra corresponding to different input combinations. The 610 nm peak coincides with emission peak of Ru complexes which reflects the integrity of ruthenium molecules. With only one initiator or no initiator added, the PL intensity stayed at the same level. In contrast, when both initiators are present, its PL intensity drops 40% to baseline value. Given the fact that baseline still shows fluorescence, it is important to assess its value since it should have no fluorescence as designed. One hypothesis is that the interaction between ruthenium and DNA origami prevents fully wash of ruthenium molecules. To prove that, no DNA modified Ru dye was mixed with origami tiles along with the logic gate strands (LGC, I_1, and I_2). Same purification and measurement were performed on this solution and the PL intensity value was shown as a green curve in Figure 3.5b. This indicates that baseline fluorescence is due to interaction of Ru dyes and DNA, most likely intercalation, which hinders complete removal by filtration.[95] With this PL intensity offset problem solved, the fluorescence results are in accordance with design and the PAGE analysis. I_1 and I_2 together initiated the logic gate process for S_3 generation which leads to the release of Ru dyes from origami tiles. Neither initiator strand cannot access the analyte release process alone. This indicates that molecular release can be indeed triggered by the DNAzyme-based logic gate system.

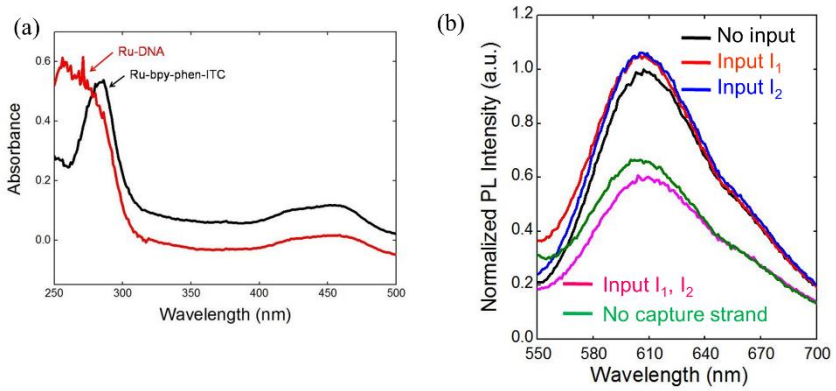

Figure 3.5. (a) Absorbance of Ru-bpy-phen-ITC molecule and DNA-conjugated Ru-dye. The absorbance peak shifts towards 260 nm after conjugation with DNA (b) Normalized PL intensity spectra of Ru-DNA interaction with origami.

With DNA logic gate-based origami capture and release system confirmed by ruthenium, protein can be brought into the system next. Thrombin, a serine protease involved in blood coagulation, is chosen as a model protein.[96] The advantage of using thrombin is because it can be specifically recognized by a 15-nt long DNA strand, which is called thrombin-binding aptamer (TBA).[97] Similar to ruthenium capture, extension strand is added to a staple in the center of each origami tile to bind to TBA domain (Figure 3.4b). Since protein is macro bio-molecule, it can be directly imaged by AFM. Thus, only one modification is applied in each origami. To examine the aptamer binding specificity, capture strand with TBA domain was added into a mixture of thrombin and GST molecules. As described in chapter 3.3.4, thrombin and GST are captured onto DNA origami first. After removal of free proteins, the captured protein was released back into solution and characterized by SDS-PAGE to confirm. Figure 3.6a shows the captured protein molecule on origami at the designed spot. With logic gate strands added, it was then released from the tiles through the logic gate process (Figure 3.6b). In order to confirm exactly which protein was captured on the origami, SDS-PAGE was performed, and clearly only thrombin was left in solution (lane 3) even though both thrombin and GST were added at the beginning (lane 2). This indicates that only thrombin was captured onto origami and released during this process which is proof for the binding specificity of DNA thrombin binding aptamer. It should also be pointed out that the DNAzyme-mediated logic gate is advantageous over using complementary strands to release the target, as it requires a significantly less amount of DNA strands to effectively release bound

analytes.[98,99] It is typical that strand displacement methods use 10-100 times excess amount of invading strands (e.g. complementary strand of TBA) to displace the analytes. In contrast, much fewer DNAzyme strands may be needed for an efficient analyte release. It is found that thrombin could be effectively released at a molar ratio of LGC: analyte = 1:1 (Figure 3.6ab). While the relatively long lower arm (16-nt) of the DNAzyme limited the signal amplification in our experiment, a DNAzyme strand with a shorter lower arm could be as effective at a lower concentration, generating even fewer chemical wastes.

Like thrombin, AuNPs were used as another model analytes to demonstrate our DNAzyme mediated capture and release system. As the DNA origami design in Figure 3.4b, two 10-nm AuNPs are designed to be captured on each origami with one in the middle and the other at the corner. Since DNA signal also has high specificity, with two sets of logic gate strands (S_1, S_2, S_3, I_1, I_2, and C) designed separately to two AuNPs, they can also be captured and released separately without affecting each other (Figure 3.3a and b). After the AuNPs were functionalized with 48-nt thiol-modified DNA strands (see chapter 3.3.3 for details), these two particles are bound onto DNA origami individually with two different capture strands. The sample was then purified with 1.5% agarose gel to eliminate free, unbound AuNPs in the solution. As a clean DNA origami with two captured AuNPs sample got, DNA logic gate strands could be added into the solution to trigger the release. Like the discussion before, the logic gate process could produce S_3 and cleave the capture strands to detach AuNPs from origami. The difference now is that there are two sets of logic gate strands (i.e. A or B, in chapter 3.3.2), and AuNPs could be selectively released whether it is in the middle or at the corner of the tile.

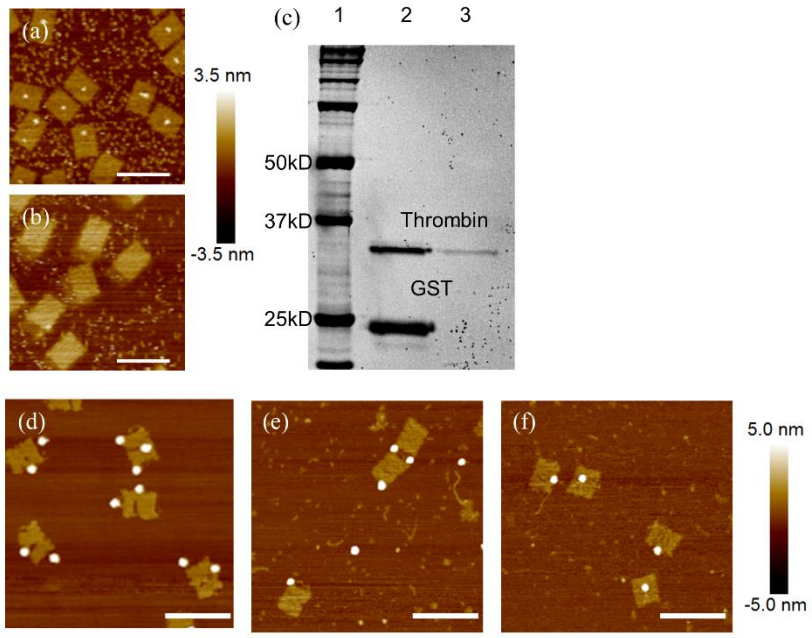

Figure 3.6. (a-b) AFM images of thrombin molecules captured on DNA origamis (a) and thrombin released from origami through DNA logic gate process (b). (c) Denatured SDS-PAGE analysis of thrombin and GST mixture before and after purification by DNA logic gate process. Only thrombin is shown after purification. Lane 1: 100 kD ladder. Lane 2: thrombin and GST mixture at the same concentration (100 nM). Lane 3: mixture purified by DNA logic gate capture and release from DNA origami. (d) AFM image of origami rectangles with both 10-nm AuNPs captured as designed (one at the corner and one at side). (e-f) AFM images of origami rectangles after releasing the AuNP at the side (e) and after releasing the AuNPs at the corner (f). Scale bar: 200 nm.

Figure 3.6d shows the representative AFM image of DNA origami with both AuNPs captured. The following images (Figure 3.6e and f) show the release of one AuNP exclusively at a time. This controlled release was performed by adding logic gate strands set A or B separately since DNAzymes released from two sets cannot recognize each other's target strand, the corresponding AuNP could be saved on origami. This indicates that there is no interference between the two sets of logic gate sequences; the initiators from one logic gate set do not cross-react and trigger the LGC of another logic gate set. It needs to be pointed out that the position of AuNPs in AFM images did not exactly match the positions designed on origami. This could be because the 48-nt capture strand is relatively long. Even though a longer strand could achieve higher capture efficiency, but its position variation may also be larger. Moreover, since only one staple extension was used to capture each AuNP, the linking between DNA origami and AuNP may not be that stable which

means the AuNP could vary more in terms of position. Overall, with the demonstration of capture and release of ruthenium, thrombin, and AuNP, DNA origami and DNA logic gate as a tool to manipulate these analytes has been well studied. These DNA techniques could be very helpful in studying liposomes which will be discussed later in this work.

3.4.3 Light triggered release mechanism

Before changing our focus to other DNA systems, DNA logic gate still has more to improve. One of the most possibilities is to introduce external signals to control DNA logic gate. As discussed in chapter 1, DNA can interact with many kinds of signals including light, pH, heat and more. Here we introduce light signal into our logic gate system by inserting a photocleavable spacer between the toehold overhang and the rest of S_1 (shown as a brown dot in Figure 3.2). Under UV irradiation, the photocleavable spacer is brunt and thus, 12-nt toehold overhang of S_1 will be released (Figure 3.2). Lack of toehold part will dramatically reduce its binding efficiency with I_1 where S_1 cannot dissociate from LGC due to the similar level of free energy between hybridizing with S_1 or not. As a result, the logic gate process could not occur, and the analytes will be retained on origami tile. Before using analytes, PAGE was performed to examine this light-controlled logic gate efficacy (Figure 3.7a). Without introducing UV light, the logic gate process is just the same as previously shown (Figure 3.7a lane 3 versus Figure 3.3a lane 6). However, with UV illumination, the toehold overhang ($S_1 \rightarrow S_1$') is cut off and the new logic gate complex of S_1'/S_2/S_3 keeps intact even in the presence of I_1 and I_2. Thus, S_3/C band is nearly unobservable which indicates that the strand displacement is much slower and less effective without the toehold segment. Further confirmation of the photo-controlled logic gate system was done with AuNPs (Figure 3.7b). Without UV exposure, AuNPs are removed from DNA origami as before when there is no photo-cleavable spacer (Figure 3.7c). In contrast, the particles are retained on the tiles when the spacer is destroyed by UV light, where the whole logic gate process is prohibited (Figure 3.7d).

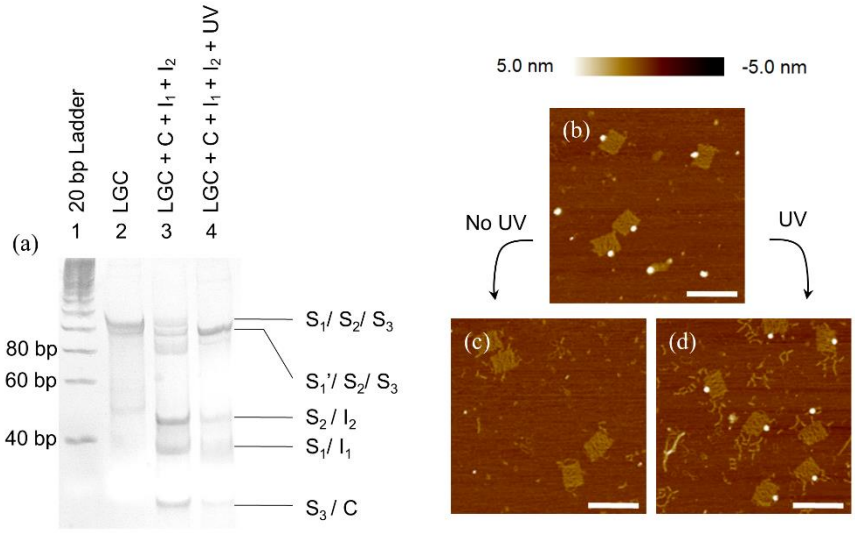

Figure 3.7. (a) 15% native PAGE analysis of the UV irradiation involved DNA logic gate process. Lane 1: 20 bp ladder. Lane 2: LGC. Lane 3: LGC+C+I1+I2. Lane 4: LGC+C+I1+I2+UV. S1': S1 sequence with toehold overhang cut off by UV irradiation. (b) AFM image of DNA origamis capturing AuNPs. (c-d) AFM image of DNA origamis after AuNPs released through logic gate process (c) and no AuNPs released through UV irradiation treated logic gate process (d). Scale bar: 200 nm.

3.5 Conclusion

In this chapter, we have demonstrated DNA origami-based site-specific capture and logic-gate-programmed release with high yield and efficiency (Figure 3.8). This robust DNA platform can be further controlled by external UV irradiation. The same strategy should be applicable to other analytes or extended to other external signals with minimal modifications. It is a demonstration and expansion of using DNA as a tool in this thesis. In the later chapters, DNA will be used extensively on other systems, including DNA origami, DNA strand displacement and logic gate and interaction between DNA strands and external signals. The study performed in this chapter built a solid foundation for further studies of engineering bio-molecules and controlling bio-systems.

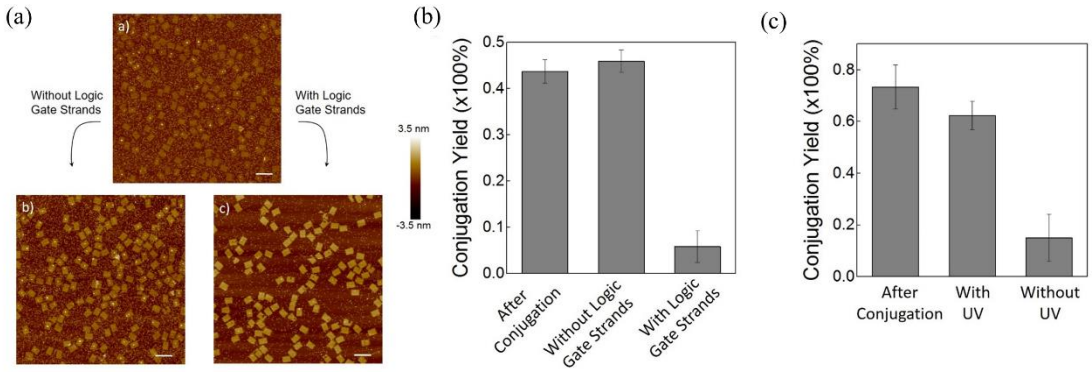

Figure 3.8. (a) Representative large-area view of AFM images for statistical analysis of thrombin release from DNA origami tiles. (b) Statistical analysis of thrombin molecules conjugated on DNA origami tiles based on the examination of more than 500 tiles. (c) Release yield of AuNPs on DNA origami tiles, in the absence and presence of UV light.

4 RELEASE OF DNA DRUG FOR CULTURED CANCER CELL TREATMENT

4.1 Introduction

The base pairing principle gives DNA high specificity and efficiency. As an engineering material, DNA could be used for many mechanical functions like molecular capture and release discussed in the last chapter. We discussed the interactions between DNA and small molecule, protein and nanoparticles earlier where DNA shows its great advantage of manipulating these analytes. In fact, DNA signal can also be used for a larger biological system, *i.e.*, a cell. DNA signals can serve as a drug to kill cancer cells specifically. In order to control DNA delivery to cells, here we introduce a new DNA system called DNA walker.

4.1.1 Carbon nanotube-based DNA walkers

DNA walkers, inspired by intracellular protein motors, are a class of synthetic molecular motors that can move processively along prescribed pathways.[100-102] As we discussed in chapter 1.1.3, a DNA walker is formed with one DNA strand or multiple DNA strands. Usually, a track full of the complementary DNA strands to DNA walker is prepared for DNA walking. The goal is to create a free energy gradient where the walker can move forward spontaneously. Such free energy gradient may be created by addition of fuel strands[103,104] or activity of DNAzymes and restriction enzymes[23,105,106]. Once the walker moves to a lower free energy state, returning it to the initial higher free energy configuration could be done by DNA strand displacement.[107]

Even though DNA walker mechanism and dynamics have been studied extensively, the interaction of DNA walker with other biological systems is relatively limited. Other than the mechanical translocation of nanoparticles with DNA walker[108], other relevant works are not much. One of the interesting ones is discussed earlier (Figure 1.3c) where He and Liu constructed a DNA walker mediated organic synthesis system by exploiting the step-by-step walking process which is a good representation of DNA walker interaction with small molecules.[27] In terms of interaction with other DNA/RNA signals, some sensing work using DNA walker have been done in recent years.[109,110]

In our group, we previously have demonstrated an autonomous DNAzyme-based walker which transports fluorescent QDs along carbon nanotubes (CNTs).[111,112] Kinetics of this DNA walker has been studied that the processivity of the walker can be controlled by metal cation type and concentration in buffer, in addition, DNAzyme sequence and structure will also affect the walker kinetics.[113] These factors will affect DNA association with each other where the mechanism behind is the same as DNA logic gate. Instead of using a particle, an DNA origami or a solid surface, we used a long CNT (a few micrometers) as the DNA walker track. The CNT track provides a relatively long distance which is sufficient for walking kinetics study as well as a 2-D direction movement which simplifies the study.

4.1.2 AS1411 for cancer treatment

Not all DNA sequences can interact with cancer cell efficiently, thus we choose a specific DNA strand called AS1411 (5' – GGT GGT GGT GGT TGT GGT GGT GGT GG – 3'). AS1411 is one of the G-rich oligonucleotides (GROs), which is an anti-proliferative drug toward multiple cancer cell lines at relative low concentrations, while it does not show fatal effects to normal cells at the same concentration level.[114] It can form G-quadruplex structure which is more resistant to nuclease in the cell as well as enhanced cell uptake compared to normal DNA chain. This drug can specifically target and bind to nucleolin, a protein overexpressed on the surface of cancer cells.[115] The AS1411-nucleolin binding may affect cancer cell growth via nucleolin-mediated destabilization of mRNA for B-cell lymphoma 2 (BCL-2) proteins, ultimately resulting in the anti-proliferation of the cells.[116,117] The oligonucleotide drug is currently in phase II clinical trials.

4.1.3 Interaction between DNA walkers and cancer cells

In order to expand our work studying interactions between DNA and other systems, CNT-based DNAzyme walker system and AS1411 oligonucleotide drug are combined as a controlled drug release platform for breast cancer treatment. While DNA walker moves along the CNT track, the anti-cancer drug AS1411 is released from fuel strands as they are decorated onto those fuels. Compared to other DNA walker systems like nanoparticle-based or polymer-based, more factors could be controlled with this design including buffer conditions, light, heat, pH and more importantly, DNAzyme itself and CNT track.[118,119] With integration of these factors, a better solution for drug release control may be presented. The cell used in this work corresponding to

AS1411 is a human breast cancer cell (MCF-7). Using our ability of manipulating DNA systems, walker kinetics can be accurately controlled and so do the cleavage rate and the number of released AS1411, and ultimately stop the proliferation of cancer cells. Furthermore, the collagen extracellular matrix (ECM) was also used to study the real-time interaction between DNA walker system and cell. This will be a more direct study of using DNA signals to control cell growth as MCF-7 cells and DNA walker are cultured together. It turns out that AS1411 based DNA walker system can reduce 40% of MCF-7 growth inside ECM. In contrast, DNA signal has no effect on normal fibroblast cell CCD-1064SK.

4.2 Scheme

Figure 4.1 shows the principle of the DNA walker mediated in-situ drug release platform embedded in the collagen ECM. Here, 10-23 DNAzyme (green) with its strong cleavage ability is used as the walker strand. The cleavage mechanism will be the same as used in DNA logic gate. The DNAzyme is bound on CdTe/CdS QD (orange dot) for better localization purpose while the fuel strand is a little different from previous work where it is consisted of AS1411 sequence (blue) and anchor sequence (navy). The fuel strands on grafted on CNT track where the method is discussed in chapter 2. Once DNAzyme hydrolyzes the rArU site (brown dot) connecting AS1411 and anchor, the cleaved AS1411 will diffuse away. As driven by lower free energy, the DNAzyme upper arm needs to migrate to the next available intact fuel strand along the track. The lower arm will then dissociate with current anchorage and migrates to the next fuel strand, completing the so-called single turnover reaction. This mechanism is the same as we discussed in the first chapter but having specific meaning to the released fuel strand. The AS1411 segment has an extra RNA base on it (5’- GGT GGT GGT GGT TGT GGT GGT GGT GGrA -3’) to make sure it can be cut off by 10-23 DNAzyme. Under the presence of potassium in solution, AS1411 can form dimeric guanine (G) quadruplex. The whole DNA walker system is then incorporated into ECM with MCF-7 cultured on the top for study of the interaction between DNA signal and cell.

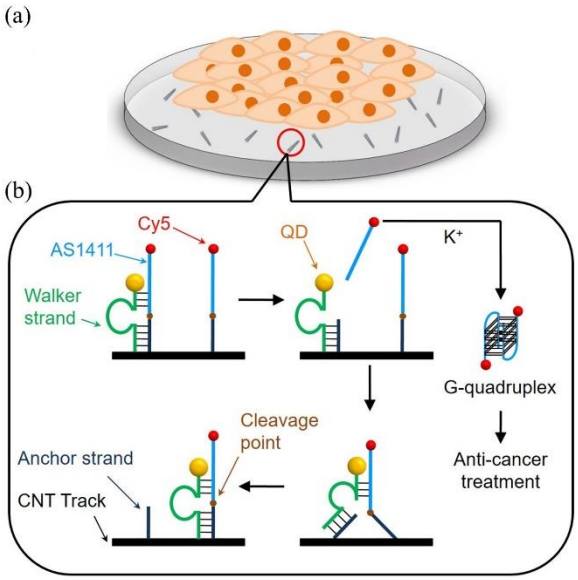

Figure 4.1. (a) DNA walker mediated cancer cell growth anti-proliferation system. Collagen ECM is prepared with DNA walker system embedded, while MCF-7 breast cancer cells are cultured on top of it. (b) Mechanism of DNA walker based AS1411 release system. As the CdTe/CdS QD (orange) conjugated DNAzyme (green) moves along the CNT track (black), anti-cancer oligonucleotide AS1411 (blue) is released from the anchor strand (navy) which can form a dimeric G-quadruplex structure for inhibiting MCF-7 cell growth. A Cy5 dye (red) is labeled on AS1411 for fluorescence measurement.

4.3 Experimental Methods

4.3.1 Materials

Advanced Dulbecco's Modified Eagle Medium/Ham's F-12 (DMEM/F-12) cell culture medium, Rat Tail collagen solution, Trypsin-Ethylenediaminetetraacetic acid (Trypsin-EDTA, 0.05%) and Dulbecco's phosphate-buffered saline (DPBS) are purchased from Fisher Scientific. HiPco carbon nanotubes are purchased from Unidym.

4.3.2 DNA walker measurement

Different from DNA walker measurement in other work, we use visible/near-infrared (NIR) single-particle/single-tube spectroscopy measurement to track DNA walker because both QD and CNT are fluorescent. The details and parameters of this measurement are reported in another publication of our group.[101] Briefly, we use a custom-built inverted, wide-field epi-fluorescence microscope

system (Axio Observer D1, Carl Zeiss) with two laser diodes and two imaging cameras as our imaging platform. CdTe/CdS QDs were visualized by an EMCCD (Andor Technologies iXon3, 512×512 pixels), and NIR emission from CNTs was collected and visualized by an OMA-V 2-D liquid N_2-cooled InGaAs camera (Princeton Instruments, 320×256 pixels). The position of DNA walker on the CNT track was determined by overlaying fluorescence images of QD and CNT.

4.3.3 AS1411 collection in the microfluidic channel

DNA walker system was immobilized inside a hand-made microfluidic channel for released DNA drug collection. First 2% agarose solution was heated to boil and then deposited on a glass slide and wait until dry. Then mixture of pre-assembled DNA walker on CNT samples was placed on top of the agarose film. A coverslip was then placed on top of the film and sealed with double-sided tape. After assembly, 1x TAE buffer was used to flush the channel with a syringe pump (Fusion 100, CHEMYX) until no fluorescence can be found from the output solution. Then, 10 mM extra Mg^{2+} was added into 1x TAE buffer to initialize DNA walking. The buffer was slowly pumped into the channel at a speed of 70 μL/hour. Solution was then collected from the outlet of the channel to determine its fluorescence.

4.3.4 Breast cancer cell culture with anticancer DNA

To prepare the cell culture medium for MCF-7 breast cancer cell, 25 mL FBS, 5 mL L-glutamine, and 5 mL penicillin/streptomycin were added into 500 mL commercial advanced DMEM/F12 culture medium. For CCD-1064SK cells, 50 mL FBS, 5 mL L-glutamine, and 5 mL penicillin/streptomycin were added into 500 mL advanced DMEM/F12 cell culture medium to prepare specific cell culture medium for fibroblast cell.

A 96-well plate was used for cell culture with approximately 60 MCF-7 cells (120 cells in case of CCD-1064SK cells) per well. The cells were incubated in 100 μL cell culture medium from last step for 24 hours in a cell incubator (at 37 °C in 5% CO_2 environment) first. The medium was then replaced by AS1411 included cell culture medium. The replacement of this new cell culture medium was performed every 24 hours for 4 consecutive days before cell imaging and counting.[120]

4.3.5 Walker system embedded in ECM for cancer cell treatment

Preparation of collagen ECM

Collagen ECM was prepared by mixing 358 μL 8.68 mg/mL rat tail collagen solution with 100 μL 10× PBS, 30 μL 0.1 M HEPES, 8.2 μL sterile 1.0 N NaOH, 1 μL penicillin-streptomycin, 10 μL L-Glutamine, 10 μL 1 M $MgCl_2$, 60 μL FBS and extra sterile H_2O to 1 mL mixture.

In order to incorporate walker/track samples into the collagen ECM, the aqueous solution, part of the sterile water was replaced by 100 μL of CNTs coated with 500 nM fuel strands and 1 μL of 1 M DNAzyme samples. During preparation, the mixture should be placed on an ice-bath and then transferred onto a Petri dish (MatTek Corp.) upon finishing. With 30-minute incubation in an incubator, collagen could be polymerized and then the Petri dish was placed under UV light for sterilization for 1 hour before cell culture.

Cell culture on collagen ECM

Approximately 4,000 cells were loaded onto the top of the polymerized collagen and incubated with 1 mL cell culture medium. Like the previous description, the medium was replaced every 24 hours for consecutive 5 days. Fluorescence images of the cells were obtained to evaluate the viability and drug efficacy.

4.3.6 Cell imaging and counting

Cell viability could be evaluated by Hoechst dye which is a common dye used for staining live cells.[121] To perform staining, cell culture medium was replaced with 1 mL DPBS solution containing 10 ug/mL Hoechst dye and incubated for 30 minutes in the cell incubator. After incubation, each well was washed once by DPBS solution to remove free dyes and an additional 100 μL DPBS solution was added for optical imaging.

Optical fluorescence imaging was performed using an Olympus IX71 microscope with a 10× objective lens. ImageJ was used to process fluorescence images to evaluate cell viability. Cell viability was determined by calculating the ratio of the area covered by AS1411-treated cells to the area covered by control cells.

To evaluate the cytotoxicity on ECM, a similar method was used. Typically, 10-12 fluorescence images were taken in each Petri dish to get more accurate results. Student's t-test was performed based on two sets of data collected to determine its statistical significance.

4.4 Results and Discussion

4.4.1 DNA walker characterization

To demonstrate DNA signal interaction with cell system, proof of DNA walker is the prerequisite. To show DNA translocation, DNAzyme based DNA walker with QD was immobilized and placed onto a CNT track full of DNA fuel strands.[111] Visible and NIR images were taken separately for QD and CNT in their respective spectral range. In our custom-built inverted microscope, an electron-multiplying charge-coupled device (EMCCD) was used to measure the fluorescence from visible QD while a 2D InGaAs photodiode array was recording the near-infrared CNT emission. DNA translocation was monitored as shown in Figure 4.2a with the fluorescence of QD (red dot) moves along the stationary CNT on the surface. The time interval between each measurement is 2 hours in order to make sure the detectable travel distance of DNA walker on CNT track. As the requirement for DNAzyme to perform cleavage, 10 mM Mg^{2+} was added to 1x TAE buffer to serve as the working buffer. After 6 hours, the DNA walker has traveled around 700 nm which leads to a speed of ~110 nm/hr. Single turnover reaction rate could also be determined based on the speed calculated and the distance between two neighboring fuel strands (~3.5 nm). It characterizes the speed of DNA walker moving from one fuel strand to the next fuel strand, in this design, the single turnover reaction rate is 8.9×10^{-3} s^{-1}.[113]

In order to generalize the walking kinetics, single turnover reaction rate of DNA walker is further confirmed by ensemble measurement. By immobilizing CNT based DNA walker system in a microfluidic channel (Figure 4.2b) and decorating the fuel strand with Cy5 dye (Figure 4.1b) for fluorescence measurement, an ensemble DNA walker moving speed or single turnover reaction rate can be determined. Mg^{2+} included 1x TAE buffer was flushed into the channel at a flowrate of ~67 μL/hour. It should be pointed out that this low flowrate has been proven not affecting the walker operation significantly.[111] The walking continues for 3 hours and solution was collected at outlet. PL intensity of the solution was determined, and the amount of released fuel strands can

further be calculated. With the number of fuel strands and walking time, single turnover reaction rate is 9.2×10^{-3} s^{-1} using the same calculation method for single-particle tracking. The similarity of these two single turnover rates indicates the robustness of DNA walker system (Figure 4.2c).

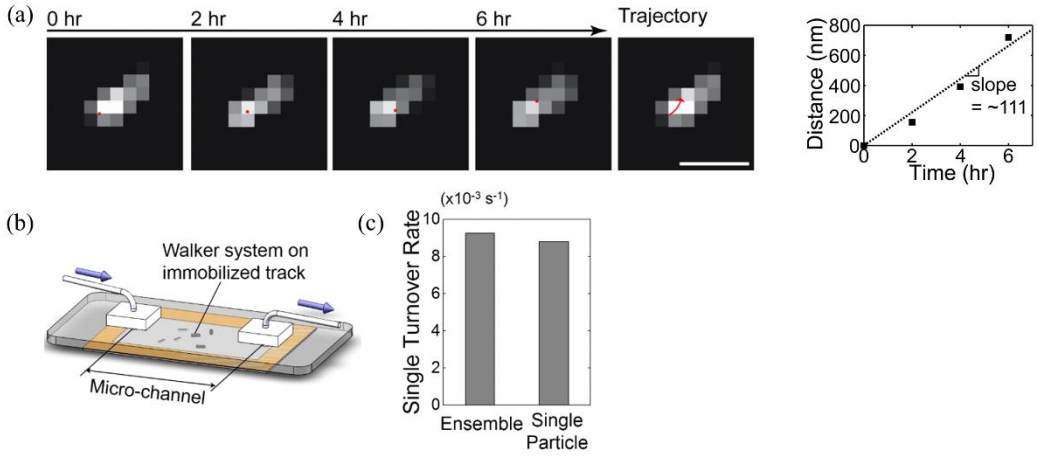

Figure 4.2. (a) Fluorescence images of translocation of the DNAzyme walker. The CdTe/CdS QD and CNT track are used as visible and near-infrared fluorophores, respectively. The red dot indicates the DNAzyme walker. It moves on the immobilized CNT track over a 6-hour period in standard TAE buffer with 10 mM Mg^{2+} with the trajectory represented by the red arrow. The speed of the walker is approximately 110 nm/hr. (b) Schematic of ensemble DNA walker release experiment. The DNA walker system is deposited on an agarose film to immobilized inside the channel. The channel is flushed with TAE buffer with 10 mM Mg^{2+} at room temperature to trigger DNA walking and released AS1411 strands are collected at the outlet. (c) Single turnover reaction rates calculated from a single (a) and ensemble (b) motor measurements.

4.4.2 Collection of released DNA strands

The demonstration of DNA walker system was performed in 10 mM Mg^{2+} buffer. As we mentioned multiple times before, one of the reasons we chose DNA to be the signal to interact with other systems is because of its controllability by external signals. Here Mg^{2+} concentration is also an important factor that we use extensively for DNA control. To test the effect of different Mg^{2+} concentration (Figure 4.3a and b) same DNA walker experiment in microfluidic channel was done but with different Mg^{2+} concentration. As expected, no fuel strand could be released if no Mg^{2+} was present in solution, and compared to 5 mM Mg^{2+}, 10 mM can release a twice greater amount of fuel strands from CNT track. Since DNA walker will be cultured together with cell eventually as the experiment goal, DNA walker release in the cell culture medium (Advanced DMEM/F12) was also examined. Without any addition, the medium only contains 1 mM Mg^{2+},

which is not enough for DNA walking. Thus, the Mg^{2+} level was made up to 10 mM by adding additional Mg^{2+} solution. Similar Cy5 PL intensity was found with cell culture medium which indicates that DNA walker system was not affected by other components in cell culture medium. These results suggest that DNAzyme based walkers can function well in cell culture environment and serve as an AS1411 release platform.

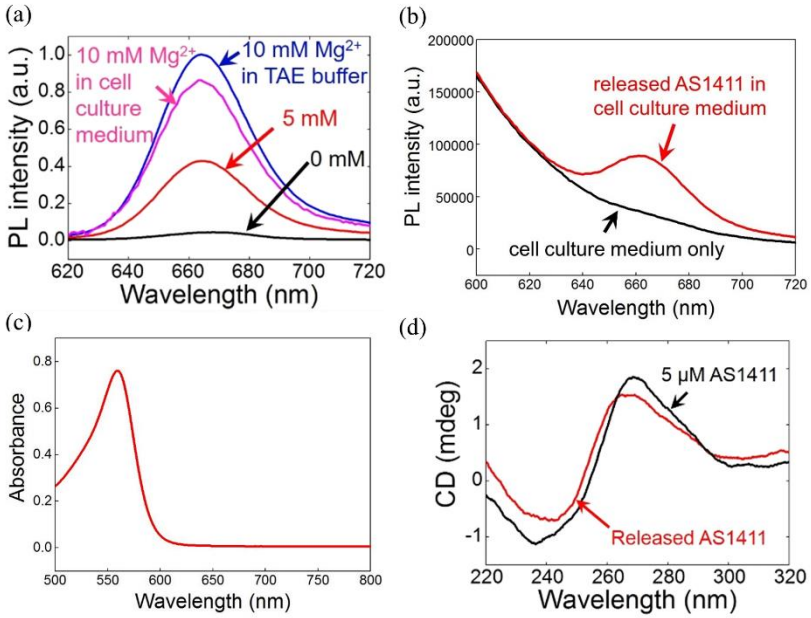

Figure 4.3. (a) PL spectra of Cy5-labelled AS1411 strands collected, which represents the relation between DNA walking speed as a function of Mg^{2+} concentration in 1xTAE buffer (blue, red, black). The pink curve indicates the DNA walking in cell culture medium with 10 mM Mg^{2+}. (b) PL spectra of cell culture medium (black) and collected AS1411 in cell culture medium (red). To obtain the PL spectrum of AS1411 (pink curve in a), the black curve was subtracted from the red. (c) Absorbance of cell culture medium. No significant absorbance above 600 nm is found indicating cell culture medium will not affect Cy5 measurement. The peak around 550 nm should be the absorbance of phenol red in cell culture medium. (d) Circular dichroism spectra of DNA walker-released and synthesized AS1411 strands in the presence of 10 mM K^+ indicating the formation of G-quadruplex structure.

Another important thing to confirm before introducing DNA walker into cell culture is the function of released strand. Synthesized AS1411 strand forms a dimeric G-quadruplex structure (Figure 4.1b) in the presence of 50 mM K^+. This secondary conformation was the key to maintain AS1411 anti-proliferation effect.[122,123] Because this structure has different absorption for left- and right-handed circularly polarized light, the circular dichroism (CD) could be a perfect tool for the test. From CD measurement of synthesized AS1411, we can find a peak at ~265 nm and a valley at

~240 nm (Figure 4.3d) which is a feature characterization for G-quartet conformation. To show the same function of released AS1411 from DNA walker in cell culture medium as the synthesized AS1411 sequences, both CD absorbance are measured. It clearly shows that AS1411 released from DNA walker could also maintain G-quartet conformation.

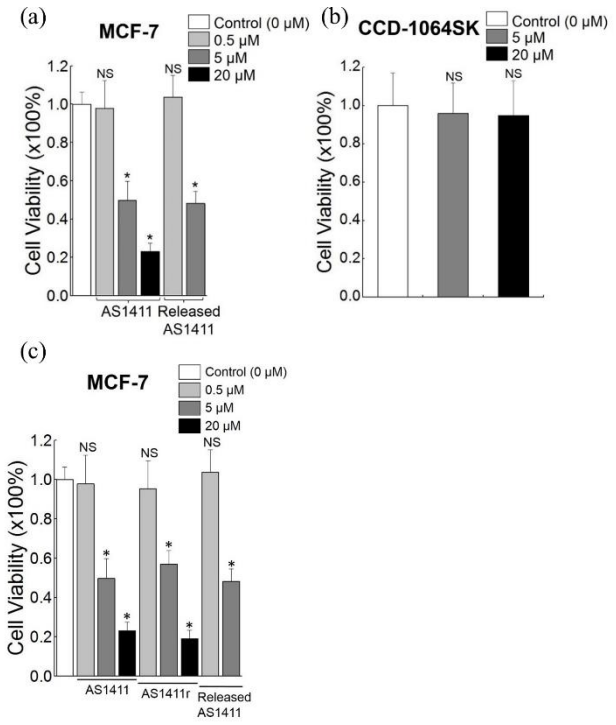

Figure 4.4. (a) Viability of MCF-7 breast cancer cells after treating by released and synthesized AS1411 strands. Cells with no drug treatment is evaluated as control. (b) Viability of CCD-1064SK normal fibroblast cells after 96-hour incubation with synthesized AS1411. (c) Viability of MCF-7 cells after 96-hour incubation with AS1411 strands with extensions. The efficacy of synthesized AS1411, synthesized AS1411r (AS1411 strand with an extra RNA base) and released AS1411 strands are compared. It turns out that the cytotoxicity level of released AS1411 and AS1411/AS1411r is similar, so the additional base (rA) of AS1411r and released AS1411 does not affect the cytotoxicity significantly.

4.4.3 Effectiveness of released AS1411 strands

Even the structure of AS1411 can be maintained after released in cell culture, its anti-proliferation function to cancer cell still needs to be proved. To do that, released and synthesized AS1411 were collected and cultured together with MCF-7 cells for 4 days (see methods for details). From the cell viability data in Figure 4.4a, it can be found that statistically there are almost no differences in cell viability between released AS1411 treated cell and synthesized AS1411 treated cell. Both

at 0.5 μM and 5 μM, AS1411 strands reduce MCF-7 cell viability by 5% and 50% respectively. It indicates that the additional RNA base (rA) in released AS1411 does not affect its efficacy. More controls were performed with synthesized AS1411 strands with an extra rA base, and this sample also shows similar level of cytotoxicity.

To examine the specificity of the sequence, same level of AS1411 dosage was also cultured with normal fibroblast CCD-1064SK cells. Almost no cytotoxicity found at 5 μM AS1411 and even 20 μM which represents the non-toxicity of AS1411 to fibroblast cells (Figure 4.4b).

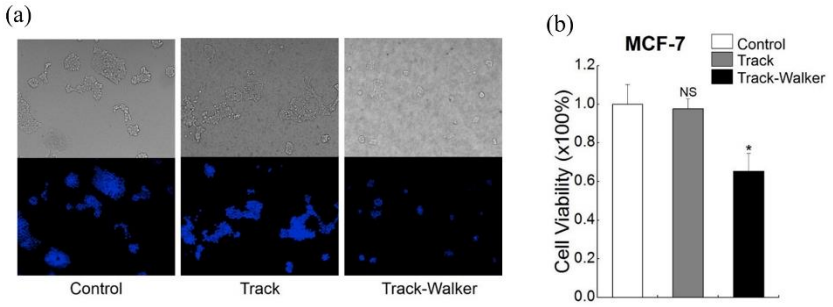

Figure 4.5. (a) Bright-field (top) and fluorescence (bottom) images of MCF-7 cells on collagen ECM after 120-hour culture with the treatment of different conditions. The area of blue fluorescence indicates the number of live cells under that experiment condition. (b) Viability of MCF-7 cells on collagen ECM after 120-hour culture. NS: not significant; *: p-value < 0.05. The cell viability is determined by comparing the blue area in (a) while the area under control experiment condition is set as 1 for cell viability.

4.4.4 Anti-proliferation of cancer cells by DNA walker system

With all previous proof of successful release of AS1411 from DNA walker and maintained AS1411 function after released, the DNA walker system was then explored in collagen ECM, to study real-time DNA interaction with cells which is also closer to *in vivo* tumor microenvironment. Here the DNA walker was mixed with unpolymerized collagen first and when collagen got polymerized, DNA walker system would be embedded into the ECM matrix. MCF-7 cell was cultured on top of ECM to avoid the possible cytotoxicity of CNT. Since whether CNT has cytotoxicity is still a controversial topic, here we choose to avoid the uncertainty.[124-127] Control experiments where only CNT with fuel strands are inside collagen ECM or buffer only in ECM were done to set the baseline of cell viability. Since no AS1411 could be released under these two circumstances, cell viability should be at a high level. The results were shown in Figure 4.5a with the bright-field image (top-row) of cells and blue fluorescence image (bottom-row) of cells stained

by Hoechst dye. The decrease of number of MCF-7 cells (blue area covered by cells) only happens in DNA-walker-embedded collagen ECM which indicates the AS1411 release from DNA walker as expected. Statistical analysis is performed as Figure 4.5b shows. It shows that significantly lower viability of MCF-7 cells exposed to the released AS1411 which is only at 60% compared to cells in the control environment. In contrast, there is a very limited statistical difference of viability between the cells cultured on the ECM with AS1411-decorated CNT tracks alone (i.e. without walkers) and cells cultured on ECM with buffer only. The total amount of AS1411 strands was estimated to be roughly 5 μM based on the amount of CNT and fuel strands associated. Compared to cell culturing with 5 μM released AS1411, the cell viability is slightly higher under this experiment condition. The difference may come from the different experimental setup and more importantly, drug amount. Here, drug was continuously released into ECM during the 5 days cell culture. However, in the previous experiment, cell culture with AS1411 was refreshed every 24 hours. This makes a big difference to the actual drug amount taken by the cells and thus will affect the cell viability. In fact, the purpose of introducing DNA walker system to ECM is to study the real-time DNA signal interaction with cell system, which has a totally different meaning compared to studying the anti-proliferation effect of released AS1411 by DNA walker system. So, the numbers here are not comparable with each other.

4.4.5 Effect of carbon nanotubes on cell viability

Before closing this chapter, I would like to extend the discussion of the cytotoxicity of carbon nanotube a little bit. Cytotoxicity of carbon nanotubes has been a very popular topic in the past decade. Based on its chemical and mechanical properties, CNT has always been a good candidate for biological applications like drug delivery shuttle, bio-sensor or novel bio-materials. However, its cytotoxicity has been unclear all the time. Scientists have opposite opinions on cytotoxicity of CNT and both have done numerous research works to support them. In this work, though the study of cytotoxicity of CNT is not the main target, we are still able to make some judgments based on the experiment results. From Figure 4.5, it is shown that with CNT embedded into the ECM, the cell viability is not different from the cells with no CNT involved. Since adding CNT or not is the only difference between these two experiments, the bio-safety of CNT in this experiment should be valid. With no direct interaction, it seems CNT is not affecting cell viability.

4.5 Conclusion

In summary, in this chapter, still using DNA as the engineering material, a DNA-walker-mediated platform that inhibits cancer cell growth is created. This takes us one step further of using DNA as a tool since now DNA is shown to be able to interact with cell systems. The culture of DNA walker inside collagen ECM also indicates the dynamic interaction between cell and DNA based systems. In addition, the use of AS1411 oligonucleotides also expands the possibility of our research. Other than molecular capture and release, DNA aptamer sequences can also be used for cell anti-proliferation. Moreover, given the robustness of DNA walker platform, it may be extended for treatment of other cancer cell lines with appropriate drugs either by DNA aptamer or molecules attachment.[128] For this work, we envision that additional regulating mechanisms could be introduced into the system like external photo-irradiation or environmental changes, where a unique powerful molecular regulating system could be produced later. For this thesis, we have already studied DNA functionality extensively by using its base-pairing hybridization and sequence-specific aptamer effect. As a mechanical engineer, the mechanical properties of DNA strands are also important to study. Thus, in the next chapter, we will bring in a new system called motor protein systems to study the mechanical properties of DNA and their interactions with motor proteins.

5 DIRECTION CHANGE OF SURFACE GLIDING MICROTUBULES WITH DNA

5.1 Introduction

In previous chapters, DNA has been used as an engineering material for chemical and biological applications based on its properties. The interaction of DNA signal with other systems has been explored. However, as an engineering material, its mechanical property is another important factor that needs to be characterized. Here we introduce motor protein systems into this work. By using immobilized DNA molecules changing microtubule moving direction, the mechanical property of DNA strand could be studied.

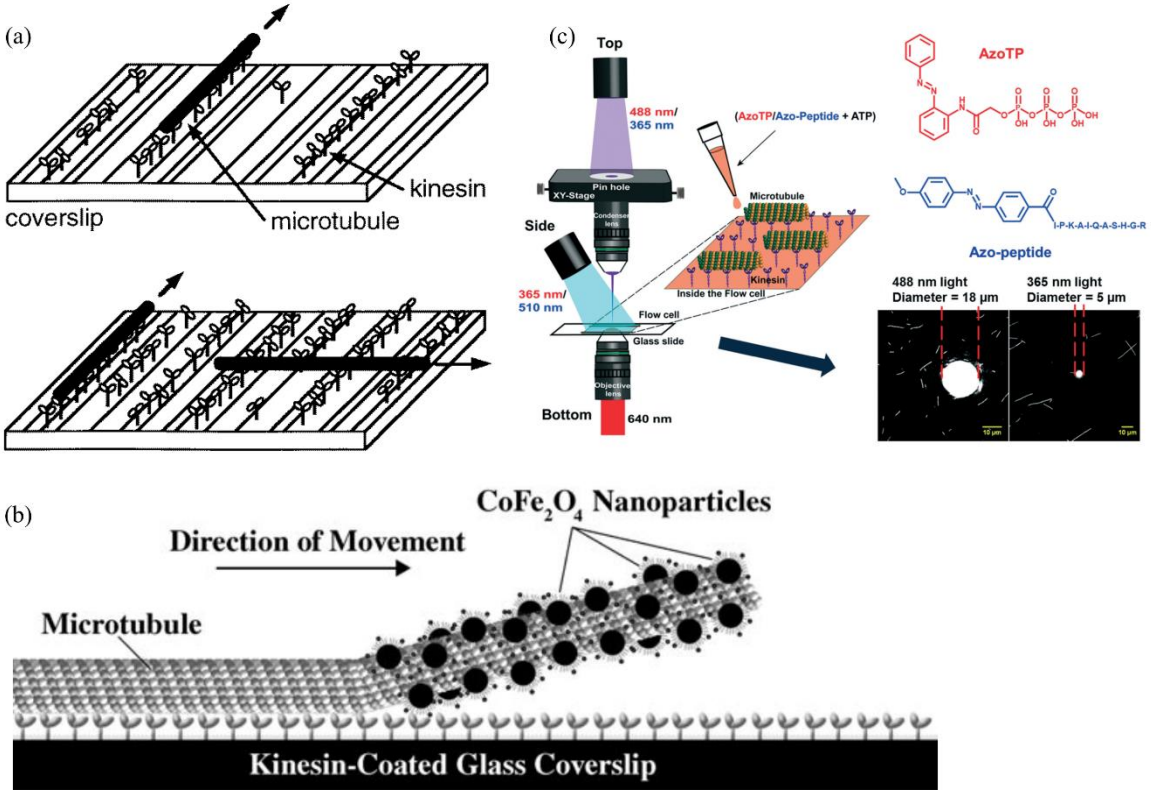

Figure 5.1. (a) Microtubule gliding direction control by kinesin placement. Kinesin molecules are coated on designed microfluidic channel and microtubules can only move on kinesin coated area.[129] (b) Microtubule gliding direction change controlled by the magnetic field. Cobalt iron oxide ($CoFe_2O_4$) particles are coated on the leading part of the microtubule. When the magnetic field changes, the direction of microtubule gliding can be changed too.[130] (c) Photocontrol of microtubule gliding. With shining UV and visible light respectively, microtubule gliding can be stopped and activated. Thus, the gliding of microtubules can be controlled by the light signal.[131]

As discussed in chapter 1, there are mainly three types of motor proteins, while in this work, we choose to use kinesin-microtubule motor protein, since they have been studied the most and they can interact with DNA easily. Despite microtubules are important cytoskeleton proteins in a cell which are important for cellular activities such as mitosis, intracellular trafficking, and cell division, here microtubule is used for its motility. One way to engineer this in vitro translocation is to immobilize kinesins onto a surface and with ATP molecules in solution, kinesins will 'walk' on microtubules. Since kinesins are immobilized, microtubule instead, will glide on the surface or so-termed gliding or motility assay.[132-136]

Motility assay itself can also interact with different signals for certain applications like molecular cargo transport, analyte detection, and a combination of both[137-139] as shown in Figure 5.1. Similar as DNA system, good control of motility assay especially velocity and direction, is the key to make it adaptive in broader systems as different engineering applications could take advantage of microtubule motility assay.[140,141] Translocation velocity can be easily controlled by varying concentration of ATP, density of kinesin[142], temperature[143], buffer pH, external field including electrical field[144] and light irradiation[145-147] or combinations of these factors[148]. In contrast, methods to control moving direction are relatively limited. The most obvious method is to selectively place kinesin on microfluidic channels where specific micrometer-level pattern has been created[149-151] or chemical modification[152] has been done on it. Other than that, direction controlling by external field is also a popular method including electrical field[45,153,154] and flow field[155,156] associated physical model studies[157,158]. In addition, the magnetic field could also be used to direct microtubule gliding if magnetic nanoparticles are functionalized on them[130,159-161]. All these methods are effective, but they cannot control the direction of a single microtubule as either external field or kinesin pattern applies to all microtubules termed as ensemble method. On the contrary, a local method that affects only one microtubule at a time should be developed. As we discussed in the previous chapters, DNA is a great tool in signaling, both to specific object (DNA logic gate), or affecting the whole system (cancer cell anti-proliferation). Thus, with introducing DNA into motor protein system, it is possible for us to solve the problem. In the meantime, the interaction between DNA and microtubules could be more than a biological or chemical reaction, but there will be mechanical interaction involved as microtubules mechanical motion has been affected. This becomes a great opportunity for us to expand the application of

DNA signal further, so a DNA based method to locally control microtubule gliding direction without external field or complex track designs need to be explored.

In this chapter, we introduce an approach that use DNA as a tool to actively change microtubule gliding direction. The interaction between DNA and microtubules has been widely studied for microtubules connecting or microtubule-surface interaction[162-165], while in this work, DNA is not used as a connector or a cargo[166], instead, it is used as a capture arm. Biotin-streptavidin system is incorporated into the system for linking DNA and microtubule. The focus of this work is to use the force exerted by splitting a double-stranded DNA (dsDNA) to redirect microtubule moving direction. The dsDNA decorated with streptavidin will first be associated on an immobilized nanoparticle when a biotinylated microtubule is in the proximity, the microtubule will be captured by dsDNA strand via biotin-streptavidin interaction and change its moving direction. Our physical model reveals that the outgoing angle of redirected microtubules is determined by the interplay between the dsDNA unzipping force (pulling force) and collective kinesin forces exerted on the microtubule. The direction of microtubules gliding will change approximately 10° on average with respect to their incoming angles. When no streptavidin is attached on a dsDNA capture arm, no significant angular change could be found other than a Brownian-type random redistribution (i.e. normal distribution centered at 0°). A traditional gliding assay without DNA-particle involved will also follow this distribution on their gliding angle change. However, if DNA is not introduced into the system, with streptavidin directly on the particle, instead of being a direction change center, the particle will then either stop the microtubule passing by or be dragged away by the microtubules.

To further study the difference and advantage of using DNA into this system, compared to other ensemble methods, we also developed mathematical models for both cases. For the microtubule direction change by using crossflow[167,168] and for the DNA based microtubule gliding direction change, two different models are developed and compared with experimental data. Under crossflow condition, flow speed, kinesin density, gliding speed, and initial direction together determine the time needed to align microtubules with flow direction while in DN-particle based local scheme for microtubule direction change where no flow associated, microtubule gliding speed, kinesin force, and DNA dissociation forces play important roles.

5.2 Scheme

Figure 5.2 illustrates the overall design of local direction change of gliding microtubules. The immobilized polystyrene particle (black) sits on the coverslip surface via non-specific adsorption. DNA signals are introduced as double helices (dsDNA, blue and green) which are covalently linked to the particle. In order to interact with biotinylated (yellow) microtubules, a streptavidin molecule (red) is attached to the end of each dsDNA (Figure 5.2 left). When a microtubule (grey) moves within the effective distance of DNA strands, the streptavidin on DNA and the biotin on microtubule will form a tight conjugation (Figure 5.2 middle). Because of the strong binding force, DNA arm will pull microtubules in a different direction compared to its moving and force it to change (Figure 5.2 right). As microtubule keeps moving forward, the hybridization between dsDNA will break as the unzipping force of dsDNA much smaller than the force generated by kinesins and the direction change of one microtubule gliding is completed.

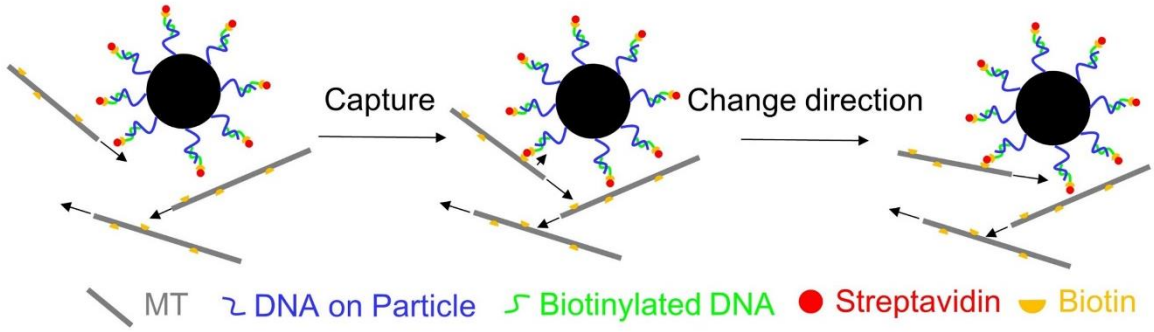

Figure 5.2. Schematic of DNA-nanoparticle based microtubule gliding direction change. Through non-specific binding, the DNA-particle (black) is immobilized on coverslip surface. One type of DNA sequence (blue) is coated on the particle, and its complementary strands (green) with a biotin-streptavidin conjugate at the end are hybridizing with the strand. Black arrows indicate the moving direction of microtubules. Once a microtubule moves in close proximity of DNA-particle, the streptavidin molecule can bind with the biotinylated microtubule, pulling and thus redirecting the microtubule.

5.3 Experimental Methods

5.3.1 Materials

Polystyrene particles with an average 200 nm diameter were obtained from Invitrogen (F8807). Gliding assay related materials including biotinylated tubulin (T333P), Hilyte dye-labeled tubulin (TL670M), kinesin (KF01, motor domain of human KIF3C, 73 kD), paclitaxel (TXD01), and

BRB80 buffer (BST01 and BST05) were all purchased from Cytoskeleton. Streptavidin was acquired from Prospec (PRO-283).

5.3.2 Preparation and characterization of particle-DNA

Association of DNA and streptavidin

DNA and streptavidin are linked based on biotin-streptavidin conjugation. First, 10 times more biotin-labeled complementary DNA (5' –/biotin/ TTT TTT TTT TGC CCC TTA ACT CCC ACG ACT AAG CCT GAC CGA TGC – 3') were mixed with 10 nM conjugated particles with ssDNA (5' – /amine/ TTT TTT TTT TTT TTT ATC GGT CAG GCT TAG TCG TG – 3') (methods described in Chapter 2.2.1). In addition, 1 μM streptavidin was also added into the solution and extra TAEM buffer was added to make a 100 μL solution. DNA strands were left for hybridization for 2 hours at room temperature they were purified by centrifuge. The mixture was washed 3 times by centrifuge (20,000g, 30 minutes) to remove unbound DNA strands and free streptavidin. Precipitate from each centrifugation was kept and dissolved in 200 μL 1x PBS buffer while the supernatant where free DNA was in was discarded. This purified particle with dsDNA/streptavidin was ready to use for the experiment. To prepare a sample of particles with DNA strands but no streptavidin, the same preparation method was done just without streptavidin added in between. This sample was used as a control to the DNA-particle with streptavidin.

DNA-Particle Measurement

Absorbance of DNA was used to estimate the number of DNA strands per 200 nm polystyrene particle. DNA has an absorbance peak at 260 nm with an extinction coefficient of $3x10^5$ $M^{-1}cm^{-1}$. The extinction coefficient of polystyrene particle is approximately ~$2x10^9$ $M^{-1}cm^{-1}$ at 660 nm. The particle and DNA concentrations were determined respectively based on the absorbance value at 660 nm and 260 nm. The DNA-to-particle ratio could then be determined from the concentration ratio given the assumption that DNA was distributed uniformly among the particles. The DNA density on the particle was found to be 1 DNA per ~30 nm^2, which corresponds to roughly 4000 DNA strands per polystyrene particle. This result is similar compared to DNA density in other reports [169].

5.3.3 Microtubule direction change with particle-DNA

The DNA-particles conjugated with streptavidin in 1x PBS buffer from previous preparation were flowed into the microfluidic channel for incubation until there were approximately 50 particles within a 100-μm x 100-μm area. PBS buffer was then flushed through the channel to wash away unbound DNA-particles. After this surface decoration with particles, standard microtubule motility assay preparation was done by adding kinesins, caseins, and microtubules sequentially as described in chapter 2. For control experiments, DNA-particles without streptavidin was used instead of the streptavidin ones.

5.3.4 Localization of fluorescent nanoparticles

Because of diffraction limit and strong fluorescence, 200 nm polystyrene could occupy several micrometer areas under the fluorescence microscope. In order to locate the accurate position of each particle by overcoming the optical diffraction limit, image processing to generate super-resolution images is executed. Around 100 raw images of particles with 10 s intervals were taken and used as inputs. After removing background noise using background subtraction from ImageJ, peak fit of single-molecule light microscopy (SMLM) tool was applied to localize each particle. The position of a particle in a series of images were fitted by a gaussian function and the localized center position of the particle was calculated. Coordinates of the particle position were calculated to indicate the exact position of the particles. Same processing was done to the rest polystyrene particles and a plot of localized particles was drawn.

5.3.5 Kinesin density on the surface

As an important factor in microtubule gliding direction change, kinesin density on the surface was characterized by using antibody targeting glutathione (anti-GST-antibody) conjugated with AlexaFluor647 fluorophore from Thermo Fisher Scientific Inc. Since there is a GST moiety on kinesin, this conjugate can target at kinesins on the surface. After depositing kinesin and casein molecules on the coverslip surface, approximately 10 nM AlexaFluor647 conjugate with anti-GST antibody was filled the channel. The PL intensity on the surface was measured on a time basis and the kinesin density was finally determined as ~80 μm^{-2} (Figure 5.3). For simplicity, n_s = 100 μm^{-2} or $\sqrt{n_s}$ = 10 μm^{-1} are used in the theoretical calculations. Control experiment was done by covering the surface with casein only.

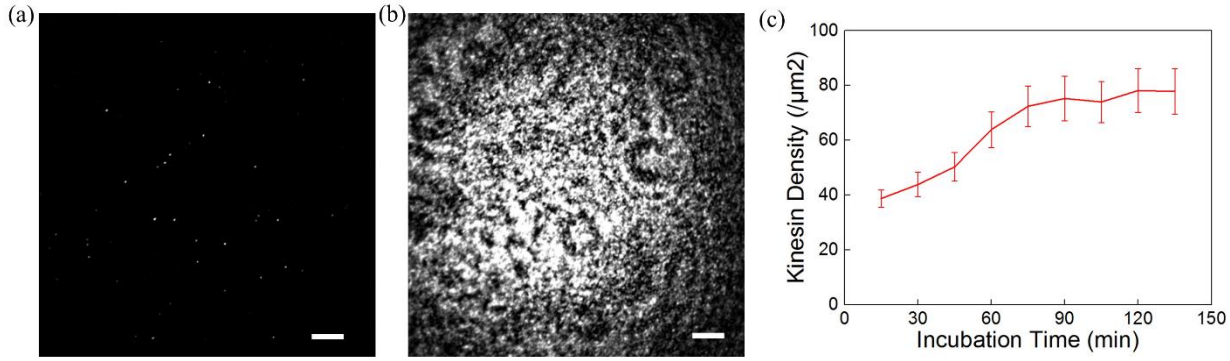

Figure 5.3. Kinesin density characterization. (a) A kinesin coated coverslip glass surface was incubated with 10 pM anti-GST tag antibody, Alexa Fluor 647 conjugate (alexa647). Each dot represents a kinesin molecule and its intensity is around 630 (arbitrary unit). (b) Same kinesin coated surface was incubated with 10 nM alexa647. Overall intensity is around 60,000/μm^2 on average. The kinesin density is calculated around 80/μm^2. (c) The fluorescence intensity (kinesin density measured) increases as alexa647 was incubated longer on surface. Eventually, the kinesin density measured is approaching 80/μm^2. Scale bars are 10 μm for both images.

5.4 Model Development

5.4.1 Modeling of DNA-particle based microtubule gliding direction change

Typically for a microtubule on a channel surface, four different types of forces apply on it: gravity, van der Waals, drag and lift forces. However, rest three forces are all in vertical direction which is not related to our analysis, only drag force is considered. Here, the drag force is eliminated from the system because DNA-particle is immobilized on surface statically. So other than the channel environment, forces are mainly from the components inside the channel. Theoretically, when a biotinylated microtubule is close to an immobilized DNA-particle with streptavidin attached, the particle will interact with the microtubule through the binding between dsDNA-streptavidin capture arm and biotin groups on the microtubule. If the microtubule is moving towards a different direction compared to the DNA-particle pulling force, it will be forced to take a circular type motion as illustrated in Figure 5.4. Correspondingly, its moving direction will change θ degrees during this circular motion around the DNA-particle. More specifically, if the microtubule has an incoming angle φ when it moves close to the particle (the angle with respect to the dashed line in Figure 5.4a), the outcoming angle of microtubule will be θ+ φ degrees. By studying the components of this system, there are three main forces applied on the microtubule during this process: the dragging force generated by kinesin ($F_{kinesin}$), the pulling force exerted by

biotin/streptavidin interaction or dsDNA hybridization (F_{pull}), and the centrifugal force generated from the circular motion ($F_{centrifugal}$). During this process, the force balance equation can be written as

$$F_{kinesin}\sin(\theta+\varphi)+F_{centrifugal}=F_{pull} \qquad \text{Eq.1}$$

Based on other studies, kinesins can change the force it exerts to maintain the motion of microtubules if the external force applied on microtubules change, with maximum a from kinesin ~7 pN/kinesin [170,171].

On the right side of the equation, F_{pull} is determined by dissociation of DNA strands and streptavidin-biotin conjugation, whichever is smaller, because the smaller one will limit the pulling force applied on a microtubule. It is able to find that around 12 pN is needed to unzip a dsDNA helix with similar length in this work, while the force needed to detach biotin and streptavidin conjugation is greater than 100 pN [172-175]. Thus, F_{pull} in our experiment should be the dsDNA duplex unzipping force which is ~12 pN.

The centrifugal force can be calculated from the radius of circular motion and the velocity of microtubule gliding, which is

$$F_{centrifuagl}=m\frac{v^2}{R} \qquad \text{Eq.2}$$

where m is microtubule mass, v is the velocity of gliding microtubule, and R is the radius of microtubule's circular motion which is considered as the length of dsDNA-streptavidin/biotin linking the particle and microtubules.

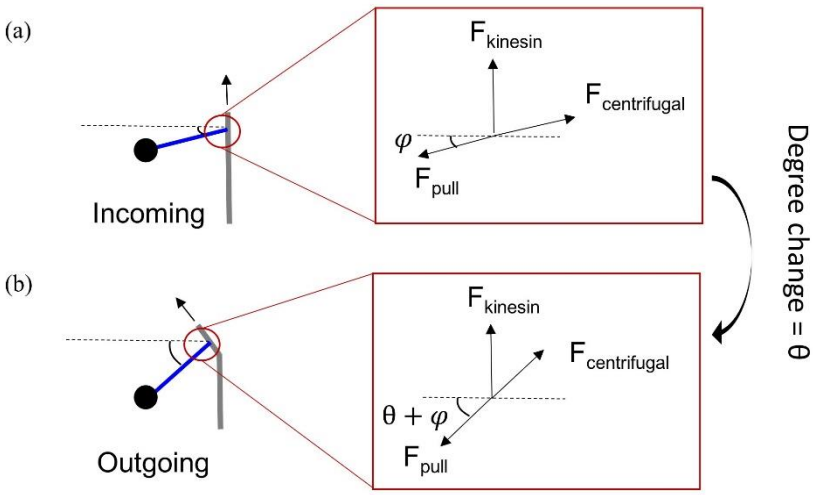

Figure 5.4. Physical model of DNA-particle based local direction changes of gliding microtubules. The black circle is the center of circular motion which indicates the immobilized particle, and the blue rod represents the capture arm (dsDNA/streptavidin). (a) Before a microtubule interacts with the DNA-particle, when it moves close, with an incoming angle φ with respect to dashed reference line, the force balance is shown as indicated. (b) After the microtubule has changed θ degrees in its moving direction, the rod is about to break (unzipping of dsDNA). Kinesin force keeps its direction as the majority part of microtubule follows the original direction, and centrifugal and pulling force have changed their direction. Based on the new force balance, degree change θ can be calculated.

There are approximately 1650 tubulin dimers per 1-μm microtubule from the studies of its polymerization dynamics [176]. The mass of a 1-μm microtubule is calculated to be ~3×10^{-19} kg/μm given the molecular weight of one tubulin dimer is around 110 kDa. The typical gliding speed of microtubules in our experiment is approximately 3 μm/min (~50 nm/s) as discussed before in the method chapter. The length of the 32 base-long dsDNA capture arm is around 10 nm, while the size of biotin/streptavidin conjugate is approximately 5 nm [177]. That makes the overall length of circular motion radius ~15 nm and thus, the centrifugal force can be calculated as

$$F_{centrifuagl} = m\frac{v^2}{R} = 5\times10^{-26}N \qquad \text{Eq.3}$$

Since $F_{centrifugal}$ << 1 pN, which is much smaller compared to $F_{kinesin}$ and F_{pull}, it will be neglected in the following calculation. The force balance equation now becomes

$$F_{kinesin}\sin(\theta+\varphi) = F_{pull} \qquad \text{Eq.4}$$

$$\theta = \sin^{-1}\frac{F_{pull}}{F_{kinesin}} - \varphi \qquad \text{Eq.5}$$

According to our DNA-particle measurement (see method for details), roughly 4000 DNA strands are grafted on a single particle. If DNA strands are assumed to be evenly distributed on the particle, also the angle between two neighboring DNA strands is assumed to be a 2-D angle, then it could be estimated as

$$\angle_{two\ neighboring\ strands} = \frac{\sqrt{S_p/n}}{2\pi r} \times 360° \qquad \text{Eq.6}$$

where S_p is the surface area of the particle, r is particle radius and n is the number of DNA strands on a particle. The angle between two neighboring DNA strands could then be calculated as 3.2°. As microtubules in solution are placed randomly and they can move in all directions with the same probability, the incoming angle φ is assumed to follow a standard normal distribution.

$$\varphi \sim N(0°, \sigma) \qquad \text{Eq.7}$$

where σ is the standard deviation. Here we assume σ = 3.2° which is the angle between neighboring DNA strands. The incoming angle will then follow

$$\varphi \sim N(0°, 3.2°) \qquad \text{Eq.8}$$

Correspondingly, the change of microtubule gliding direction should follow

$$\theta \sim N\left(\sin^{-1}\frac{F_{pull}}{F_{kinesin}}, 3.2°\right) \qquad \text{Eq.9}$$

where F_{pull} = 12 pN. $F_{kinesin}$ is determined by the number of kinesins affecting a microtubule and the force exerted by a kinesin. Because of the limited size of DNA-particle compared to microtubule length, we assume that only the 1-μm-long leading segment of a microtubule is responsible for direction change. As mentioned in method part, on average, kinesin density on the surface is n_s = 100 μm^{-2} or $\sqrt{n_s}$ = 10 μm^{-1}. Therefore, 10 kinesin molecules could attach on a 1-μm-long microtubule and force from each kinesin is estimated to be 7 pN as the maximum force it can generate. Then Eq. 9 becomes

$$\theta = N(9.9°, 3.2°) \qquad \text{Eq.10}$$

This is the distribution representing the extent of microtubule direction change.

5.4.2 Modeling of crossflow based microtubule gliding direction change

In order to compare with the local microtubule gliding direction change method and further study the effectiveness of using DNA to interact with motor protein systems, the ensemble method to change microtubule gliding direction is also studied in this work. Besides introducing an existing

experimental work done by Kim et al. [167], we developed a physical model to explain this gliding behavior as compared to the local one we have. As part of the calculation, the microfluidic channel dimensions parameters are taken from their paper.

Different from our previous study in local gliding direction change, here crossflow is introduced in this experiment which means now the drag force is large enough to be considered. Since the drag force is created by flow, and its direction is on the same plane as the microtubule gliding direction. This force will affect the microtubule's motion [178-180].

Since different types of flow could have distinct effects on microtubules, it is important for us to calculate Knudsen number $Kn = \lambda/L$, where λ is the mean free path of the water molecule ($\lambda \approx 0.25$ nm) and L is particle size. For microtubules we are studying, the diameter is around ~25 nm which is L in this case. Thus, Knudsen number is Kn = 0.01, and the interaction between flow and microtubules is considered as continuum mechanics inside the channel. To further determine the force, Reynolds number is calculated as $Re = \frac{\rho v L}{\mu}$ (ρ is density of the fluid, μ is fluid viscosity, v is flow velocity, and L is characteristic length). Here the solution in channel is considered as water, so the fluid properties could be found directly. For characteristic length, it is estimated as the diameter of the microtubule which is ~10 nm since the leading domain determines the direction change of microtubule gliding. In order to calculate flow velocity v at the microtubule position, the maximum flow rate in the channel needs to be calculated first. From the work we reference [167], the length, width and depth of the channel are l = 15 mm, w = 400 μm, and d = 100 μm, respectively. The pressure difference between channel inlet and outlet could then be determined [181].

$$\Delta P = \frac{4 l \tau_w}{D_h} \qquad \text{Eq.11}$$

where D_h is the hydraulic diameter of the channel (D_h = 160 μm) and τ_w is wall shear stress. The pressure difference between channel inlet and outlet is directly related to maximum flow velocity which can be then calculated under the condition of wall shear stress 0.45 Pa as used in the paper [180].

$$v_{max} = \frac{\Delta P (\frac{D_h}{2})^2}{4 \mu l} = \frac{D_h \tau_w}{4 \mu} = 0.018\, m/s \qquad \text{Eq.12}$$

This v_{max} is the flow rate at the centerline of the channel ($d/2$ = 50 μm). As a Poiseuille flow, to calculate the flow speed microtubule position, the distance between microtubule position to the centerline is analyzed. With the height of a kinesin around 10 nm and the radius of a microtubule R_{MT} = ~12.5 nm, the distance of the microtubule to the bottom surface is approximately 20 nm. Thus, the flow speed could be calculated as $v \approx 1.4\times10^{-5}$ m/s at the microtubule position.

With all four parameters known, Reynolds number could be determined as significantly less than unity (~$3.6\text{x}10^{-7}$, $Re \ll 1$). With this knowledge, the flow force applied on microtubule could be determined. But given an irregular shape of microtubule, it is important to calculate a simpler situation first which is the drag force (F_D) applied on a spherical particle. This force can be determined by the Stokes' law

$$F_D = 6\pi\mu v R_p \qquad \text{Eq.13}$$

Here, R_p is the particle radius. For a non-spherical particle including a microtubule-type cylinder [182], the drag force can be expressed as

$$F_D = 6\pi\mu v\left(\frac{R_n}{3} + \frac{2R_s}{3}\right) \qquad \text{Eq.14}$$

where R_n is the radius of a sphere that has equivalent area compared to the projected area of the cylinder (microtubule) on the direction of perpendicular to flow which is explained in Figure 5.5a. R_s is the radius of a sphere that has the same area compared to the cylinder surface area (Figure 5.5b).

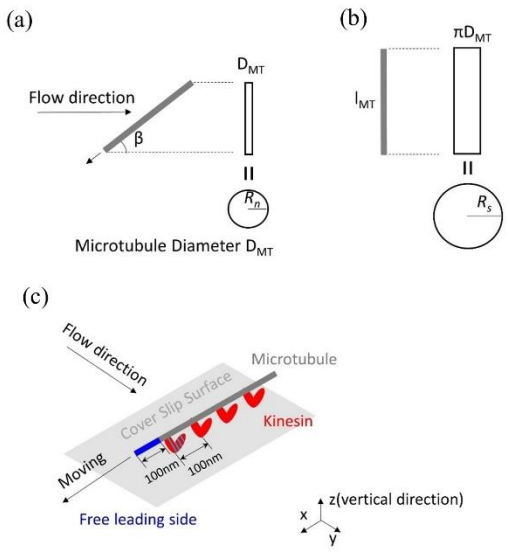

Figure 5.5. (a) Determine Rn through the projection of a microtubule to flow direction. The projected rectangle D_{MT} (projected width) × l_{MT} sinβ (projected length) should have the same area of a hypothetical sphere with a radius R_n. (b) Determine R_n by unfolding a microtubule cylinder into 2-D. The surface area of a microtubule $l_{MT} \times \pi D_{MT}$ should be equal to the area of a hypothetical sphere with a radius R_s. (c) Schematic of a microtubule gliding affected by flow. The whole microtubule is attached on kinesins and cannot move, except the leading segment (blue part). Thus, this is the only domain which could be affected by flow and changed moving direction. The length of this segment is assumed to be 50 nm which is half of the average distance between two adjacent kinesins (100 nm).

Since a microtubule keeps changing direction when it moves in crossflow, finding R_n and R_s is a dynamic process. For a microtubule, all parts have force balance on flow direction because of kinesin, except for the leading domain where it is waving in flow before it binds to the next kinesin (Figure 5.5c). This domain has the length x assumed to be half of the distance between two adjacent kinesins ($x = d_s/2$ = 50 nm) given uniform distribution of microtubule leading domain position between these two kinesins. Thus, as explained in Figure 5.4ab, R_n and R_s can then be expressed as

$$\pi {R_n}^2 = 2xR_{MT} \sin\beta \qquad \text{Eq.15}$$

$$4\pi {R_s}^2 = 2\pi xR_{MT} \qquad \text{Eq.16}$$

where β is the direction of microtubule gliding versus flow direction defined in Figure 5.5. R_s can be calculated based on microtubule radius and length of the free leading domain which is 18.0 nm. For R_n, the angle β will be incorporated into its calculation because it is a function of microtubule

moving direction. In this case, flow drag force $F_D(\beta)$ is also a function of orientation of the microtubule.

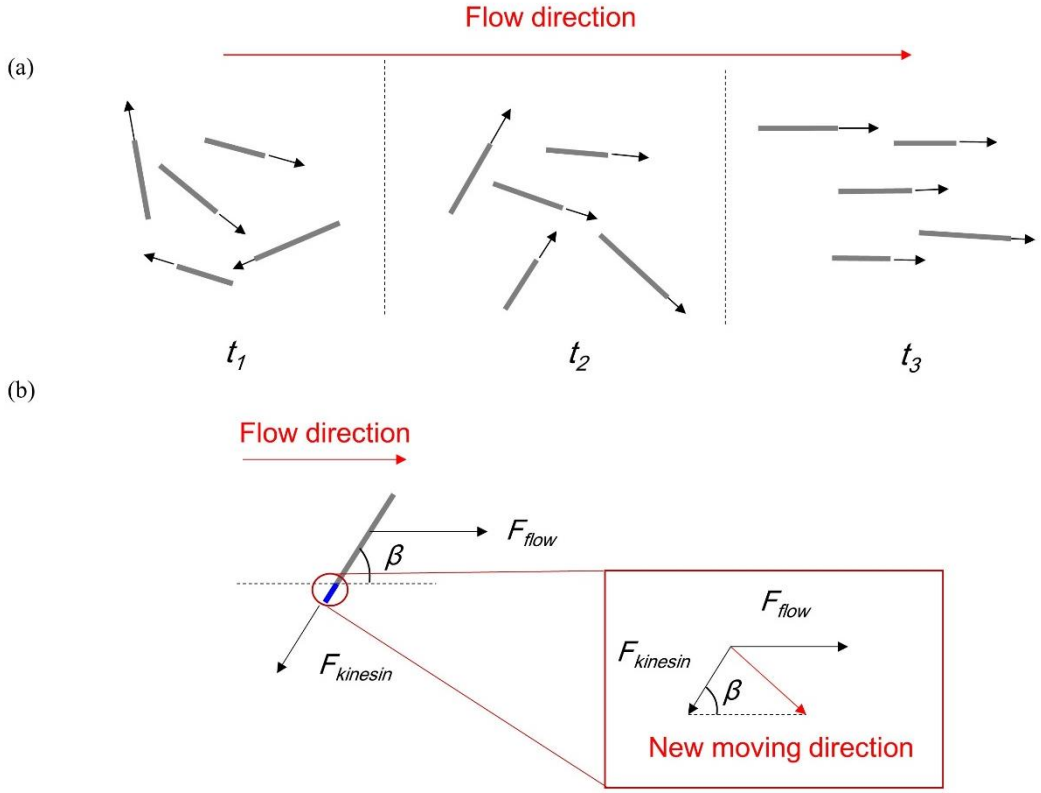

Figure 5.6. (a) Schematic of alignment of microtubule gliding direction by flow ($t_3 > t_2 > t_1$). (b) Force balance analysis under flow affection. The majority of the microtubule is balanced by kinesin force and flow force while the unbound leading segment is not balanced. The combination of flow force and kinesin force determines the new moving direction of the microtubule (red). The angle β is used to represent the microtubule's moving direction as it is the angle between microtubule's moving direction and flow direction.

Given that the Reynolds number is much less than 1 from previous calculation, inertia is negligible under our experimental conditions. Thus, the gliding direction of microtubules will be fully determined by force balance between flow and kinesins, as illustrated in Figure 5.6. Most of the microtubule is held and transported by kinesins while only the leading domain could be redirected by flow in solution. This redirection flow could be expressed as:

$$F_{flow} = F_D = 6\pi\mu v\left(\frac{\sqrt{\frac{2xR_{MT}\sin\beta}{\pi}}}{3} + \frac{2R_s}{3}\right) \qquad \text{Eq.17}$$

Where all parameters have been determined from previous calculation and β is the only variable.

Different from the local-based direction change method, here flow force (~0.001 pN) is not at the same magnitude level as kinesin force. So, there is no way for a kinesin to exert its maximum stall force 7 pN. In fact, the average force from a kinesin was found to be around 0.3 pN by Palacci and co-workers [183]. Only one kinesin is directly affecting the microtubule leading domain. Therefore, we use $F_{kinesin}$ = 0.3 pN in our calculation for flow-based microtubule direction change.

Since there is a square root of sin β term which cannot be integrated in the real number system, it is important to use the numerical method to calculate. Here the time needed for a microtubule moving from one kinesin to another is considered time interval Δt. A microtubule completes one moving direction change behavior during this time period. With that, the direction changes during each Δt could be added up over time to determine the overall direction change of microtubules. This time interval can be calculated as

$$\Delta t = \frac{1}{v_{MT}\sqrt{n_s}} \qquad \text{Eq.18}$$

where v_{MT} is gliding speed of microtubules, and $\sqrt{n_s}$ is 10 μm^{-1} as characterized before. In the experimental work referenced, native or full-length recombinant kinesin was used, whose corresponding microtubule moving speed is 30 – 40 μm/min [184]. Thus v_{MT} = 30 μm/min or 500 nm/s was estimated and used in our calculations, with the time interval set Δt = 0.2 s.

With time interval determined for this discrete function, the microtubule gliding direction could be determined by the parameters we have. At each time interval, a microtubule experiences $F_{kinesin}$ on its gliding direction as it always has and F_{flow} along the flow direction. The sum of these two vectors will determine the new microtubule moving direction which could be expressed as

$$\overrightarrow{F_{moving}} = \overrightarrow{F_{flow}} + \overrightarrow{F_{kinesin}} \qquad \text{Eq.19}$$

To convert this equation into scalar parameters, the moving direction could be determined

$$\tan\beta_k = \frac{F_{kinesin}\sin\beta_{k-1}}{F_D(\beta_{k-1}) + F_{kinesin}\cos\beta_{k-1}} \qquad \text{Eq.20}$$

where β_k is the direction of microtubule moving at the kth time interval.

It should be noted that microtubule gliding direction at the current time interval is related to the direction at a previous time interval, this is because we assume the moving direction of a microtubule will not change before it finishes the current time interval in order to simplify the calculation. With start point β_0 and time interval 0.2 s set, the following angles β_0 to β_{k-1} can be determined sequentially from Eq. 20. At time t_k, the microtubule direction is β_k.

To determine the error of this model, experimental direction change is included and compared

$$error = \sqrt{\frac{\sum(\beta_{model} - \beta_{exp})^2}{N}} \qquad \text{Eq.21}$$

where β_{model} is the theoretical moving angle from the model, β_{exp} is the experimental moving angle, and N is the total number of cases.

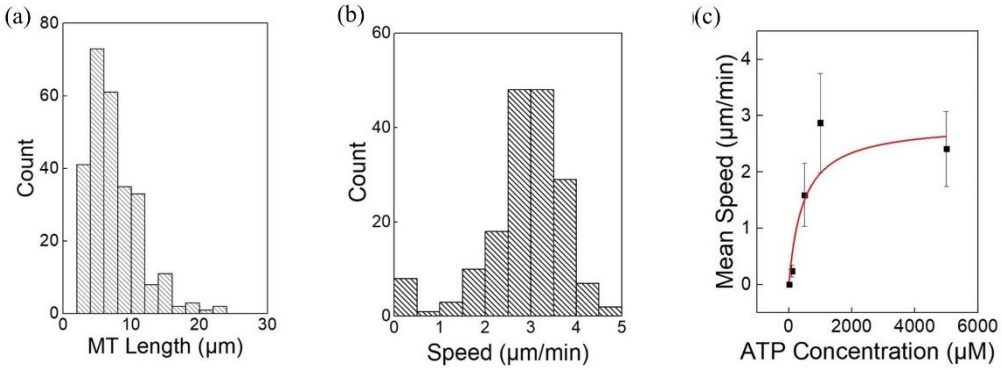

Figure 5.7. (a) Length distribution of polymerized microtubules measured by fluorescence imaging. Most microtubules are 10 μm long or less. (b) Microtubule gliding speed distribution with 1 mM ATP in solution. Average speed is ~3 μm/min. (c) Microtubule gliding speed as a function of solution ATP concentration. It increases as ATP concentration increases and gradually stops increasing after around 1 mM ATP.

5.5 Results and Discussion

5.5.1 Microtubule motility assay characterization

Before introducing DNA-particle into the system, the microtubule motility assay is analyzed. The length and gliding speed distribution of polymerized microtubules are found from fluorescence imaging. As polymerization conditions optimized, the average microtubule length is found to be ~10 μm and the gliding speed under our experimental conditions is found to be ~3 μm/min (Figure 5.7a and b). In addition, the microtubule gliding speed versus ATP concentration is also analyzed

(Figure 5.7c) and it is found that higher than ~1 mM concentration of ATP, microtubule speed reaches a plateau.

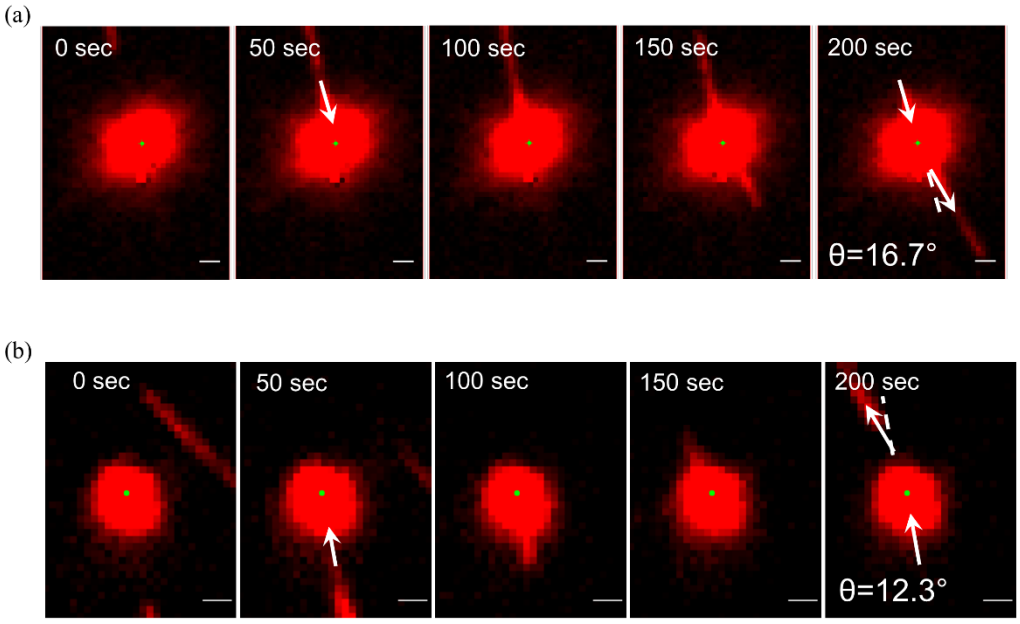

Figure 5.8. Pseudo-colored fluorescence images of microtubule gliding direction change by DNA-particles. The red circle represents a DNA-particle, and the red rod indicates a microtubule. The green dot is a localization of the nanoparticle as red circle is much larger than the particle's actual size due to the diffraction limit. The green dot is exact 200 nm in diameter. The microtubule moving directions change ~12.3° (a) and ~16.7° (b) after the microtubule passes the DNA-particle. Microtubule incoming and outgoing directions are shown as the white arrows. The dashed line is the extension of the incoming angle for better comparison with microtubule's leaving direction. Both microtubules and nanoparticles are imaged by 658 nm excitation laser. Scale bar is 1 μm in both images.

5.5.2 Local direction changes of gliding microtubules by DNA-particles

Two representative cases of local directional changes of gliding microtubules are shown in Figure 5.8. Here, incoming and outgoing gliding directions are represented by two white arrows and the dashed line is the extension of the incoming moving direction of the microtubule. The direction change could be found to be $\theta \approx 12.3°$ and 16.7° respectively while in contrast, if no streptavidin is attached on DNA-particle, the direction change is much smaller (Figure 5.9). It is noted that there is also a small green dot at the center of each red nanoparticle. This represents the actual size and location of the particle calculated by the localization tool in ImageJ (more details in method chapter). The main purpose of doing this calculation is to eliminate ineffective cases from the

dataset. Because of the diffraction limit, the particle appears to have 2 μm in diameter which is significantly larger than its actual size 200 nm diameter. The loss of quality here could create problems in determining whether there is an interaction between DNA-particle and microtubules or not. Thus, in order to make it clear, green dot is plotted as the actual nanoparticle and only the microtubules passing through it will be considered as possible interaction candidates. Even though microtubule is not localized because it has larger size and also moves during image taking process, particle localization has already filtered out most non-interacting DNA-particles and microtubules. By doing that, it becomes evident that microtubule moving direction changes significantly after interacting with the DNA-particles.

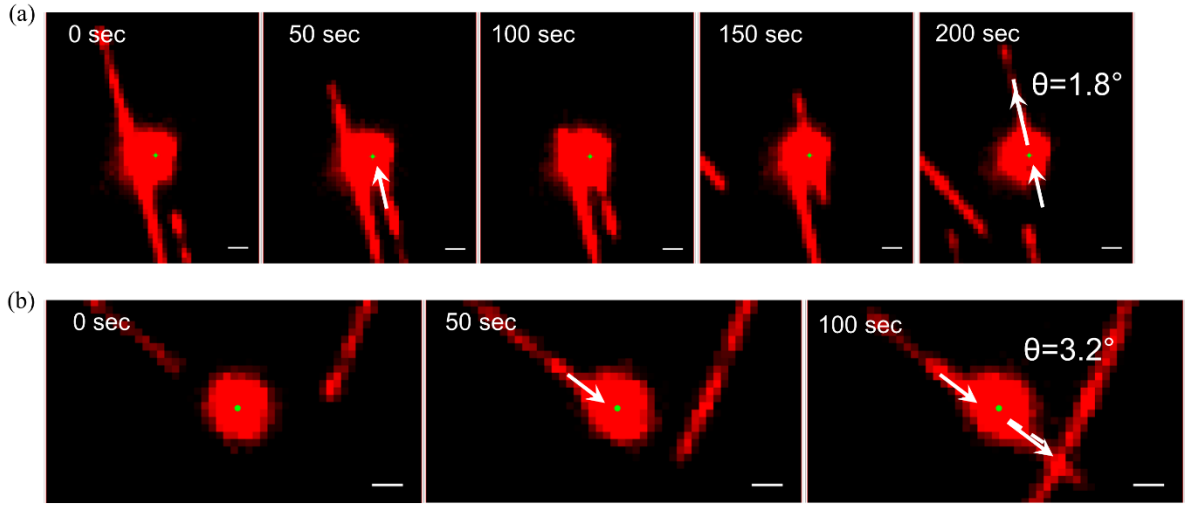

Figure 5.9. Pseudo-colored fluorescence images of direction changes of gliding microtubules by DNA-particles without streptavidin. Almost no direction change is found. Image components are the same as Figure 5.8. The microtubule moving directions change ~1.8° (a) and ~3.2° (b) after the microtubule passes the DNA-particle. This indicates that without streptavidin, no interaction happens between DNA-particle and microtubules, so no significant microtubule moving direction change can be found. Scale bar is 1 μm in both images.

5.5.3 Direction change angle distributions

To unambiguously confirm this local direction changes by DNA-particle, statistical analysis is needed. As a comparison, DNA-particle with (green curve) and without (blue curve) streptavidin has been tested separately on their ability to change microtubule gliding direction. As Figure 5.10a shows, both cases have direction change to some extent, but DNA-particle with streptavidin exerts a larger and broader direction change distribution where it can be approximated with a normal distribution $N(0°, 9.6°)$ which is centered at 0° and has a standard deviation $\sigma \approx 9.6°$. In contrast,

without streptavidin on DNA-particle, biotinylated microtubules cannot be captured and redirected and thus the angle distribution is also much narrower as expected. Based on calculation, it can also be concluded as a normal distribution $N(0°, 4.0°)$ however with a smaller standard deviation $\sigma \approx 4°$. In addition, we also find that all angle changes without streptavidin involved are less than 10°, which is also an indicator of the function of DNA-capture arm on the immobilized particle to redirect microtubules.

Furthermore, the histograms can be generalized into relative frequency plots for better comparison. Here in Figure 5.10b, addition to DNA-particle with and without streptavidin cases, free gliding of microtubules without DNA-particle involved is also taken into consideration (black curve). It is clear from the plot that without streptavidin, whether or not a DNA-particle exists doesn't make differences in direction change. In fact, the black curve is a random direction change due to Brownian effect which is common in *in vitro* motility assay.[185,186] To quantify the differences between the distributions using DNA-particle with streptavidin and without streptavidin, Kolmogorov-Smirnov test (KS test) [187] is performed (Figure 5.10c). As a nonparametric statistical test, it can evaluate how similar two datasets are statistically. If the empirical cumulative distribution functions of these two datasets are close to each other, the two datasets are considered similar. In this test, similar datasets indicate no effect of DNA-particle on microtubule direction change. By making the cumulative probability plot, we found that the largest distance between these two cases is D = 0.375 which corresponding p-value can be calculated as 0.000.[188] So the hypothesis of the same distribution of DNA-particle with and without streptavidin should be rejected, which means there are significant differences between these two conditions. This statistical result also supports our experimental design in microtubule direction change.

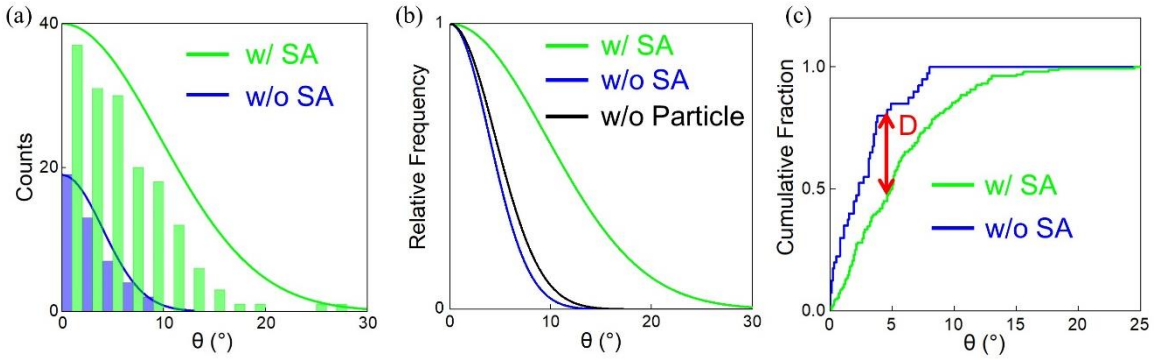

Figure 5.10. (a) Histograms of microtubules gliding direction change angles for different cases including DNA-particles with streptavidin (SA) (green) and without streptavidin (blue). The streptavidin-coated DNA-particles exhibit a significantly broader distribution compared to the no streptavidin particles, and it also has a larger maximum gliding direction change angle. (b) Relative frequency is plotted against microtubule direction change for DNA-particles with (green) and without (blue) streptavidin. A control experiment with no particles in solution is also presented (black) and it has a similar distribution compared to DNA-particle without streptavidin. This indicates that DNA-particle needs streptavidin to show their direction change function. (c) Kolmogorov-Smirnov test of two direction change datasets. The distance between the cases of DNA-particles with (green) and without (blue) streptavidin is measured in the cumulative probability. Because of the distance D = 0.375 has a corresponding p-value of 0.000, it indicates that the hypothesis no significant difference between these two cases has been rejected. So DNA-particles with and without streptavidin have differences in microtubule direction change.

5.5.4 Comparison of model and experiment of direction change by particles

With the confirmation of differences in two cases, the next is to compare the experimental data with the model predicted result. The physical model is calculated in Chapter 5.4.1 which shows the microtubule direction change follows *N(9.9°, 3.2°)* based on experimental conditions used in this test. The curve is plotted in red in Figure 5.11.

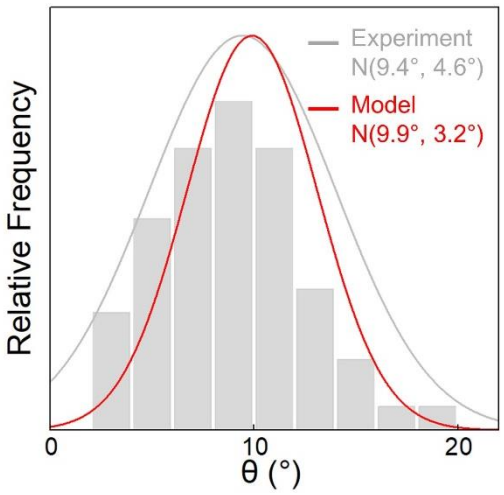

Figure 5.11. The histogram (grey) of microtubule gliding direction angles θ has been fitted by a normal distribution (grey) and compared with the theoretical calculations (red). The model has mean and standard deviation of angle change approximately 9.9° and 3.2°, respectively. The experimental histogram comes from the subtraction of the blue histogram (DNA-particles without SA) from the green histogram (DNA-particles with SA) in Figure 5.10a. The experimentally obtained statistics are fitted by a normal distribution N(9.4°, 4.6°).

However, in real experimental data, it is found earlier that random direction change exists even in traditional motility assay. To accurately evaluate the function of DNA-particle, it is important to eliminate the random effect on direction change. To achieve that, direction change generated by Brownian motion (blue histogram in 5.10a) is subtracted from the distribution of DNA-particle-streptavidin based direction change (green histogram in 5.10a). The resulting histogram as a function of the difference angle θ is shown in grey in Figure 5.11. This distribution rules out the random direction change and fully represents the DNA-particle based microtubule direction change. With a normal distribution *N(9.4°, 4.6°)* fitting, the similarity of theoretical model prediction (red) and experimental data (grey) is shown in Figure 5.11. Albeit smaller differences in standard deviation and mean value due to oversimplified assumptions, the experimental microtubule direction change is explainable by the physical model.

One thing to notice in DNA-particle based local method is that DNA strands are essential to direction change of microtubule gliding in this design. As a comparison, if a particle is fully covered by streptavidin, but no DNA, microtubules are either got stuck or dragging the particle away. The reason behind is non-specific binding of streptavidin and nanoparticle. Since the force

needed to break this non-specific binding is much larger compared to streptavidin/biotin conjugation force, without DNA involved, breaking streptavidin/biotin conjugation becomes the critical part. Since over 100 pN is needed in this case, kinesins in the leading part of the microtubules cannot generate that much force. Thus, microtubules will have a high chance to move with the particle or stop as shown in Figure 5.12. However, in our actual experiment, none of such case has been found which indicates the very limited streptavidin non-specific binding on nanoparticles. Instead, the majority of streptavidin is linked to the nanoparticle through dsDNA. With unzipping dsDNA, microtubules moving direction can be changed.

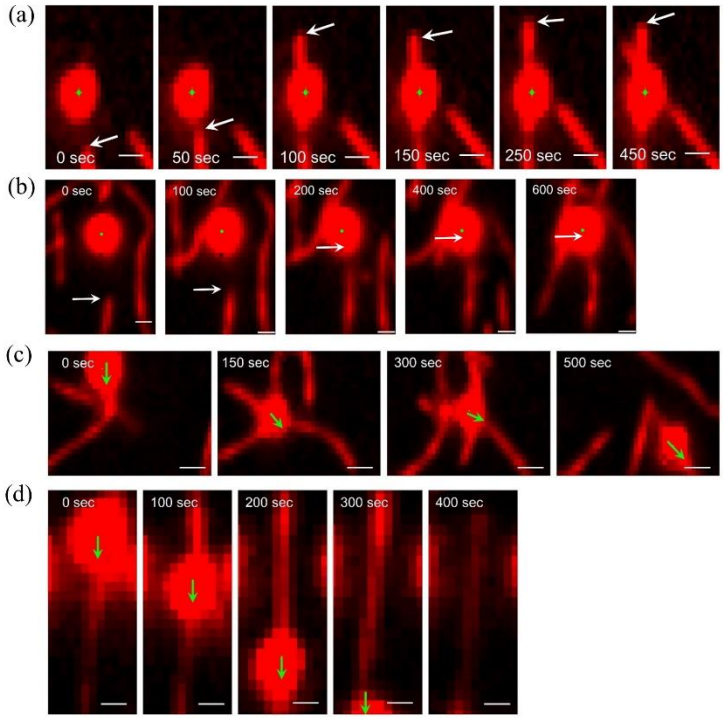

Figure 5.12. Representative fluorescence images of gliding microtubules before and after interaction with streptavidin/nanoparticle conjugates. In this control experiment, no DNA is attached on nanoparticle, instead, streptavidin molecules are conjugated onto nanoparticles. (a) – (b). Gliding microtubules are stopped after attaching immobilized particles. White arrow indicates the position of leading edge of the microtubule whose movement is halted. (c) – (d). Immobilized particles are dragged away by gliding microtubules after the microtubule interacting with the particle. Green arrow indicates the moving direction of the particle by a microtubule. Scale bars are 1 μm in all images.

5.5.5 Experimental data and modeling of direction change by crossflow

Ensemble microtubule direction change is also compared between experimental data and physical model (Figure 5.13). The experimental data are presented in dots directly taken from Kim et al.'s

work while the curves with the same color scheme are the theoretical calculation of microtubule direction in flow. As time passes, all microtubules will eventually be aligned to flow direction disregard their initial gliding direction which corresponds to reality as part of the validation of the model. With different initial angles, the time needed for microtubules to be aligned varies, gradually increasing its changing speed between 180° to 90° and decreasing the changing speed between 90° to 0° (with respect to flow direction). Different channel shear stress (or flow speed) also affect the microtubule direction change as expected. With larger pressure, faster flow speed is generated inside the channel and thus microtubules are aligned with shorter time. It takes ~200 s to align a microtubule from 180° to 0° (deviation within 1°) when the shear wall stress is 0.45 Pa, while it takes ~500 s at 0.18 Pa and ~1000 s at 0.09 Pa. The difference between experimental and modeling datasets is calculated as 0.3 rad (Eq.21).

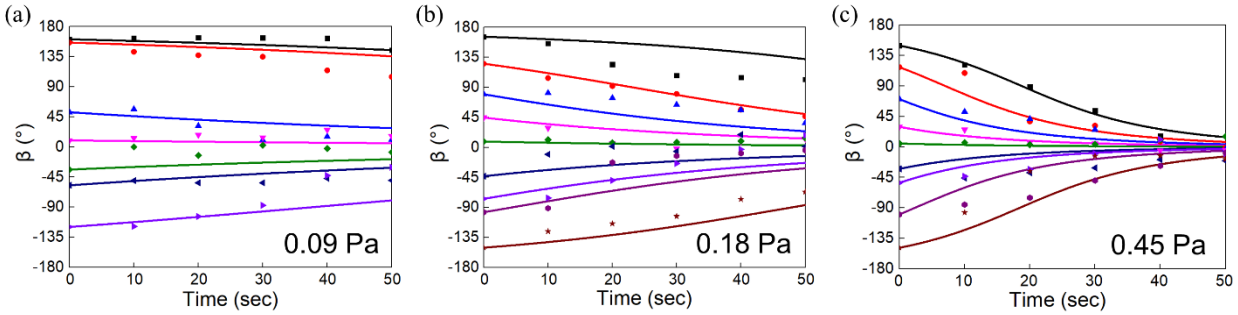

Figure 5.13. Theoretical calculations (lines) of microtubule redirection by crossflow are compared to experimental measured microtubule direction change (objects in the corresponding color) reported by Kim et al. Each curve represents a temporal evolution of a microtubule's moving direction with different initial angles under various wall shear stresses (i.e. flow speed) of 0.09 (a), 0.18 (b), and 0.45 Pa (c). It is evident that with higher shear stress (i.e. high flow speed), the time needed for alignment is shorter. The square root of mean square displacement is approximately 0.3 rad.

5.5.6 Particle-based local scheme versus flow field-based ensemble method

There are several major differences between these two methods.

- Crossflow can affect the gliding behavior of all microtubules in solution, while the interaction between a DNA-particle and microtubules is one at a time. Ensemble method may not be suitable for the case where we only want selected microtubules to be redirected. The DNA-particle based scheme should be used in this case given its ability to change microtubule gliding direction locally. To use this method, particles could be placed at designed positions where microtubules will move across to achieve the local direction change.

- The difference in gliding direction change angles by a crossflow and a particle are attributed to the time that relevant forces are exerted on microtubules. A crossflow could align microtubules completely is because the flow has continuous force applied on the microtubules which could easily be over 10 seconds level. On the contrary, a DNA-Particle could only interact with a microtubule in an extremely short time period. Based on another report, the time needed to dissociate a 20-bp-long duplex is only ~10 μs.[175] So, this huge difference in magnitude of time contributes to the fact that crossflow has a stronger alignment effect compared to DNA-particle.

Since the change of microtubule gliding direction through DNA-particle is highly dependent on the DNA pulling force and the interaction time between microtubules and the particle. The angle may be increased by using longer dsDNA strands or stronger bio-conjugates with a larger rupture force. One thing to notice is that the rupture force should not exceed overall kinesin forces on the microtubule otherwise the microtubule will be trapped as a similar situation shown earlier.

5.6 Conclusion

In summary, we take advantage of mechanical properties of DNA strands in this chapter and apply that in motor protein system. By using the dissociation force of dsDNA, a local scheme for redirecting microtubule gliding is created. A physical model is also developed to explain the function of DNA strands better in this system. Compared to conventional ensemble methods such as crossflow, DNA-particle shows distinct properties including local direction change, short interaction time and on average 10° changes in the microtubule direction. These makes DNA-particle a unique method for microtubule direction change. In addition, the differences between an ensemble direction change method and a local direction change method are also highlighted from the study of physical models and experimental results together. It is possible that the DNA-particle-based local approach may be incorporated with microfluidic architectures to provide a better and easier microtubule gliding control for various applications. Moreover, we expand and test the application of DNA strands/signals further in this chapter. With the manipulation of DNA strands based on its biological property, chemical property, and mechanical property, we can finally be comfortable introducing DNA as a tool into the complex artificial cell system to help us study and explore the potentials of it.

6 MONITORING LIPOSOMES REVERSIBLE CLUSTERING BEHAVIOR BY DNA SIGNALS

6.1 Introduction

Cell aggregation is an important phenomenon in cellular biology where cells bind and cluster together under a certain environment. Studying the cell-cell interactions during this process could contribute extensively to the understanding of cell differentiation, migration, and viability.[189] Furthermore, cell aggregation study also holds great potential in enhancing tissue engineering research as cell-cell interaction is an essential part of tissue building in real life. With this importance, plenty of research have been done on this topic, including cell reactions to certain chemicals, the kinetics and dynamics of cell aggregation, and the possible diseases related to cell aggregation. These works characterize cell aggregation behavior from all different aspects. However, given the complex inner cellular environment, to take full control of cellular aggregation and dissociation is difficult. Thus, the simplified artificial cell/liposome could be introduced to the system either for a deeper understanding of cell interactions or for better control of cell aggregation behavior.

Since liposomes cannot interact with each other spontaneously like live cells, it is important to develop another signaling pathway for liposomes to achieve a similar effect as a living cell. Related research work has been done by using Ca^{2+} as a signal to trigger liposome clustering in order to study the membrane permeability change and its application.[190,191] Even though an external signal is used to control liposome aggregation behavior, reversibility is achieved in these works. From the discussions we have in the previous three chapters, DNA could be used as perfect candidate for signaling molecules in artificial cell systems. As previous works indicate, DNA can interact with other DNA, protein, small molecule, and nanoparticles, which means all these components could be brought into the liposome system if DNA is present. In addition, the interaction between DNA signals and liposomes has also been studied extensively which provides a solid foundation for further improvement of this interaction. Either mixing DNA with liposomes for signal delivery, DNA mediated liposome fusion or constructing DNA structures as transmembrane pore, DNA contributes highly to the development of liposome. To take a step further on this connection, and

to use it as a tool for cell aggregation study, a DNA-based controlled reversible liposome clustering system is developed.

The goal of the system is to emulate actual cell aggregation with controllable and reversible behavior. To take advantage of the specificity of DNA base pairing, it is used as the signaling molecule to trigger association and dissociation of liposomes in solution. In addition, DNA origami based transmembrane channel is incorporated with liposome to have inner cellular reaction involved in this signaling which makes the system behavior closer to cell aggregation.

6.2 Scheme

Figure 6.1 shows the experiment design for DNA mediated liposome reversible clustering behavior control. A DNA strand (green) coated giant liposome (~10 μm diameter) with DNA origami transmembrane pores (brown) inserted and Exonuclease III (yellow, Exo III) coated nanoparticle (red, 200 nm diameter) encapsulated. Because of origami pores, inner liposome shares the same buffer condition with outer liposome, and, materials smaller than the size of origami pore could also diffuse in and out through the DNA origami channel. This makes it possible for the control of aggregation and release around certain liposomes locally. In order to trigger liposome aggregation, a hairpin DNA signal (purple) is added into the solution. After it diffuses into the liposome and gets digested by Exo III molecules immobilized on the nanoparticle, the protected DNA sequence will be exposed and diffuse back outside the liposome. This new released signal will link DNA strands (green) coated on large liposomes and DNA strands coated on small liposomes (blue) because it has complementary parts to both strands. Thus, small liposomes will be linked onto large liposomes due to DNA hybridization. To release this aggregation, a release DNA signal (pink) will be added which is fully complementary to linking signal generated from last step. Because of strand replacement, liposomes linking will be released.

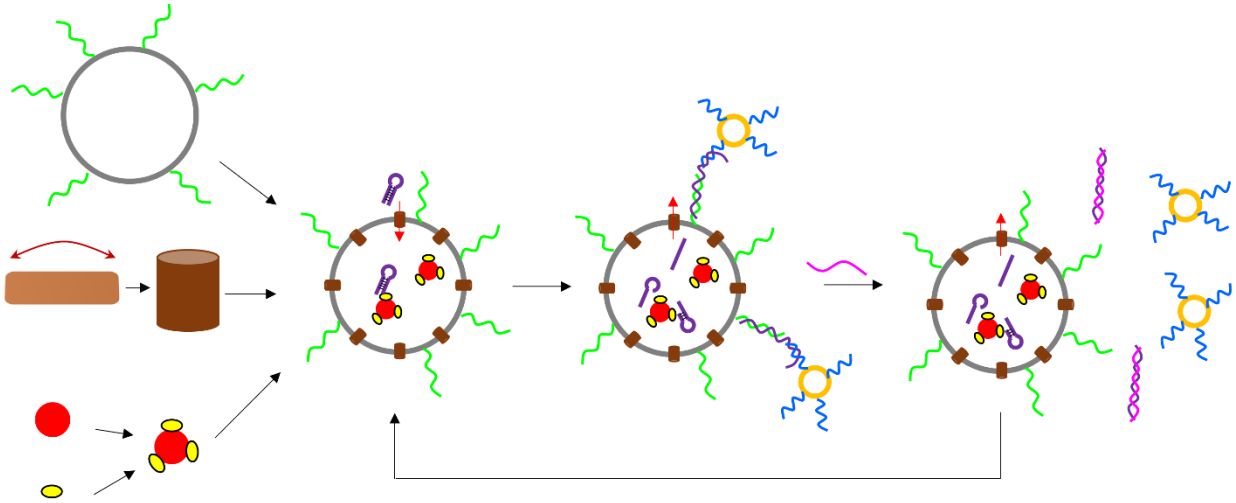

Figure 6.1. Controlled reversible liposome aggregation. DNA strand (green), DNA origami transmembrane channel (brown) and Exo III (yellow) coated nanoparticle (red) are incorporated into the same liposome. Upon addition of external DNA hairpin signal (purple), it will pass through origami pore and interact with Exo III. Once the hybridization part of the hairpin is digested by Exo III from 3' end, the remaining segment of the signal will pass origami pore again and bind with the DNAs around the liposome. As part of the signal is complementary to DNA strands (blue) decorated on small liposomes, the small liposomes will then aggregate together with the large liposome. To release the aggregation, a DNA signal (pink) fully complementary to the purple strand will be added. This association and dissociation process can be reversible by repeatedly adding aggregation signal (hairpin) and releasing signal (pink).

6.3 Experimental Methods

6.3.1 Materials

All the lipids used are purchased from Avanti Polar Inc. Anti GST antibody is purchased from Thermo Fisher Scientific Inc.

6.3.2 DNA-lipid conjugation

Amine group modified DNA sequence (5' – /amine/ GGA CAG AGT GAC ATC – 3') is used to prepare for lipid-DNA linking. First, 20 µL 1mM amine DNA was dissolved into a mixture containing 39 µL 60 mM azide-NHS (dissolved in dimethylformamide or DMF), 40 µL DMF and 1 µL triethylamine (TEA) buffer. The mixture was incubated at room temperature for two hours

to let the NHS group react with the amine. Then 200 µL ethanol and 10 µL 3 mM NaCl solution were added into the solution. The mixture was incubated at 4 °C for 30 minutes before it was centrifuged at 20,000g for another 30 minutes for purification. Supernatant was removed and the precipitate was re-dissolved in 200 µL ethanol to centrifuge again to remove excess azide-NHS molecules. After centrifuge, precipitate was collected, dried in vacuum and resuspended in 1x PBS buffer. The concentration of synthesized DNA-azide was determined by the absorption of the sample at 260 nm by a spectrophotometer.

Synthesized DNA-azide was then clicked with 1,2-distearoyl-sn-glycero-3-phosphoethanolamine-N-[dibenzocyclooctyl(PEG) -2000] (DSPE-PEG(2000)-DBCO). Azide groups can react with DBCO groups without using any catalyst, which is a very efficient method. The known concentration DNA-azide from last step was mixed with DSPE-PEG(2000)-DBCO at a molar ratio of 1:5. The mixture was left overnight in dark to complete the reaction. The sample was then purified by the same procedure discussed above, including ethanol precipitation, centrifugation, ethanol washing, and concentration determining. Then the synthesized DNA-lipid was ready to use.

6.3.3 Coating polystyrene nanoparticles with Exo III

Coating Exo III onto the polystyrene particle is almost the same as coating DNA strands onto the particle discussed in Chapter 2.2.2. DNA was replaced by Exo III molecules in this case while the amount of Exo III is less (5 µL 10 µM Exo III). In order to keep the activity of Exo III molecules, the incubation should be kept at 4 °C instead of room temperature and the incubation time should also be elongated to 3 hours for completed reaction.

The measurement of the activity of Exo III after conjugating with nanoparticles was done by monitoring the PL intensity change of a dsDNA couple. One DNA strand was conjugated with FAM dye (5’ – ATC GGT CAG GCT T/iFluorT/T TTTTTT T – 3’) and another DNA strand (5’ – /5IABkFQ/ AAG CCT GAC CGA T – 3’) has a quencher on its 5’ end. When two strands are hybridized, the quencher could absorb all fluorescence emitted by FAM dye where no fluorescence will shine and if DNA strands are digested, fluorescence will get much stronger. To test Exo III activity, 1 µM of each DNA strand was dissolved in 100 µL 1x NEBuffer (B7001S, New England

Biolabs) first and measured fluorescence. Then, the measurement was paused, 1 μL conjugated Exo III particle was added into the solution and the measurement was resumed. Based on the increasing speed of PL intensity of FAM fluorescence, the activity of Exo III could be determined.

6.3.4 Preparation of large liposomes with DNA strands, transmembrane origami pore, and encapsulated Exo III-particle

Same DNA-lipid and Exo III-nanoparticle prepared in previous steps will be used for liposome preparation. DNA origami will be a little different compared to the synthesis discussed in Chapter 3.3.4. Here the same rectangle origami was used, but it was connected on two sides to become a cylinder shape. Cholesterol modified DNA strands bind to the extension of staples at the middle of the cylinder to create an extra cholesterol ring outside DNA origami.

With these samples prepared, liposome could be prepared in a similar way as described in Chapter 2.6. To place DNA strands on the surface of the liposome, DNA-lipid was mixed with DMPC at a molar ratio of 1:1000 in a glass vial. The solution was then dried in vacuum for 20 minutes to evaporate all solvent and resuspended with 300 μL liquid paraffin. The new solution was sonicated at 50 °C for 3 hours. Lipids will disperse uniformly in the sonicated solution. Then 10 μL 10 nM DNA origami pore, 5 μL Exo III-particle, both in TAEM buffer were mixed and added with another 5 μL TAEM buffer. This 20 μL mixture was added into lipid solution and then vortexed for 25 s to make aqueous solution forming droplets inside lipid. After vortexing, the liposome solution became blurred. Then 150 μL solution was poured onto 300 μL TAEM buffer and centrifuged for 15 minutes at 8,000 g. The liposome containing DNA strands on surface, DNA origami transmembrane pore, and Exo III-nanoparticle inside was in the precipitates. Both aqueous phase and oil phase supernatants were discarded, and the precipitate was dissolved in TAEM buffer for future use.

6.3.5 Preparation of small liposomes with DNA strands

Different from large liposome preparation, the rehydration method is used for small liposome preparation. First cholesterol modified DNA (5’ – TAA CAA CCA AAC CAT TTT T /3CholTEG/ – 3’) was mixed with DMPC at a molar ratio of 1:1000 in glass vial. The solution was dried in vacuum for 20 minutes to let lipid form a dry thin film on the bottom of the vial. Then the glass vial was placed on a pre-heat hot plate at 90 °C and 1 mL TAEM buffer was poured into the vial.

The solution was stirred by a stirring bar at 500 rpm for 1 hour while it was kept heated all the time. After stirring, small liposome solution was purified by a 30 kDa molecular weight cut off spin column at 5,000 g for 5 minutes 6 times to remove free lipid molecules and free DNA molecules. The purified small liposomes were ready to use.

6.3.6 Fluorescence imaging of liposomes

Large liposomes were flowed into a hand-made microfluidic channel by a syringe. Once they were flowed, liposomes will non-specifically bind to microchannel surfaces via electrostatic interaction. After the liposomes were captured inside the channel, other samples and signals including fluorophores, DNA signals, and small liposomes could be flowed into the channel to interact with the large liposome. In addition, the buffer in the channel could also be replaced by flushing new buffer into the channel. Fluorescence images were taken by the fluorescence microscopy system as discussed in Chapter 2.7.4.

6.4 Results and Discussion

6.4.1 Characterization of liposome and DNA origami transmembrane pore

A typical liposome is shown in Figure 6.2 with roughly 10 μm in diameter which is also the size of the liposomes we are studying later in this work. The liposome is composed of DMPC and rhodamine-labeled lipids at a molar ratio of 100:1. Rhodamine dye could be excited by 561 nm laser and has its emission around 580 nm. As Figure 6.2a-d show, the liposome shows a clear ring with brighter inner liposome compared to background under 561 nm excitation which indicates the rhodamine-labeled lipids are on the liposome surface. With 405 nm or 658 nm laser, nothing could be excited which indicates that the lipids itself will not intervene emission from other components with different excitation wavelengths such nanoparticles and DNA origamis for future experiments.

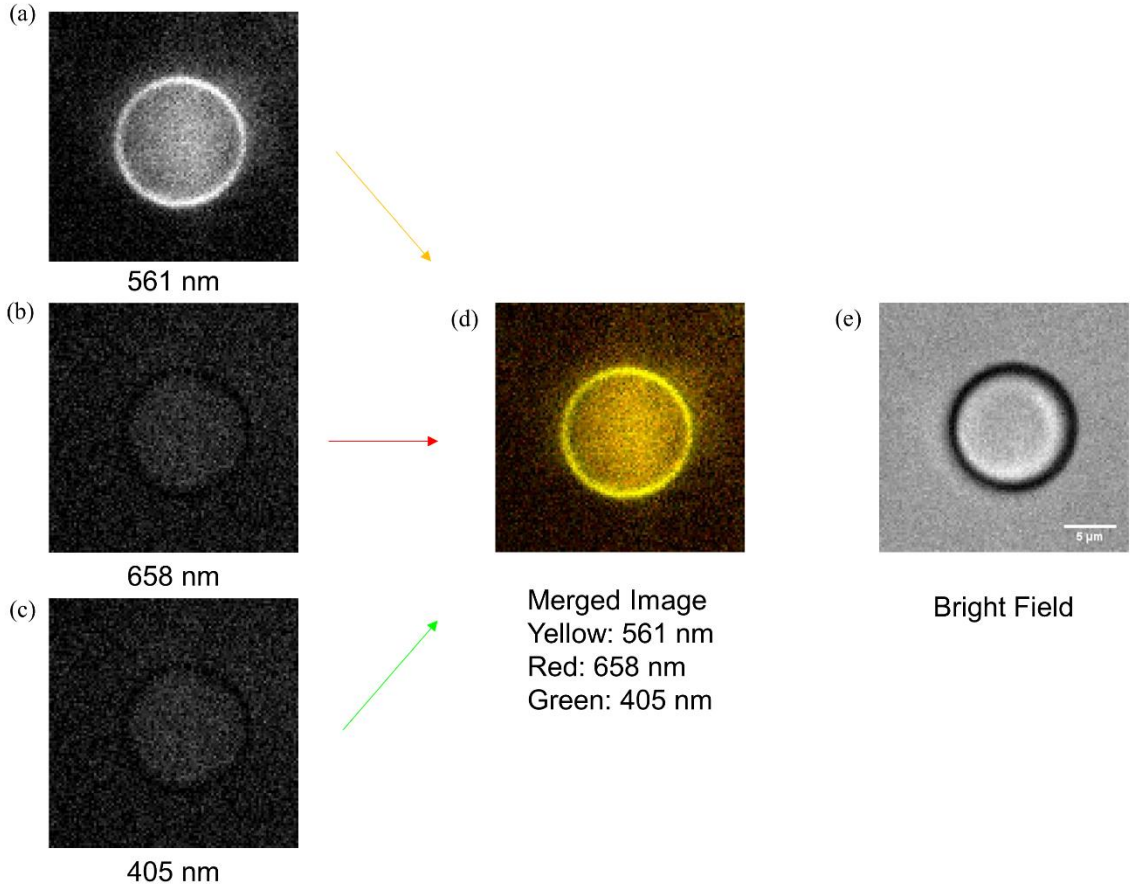

Figure 6.2. Liposome imaging under fluorescence microscopy. (a) Liposome image under 561 nm excitation. (b) Liposome image under 658 nm excitation. (c) Merged image by (a) and (b), green color indicates (a) and red color indicates (b). (d) Bright-field image of a liposome. The scale bar is 5 μm.

When DNA origami transmembrane pore is inserted into the liposome membrane, with the Cy-5 dye modified with DNA origami staples, it is expected to see the similar liposome structure under fluorescence microscopy. By using 658 nm as excitation wavelength, we can find that a brighter fluorescent ring forms on the liposome only when DNA origami incorporated into the liposome (Figure 6.3ab). This indicates that DNA origamis are indeed immobilized onto the liposome membrane.

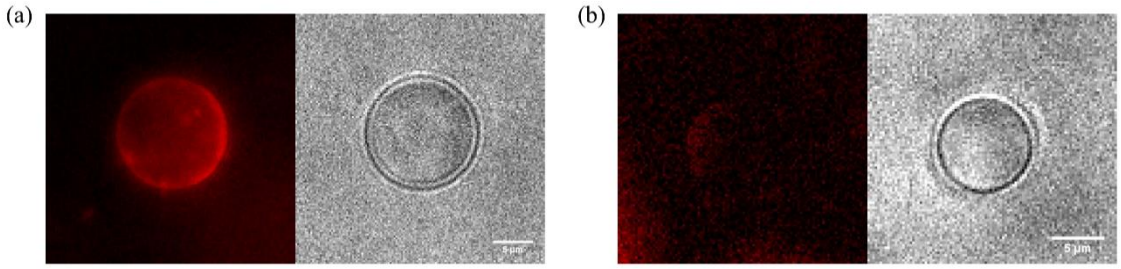

Figure 6.3. DNA origami inserting into the liposome membrane. Cholesterol modified DNA origami can be incorporated into liposome surface and show a fluorescent ring from Cy5 dye (a), while non-cholesterol modified DNA origami cannot and thus no ring can be found (b). Scale bars are 5 μm.

6.4.2 Characterization of DNA transmembrane pore

With the proof of DNA origami existing on liposome surface, it is then important to validate the function of the origami pore. The most basic function of cell pore is to serve as a channel for molecules to diffuse in and out. Thus, fluorescence dyes were used for this test. Green fluorescent protein (GFP) and Cy-5 modified DNA strands were selected as target molecules. Non-fluorescent DNA origami was inserted into the liposome, in this case, to prevent wrong fluorescence readings from DNA origami. As Figure 6.4a shows, when there is DNA origami pore existing on liposome, there is a connection between inside and outside the liposome. When GFP was added into the solution, because of the large pore size (~30 nm diameter) compared to GFP molecule size (~5 nm diameter), GFP could easily diffuse into the liposome. Thus, the fluorescence of GFP inside liposome and outside the liposome should be at a similar level. On the contrary, if no DNA origami is on the liposome membrane, then GFP would stay outside liposome, which led to the result in Figure 6.4b that GFP fluorescence only shined outside liposome instead of inside. Similarly, when DNA-Cy5 was used as a signal, the comparison between DNA origami decorated liposome and plain liposome was shown in Figure 6.4cd. These results indicate it is possible for signals outside the liposome to reach inner liposome for further reactions. One thing to notice is that the inflow speed seems to be extremely fast. Even the sample was placed under the microscope for imaging immediately after mixing liposomes with signals, the inflow effect still has completed already. That may be due to the size difference between signal molecules and origami pore which could possibly make the diffusion through the channel as free diffusion in solution.

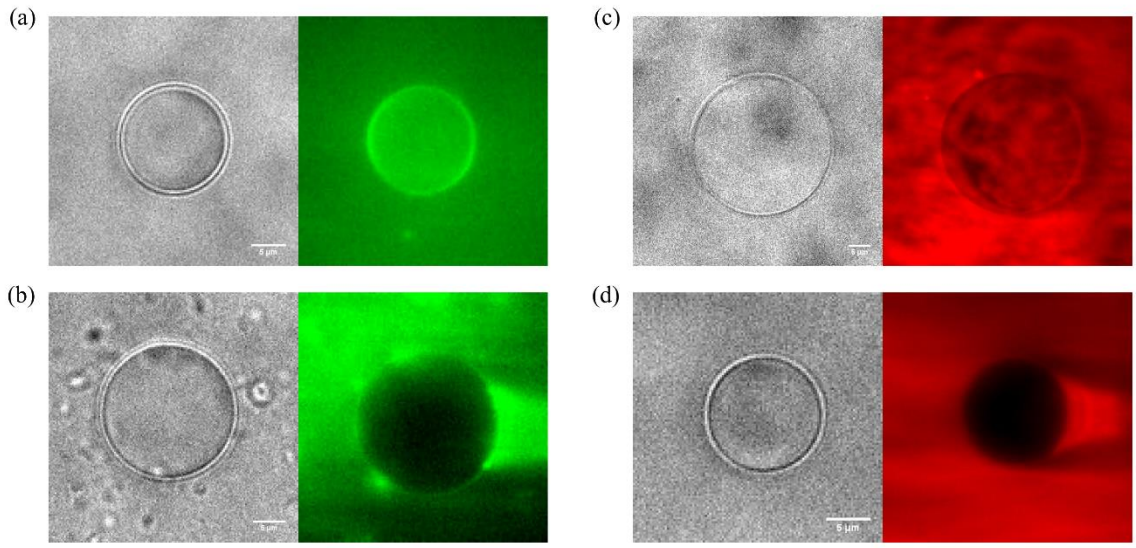

Figure 6.4. Signal influx into liposome through origami pore. (a)-(b): GFP signal can penetrate through liposome surface with DNA origami pore (a), but cannot diffuse in without DNA origami (b). (c)-(d): DNA-Cy5 signal can get into liposome with DNA origami pore existing (c) and cannot get in if no origami pore on liposome surface (d). Scale bars are 5 μm.

As a bidirectional channel, it is not enough for DNA origami pore to let signals diffuse into liposome from outer solution, signals diffusing out is also necessary. Same GFP and DNA-Cy5 molecules were used as signals again for outflow characterization. Signal molecules were encapsulated inside liposome first when the liposome was prepared. Since molecules would diffuse inside and outside through the channel to balance the fluorescence intensity, liposomes were washed by column filter to remove the free dyes in solution. If no origami pore was on liposome, the signal molecules inside would be kept well and showed fluorescence. Conversely, these molecules would be lost if liposome had no origami on it. As Figure 6.5 shows, liposome samples were first filled with GFP or DNA-Cy5 dyes separately (left column). After column filter wash, liposome samples with origami pore would lose the dyes encapsulated and the whole sample had no fluorescence. Liposomes without DNA origami, instead, would keep dyes stored inside, and the sample would only show fluorescence from inner liposome as free dyes in solution have been washed away.

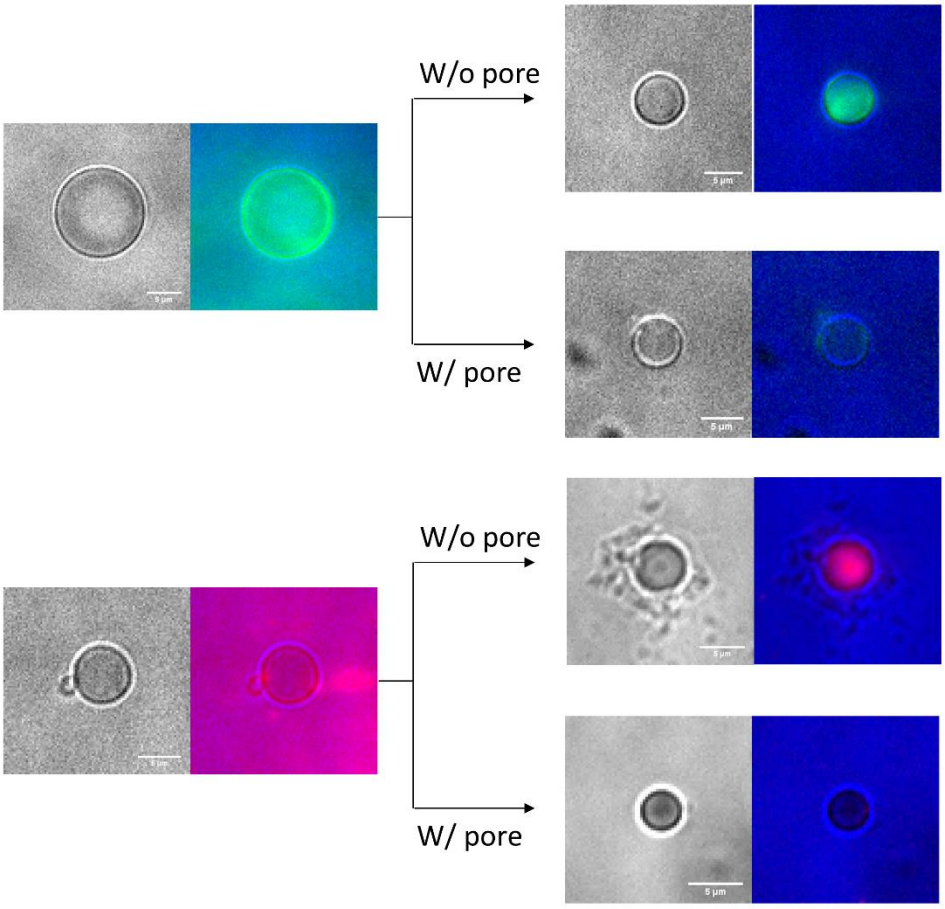

Figure 6.5. Signals outflow through DNA origami pore. GFP (green) and DNA-Cy5 (red) are encapsulated inside liposome first as the left column shows. Then the liposome sample is washed by a column filter to remove free dyes in solution. If there is DNA origami pore on liposome, dyes inside liposome will also be washed away and no fluorescence will show after wash. If there is no DNA origami pore, signals don't have connections with the outside solution and thus won't be washed away. So fluorescence will shine inside liposome only after washing in this case. Scale bars are 5 μm.

Corresponding ensemble measurement was shown in Figure 6.6. Fluorescence intensity of GFP and DNA-Cy5 were measured first right after the liposome has been made. Then column filter purification would apply on liposomes to remove the free dyes in solution as well as dyes encapsulated inside liposomes. The time interval between each purification was 2 hours to make sure it is long enough for dyes to disperse uniformly in the liposome solution. The PL intensity drops each time as purification times increase which is because of the gradual loss of dyes from liposomes. Since there are free dyes in solution when liposomes were prepared, the intensity drop for the first wash is the biggest as most free dyes were washed away. Another thing to notice is

that GFP shows a better outflow effect compared to DNA since PL intensity drops more in GFP cases. This may be due to the interaction between DNA signal added and DNA origamis on liposomes. Since part of the DNA signals may be captured by DNA origami, they could not be washed away. This possibly makes worse inflow and outflow effect for DNA signals compared to protein signals.

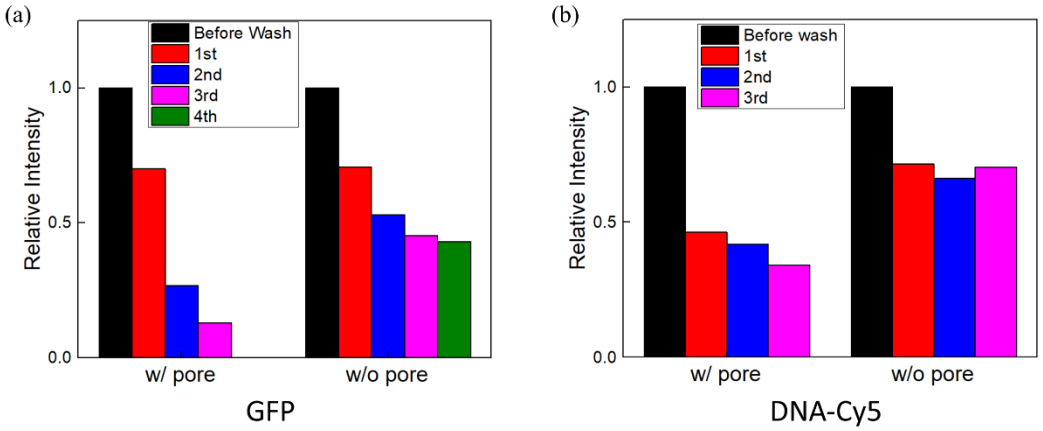

Figure 6.6. Statistical analysis of signal outflow through DNA origami pore. GFP (a) and DNA-Cy5 (b) are encapsulated inside liposomes at the beginning with fluorescence intensity determined (black column). Then column filter wash is performed for each sample. As more times column wash is done, fluorescence intensity of the sample keeps decreasing, but become slower and slower. We can find that w/ pore cases have a stronger decrease compared to w/o pore cases. This is due to the fact that fluorescent signals inside liposome cannot be washed away if no DNA origami pores on liposome. So w/o pore, liposomes will have higher fluorescence intensity compared to w/ pore.

6.4.3 Exo III activity inside a liposome

The purpose of transporting DNA signals inside liposome is to digest the DNA signal and generate the new aggregating DNA signal. Thus, it is important to maintain the activity of Exo III even when it is inside a liposome. For a free Exo III enzyme, its activity was tested by a FAM-quencher DNA couple (check details in Chapter 6.3.3). It could be found that 0.1 unit/μL Exo III can digest oligonucleotides very fast (Figure 6.7a). Almost all digestion finished within a few seconds. Given the definition of 1 unit of Exo III can digest 1 nmole oligonucleotide at 37 °C for 30 minutes, and the fact that the proceed speed for an Exo III molecule is 500 bp/minute at 37 °C, the molar concentration of 0.1 unit/μL is estimated to be 1 nM. Once the Exo III molecules were coated onto polystyrene particles and purified, its digestion activity was measured again and shown in Figure 6.7b. Theoretically, the Exo III concentration in solution is 0.1 nM based on the amount added for

conjugation with nanoparticle. However, its digestion speed is only ~1/20 of 1 nM Exo III. This indicates that the reaction yield of Exo III conjugation onto nanoparticle is around 50%. This could be due to the relatively low molar ratio of Exo III and nanoparticles (100:1), which could lower the interaction chance between these two materials and reduce the conjugation yield.

With the particle-Exo III made, it was then encapsulated into liposomes with the same liposome preparation method used before. DNA origami pore was also included on liposome to serve as the channel for the FAM-quencher DNA couple to diffuse in. It could be found that when Exo-particles were encapsulated inside the liposome, Exo III could still show its activity (Figure 6.7cd). However, with the same amount of nanoparticle-Exo III added, fluorescence increase was only about 1/10 of nanoparticle-Exo III encapsulated inside liposome compared to free nanoparticle-Exo III (Figure 6.7e). This difference may be created by the loss of nanoparticles in encapsulation and difficultness for DNA strands to diffuse into the liposome. Even though a significant amount of Exo III activity was lost during liposome preparation, the rest amount was still enough for digesting DNA signals.

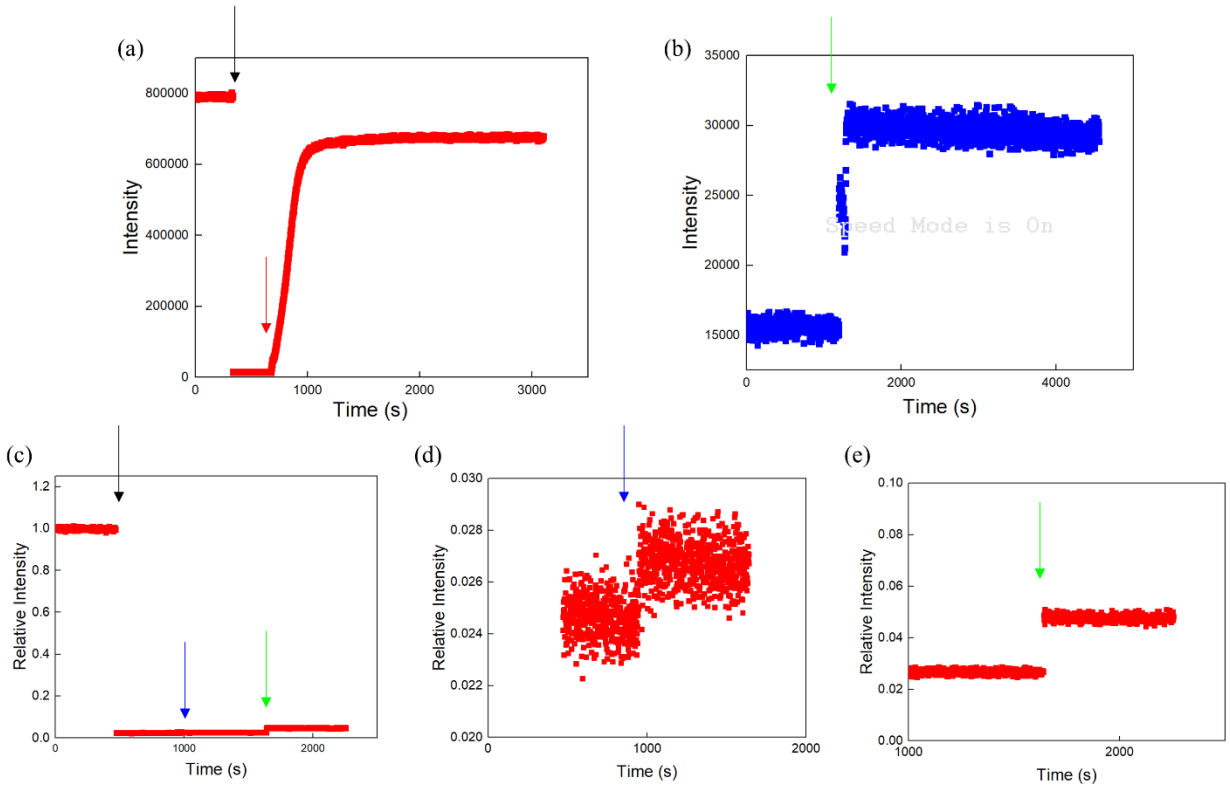

Figure 6.7. (a) Exo III activity measurement with FAM-quencher DNA couple in 1xNEBuffer (NEB #7001S). The concentration of Exo III here is 0.1 unit/μL and DNA strands are 1 μM. Initially, PL intensity is high with only DNA-FAM in solution. The intensity quickly approaches 0 after the addition of DNA-quencher (black arrow). This is because DNA double-strand is hybridizing well and most fluorescence emitted is absorbed by the quencher. Once Exo III is added into the solution as the red arrow indicates, the quencher attached DNA strand will be digested and DNA hybridization will be broken. Without proximity of quenchers, fluorescence from FAM will not be absorbed and thus the overall sample has a dramatic increase in its fluorescence. (b) The same measurement is done as (a), but Exo III coated nanoparticle is used instead of free Exo III. With the theoretical concentration of Exo III 0.01 unit/μL, it seems 50% of Exo III shows function on nanoparticle since PL intensity increase is about 1/20 compared to using 0.1 unit/μL Exo III. (c)-(e): Exo III activity measurement with nanoparticle-Exo III encapsulated inside the liposome. (d) and (e) are two enlarged portion from (c). Black arrow also indicates the addition of DNA-quencher. The liposome with Nanoparticle-Exo III is added into the solution at the blue arrow, where relative intensity increases ~0.003 as (d) shows. Compared to the addition of nanoparticle-Exo III in (e), there is 1/10 activity of Exo III kept which may be due to the loss of Exo III particle and more difficulties in DNA diffusing into a liposome.

Because we need to encapsulate nanoparticle-Exo III into a liposome, these Exo III coated particles were mixed with DNA origami at the preparation step as the inner solution. To keep the structure of the origami, it is important to make sure that they were not digested by Exo III. So, the

fluorescence image of liposomes encapsulating Exo III coated nanoparticle was taken in Figure 6.8a (due to lack of laser lines, we used the same laser line for nanoparticle and origami pore). We could find that both a large red dot (indicating the nanoparticle-Exo III) and a red ring (indicating the DNA origami pore) show on the image. Furthermore, DNA origami was also mixed with the same amount of Exo III as those encapsulated in liposomes to show whether maintaining DNA origami structure intact successful or not. It turned out that most DNA origamis would keep their structures because of the relatively low concentration of Exo III or possibly the steric hindrance between nanoparticle and DNA origami. In either way, DNA origami pores could maintain their structures and likely their functions after mixing with nanoparticle-Exo III. This leads us to the next step of testing local reversible liposome aggregation control.

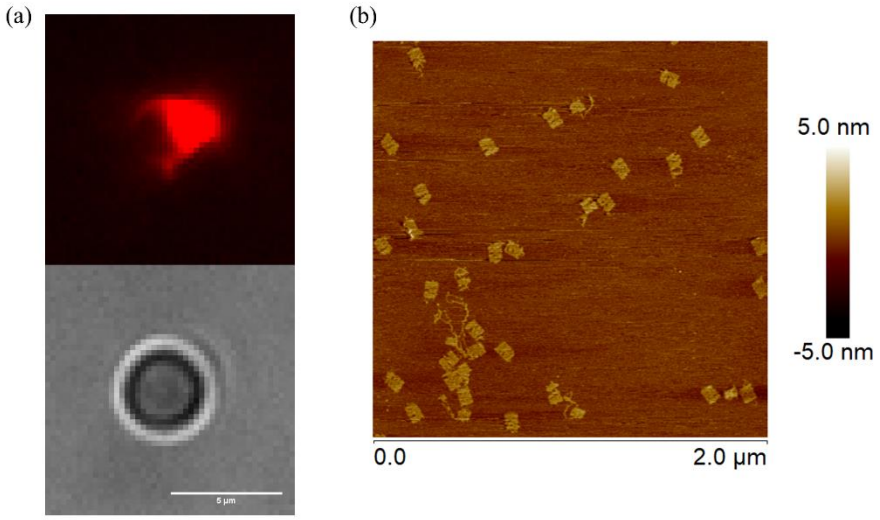

Figure 6.8. (a) With the addition of Exo III into liposome with origami pore, the ring of DNA origami pore still shows which indicates DNA origami is not digested by Exo III and could still serve as a transmembrane channel. Scale bar is 5 µm. (b) 10 nM DNA origami is mixed with 0.01 unit/µL Exo III in 10 µL TAEM buffer and incubated for 15 minutes. Most origami keeps their structure after incubation. Same 0.01 unit/µL Exo III will be used in preparation of liposome, so this indicates that DNA origami pore will not be digested by Exo III during preparation step and the liposome sample can be used for interacting with outside liposome signals.

6.4.4 DNA programmable aggregation of liposomes

Before combining DNA liposomes with nanoparticle-Exo III for local reversible clustering control, DNA signals were introduced into the system to confirm the function of DNA mediated liposome aggregation and release. Linker strand (5' – ATG GTT TGG TTG TTA GAT GTC ACT CTG TCC GAA TCA – 3') and release strand (5' – TGA TTC GGA CAG AGT GAC ATC TAA CAA CCA AAC CAT – 3', fully complementary to linker strand) were used to initiating liposome aggregation and releasing aggregated liposomes. The large liposomes were immobilized inside microfluidic channel first by non-specific binding. Excess amount of linker strands was added into the channel for incubation about 10 minutes and then washed away. With large liposomes decorated with linker strands through DNA hybridization, small liposomes were then introduced into the channel. Since DNA sequences on small liposomes were complementary to the remaining part of linker strands, small liposomes would be captured by large liposomes, and thus aggregation of liposomes formed just like Figure 6.9b. The PL intensity coming from small liposomes increased tremendously with the addition of the linker strand. Moreover, as expected, once release strands were flushed into the channel, small liposomes would dissociate from large liposomes and as a result, the PL intensity from small liposomes decreased a lot (Figure 6.9c). as a reversible clustering control, multiple cycles could be done by repeatedly adding the linker strand and release strand where the corresponding fluorescence change of small liposomes attached on large liposomes was shown in Figure 6.9.

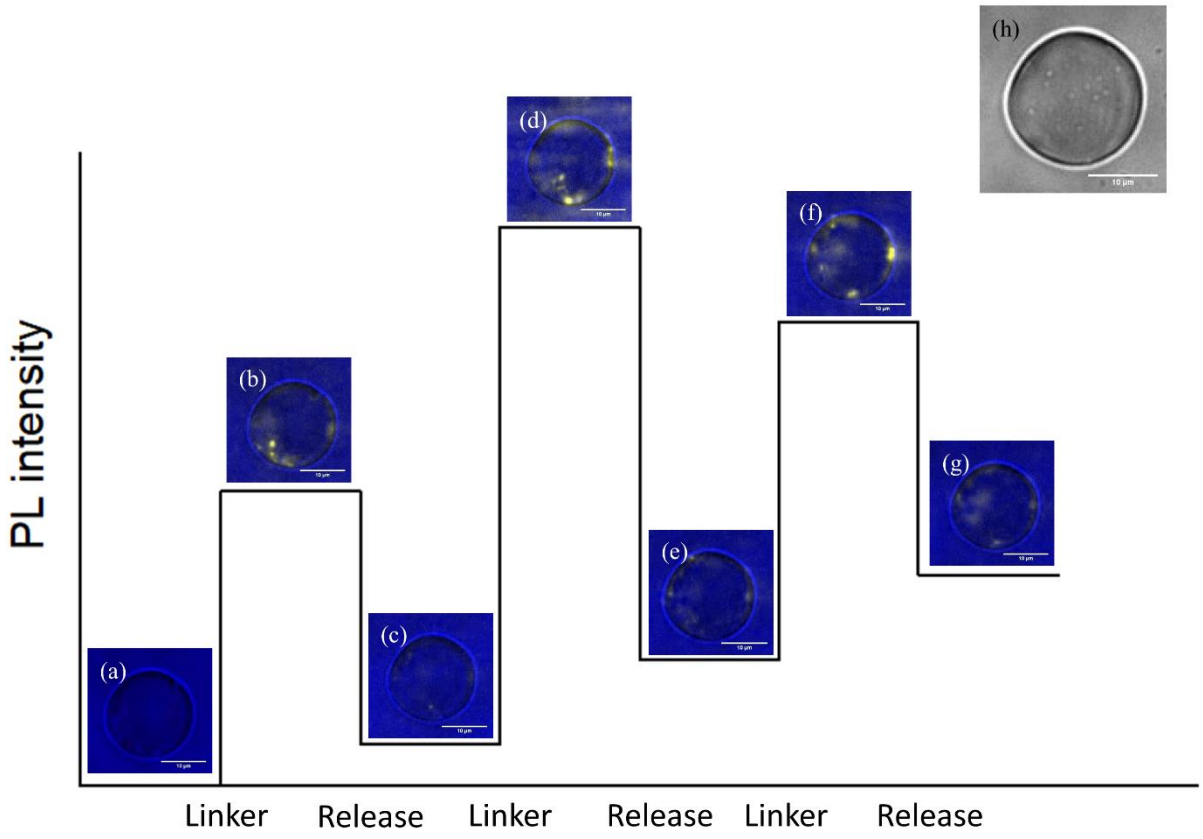

Figure 6.9. Aggregation and release control of liposome without DNA pore by addition of DNA signals. (a)-(g): A large liposome is immobilized in a microfluidic channel. With the addition of linker DNA and small liposomes, small liposomes will bind to the large liposome through DNA hybridization and thus the fluorescence from small liposomes will increase ((b), (d), (f)). Once the release DNA strand is added into the solution, it is fully complementary to linker strand so the linking between large liposomes and small liposomes will break. The small liposome fluorescence will then drop as (c), (e), (g) show. (h) is the bright field image of the large liposome. Scale bars are 10 μm for all images.

It is noted that the release of liposome aggregation is not as completed as expected while some small liposomes still attach on the large liposome and the PL intensity after releasing increases gradually as the experiment continues. One hypothesis is that some small liposomes bind to the surface instead of large liposomes. Since the majority of surface areas are not interacting with large liposomes, small liposomes can flow into the gap between large liposomes and glass surface and bind there non-specifically. When the overlaid images were prepared, these small liposomes would look like on the large liposome while they were indeed not. To further confirm the DNA dissociation release, DI water which could disrupt DNA hybridization, instead of release strand,

was used. As Figure 6.10 shows, the intensity difference between aggregation and release is larger compared to using the release strand, which could be due to a more completed dissociation of DNA strands. The remaining PL intensity after release may also come from the non-specific binding between small liposomes and glass surface.

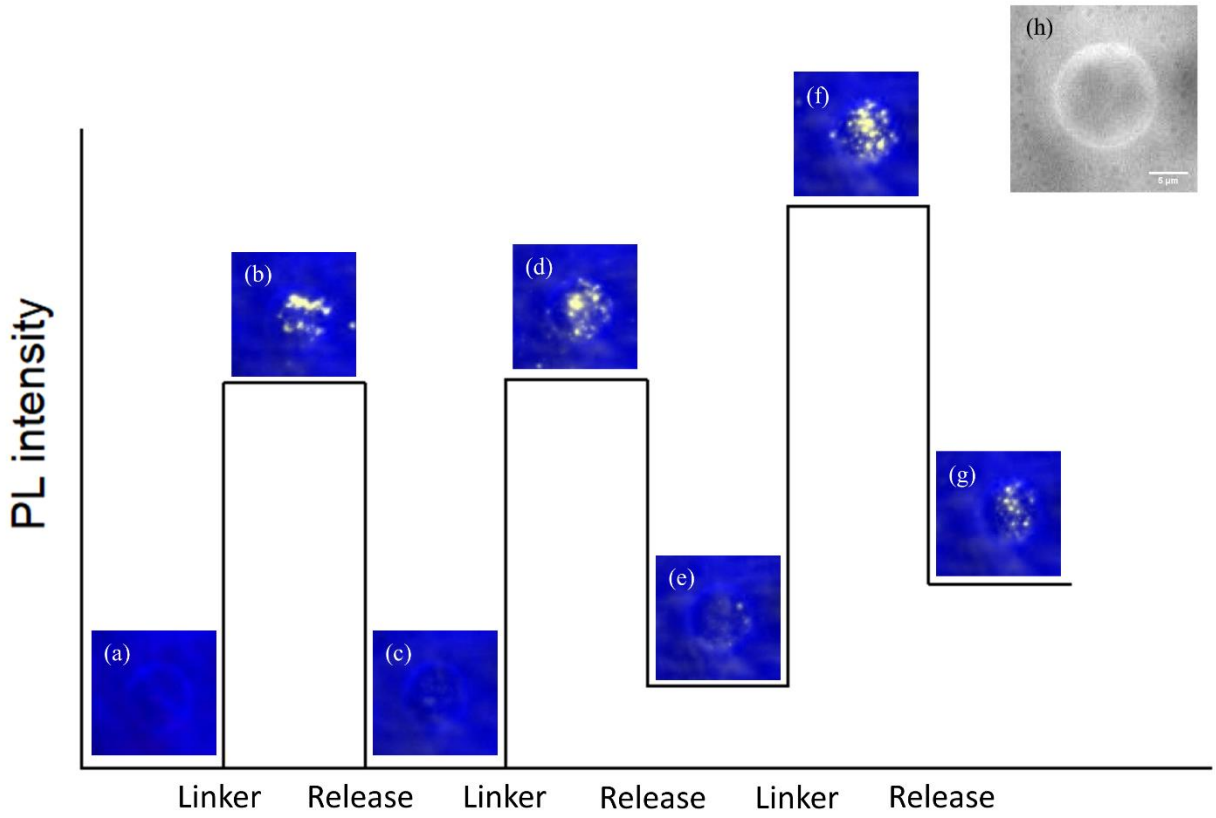

Figure 6.10. Aggregation and release control of liposomes without DNA pore, where releasing is done by addition of DI water. (a)-(g): A large liposome is immobilized in a microfluidic channel. With the addition of linker DNA and small liposomes, small liposomes will bind to the large liposome through DNA hybridization and thus the fluorescence from small liposomes will increase ((b), (d), (f)). Here instead of release strand, DI water is flushed into the channel. Since DNA hybridization needs cations in solution, with DI water only, DNA base pairing will break and small liposomes will be released from large liposomes. Thus, the fluorescence from small liposomes will drop as (c), (e), (g) show. (h) is the bright field image of the large liposome. Scale bar is 5 µm.

The test with direct addition of DNA signals proves that liposomes could be aggregated and released under DNA signal control. This makes us confident to include the last component into our system, which is the Exo III coated nanoparticle. As Figure 6.11 shows, its pattern is quite

similar to previous control experiments with adding DNA signals to aggregate and release liposomes. Here the difference is that the DNA signal we used was a hairpin strand (5' – ATG GTT TGG TTG TTA GAT GTC ACT CTG TCC GAA TCA ACA TCT AAC AAC CAA ACC AT – 3') where the linker strand is protected inside it. Once this hairpin DNA signal has interacted with Exo III molecule, the protecting oligonucleotides would be cut off and the linker signal would be exposed. Similarly, after aggregation, DNA release signal could be introduced again, and the liposome aggregation would be released. Same aggregation and release cycle could be created by the addition of DNA signals. This indicates the effectiveness of DNA signals in locally controlling artificial cells aggregation and release behavior.

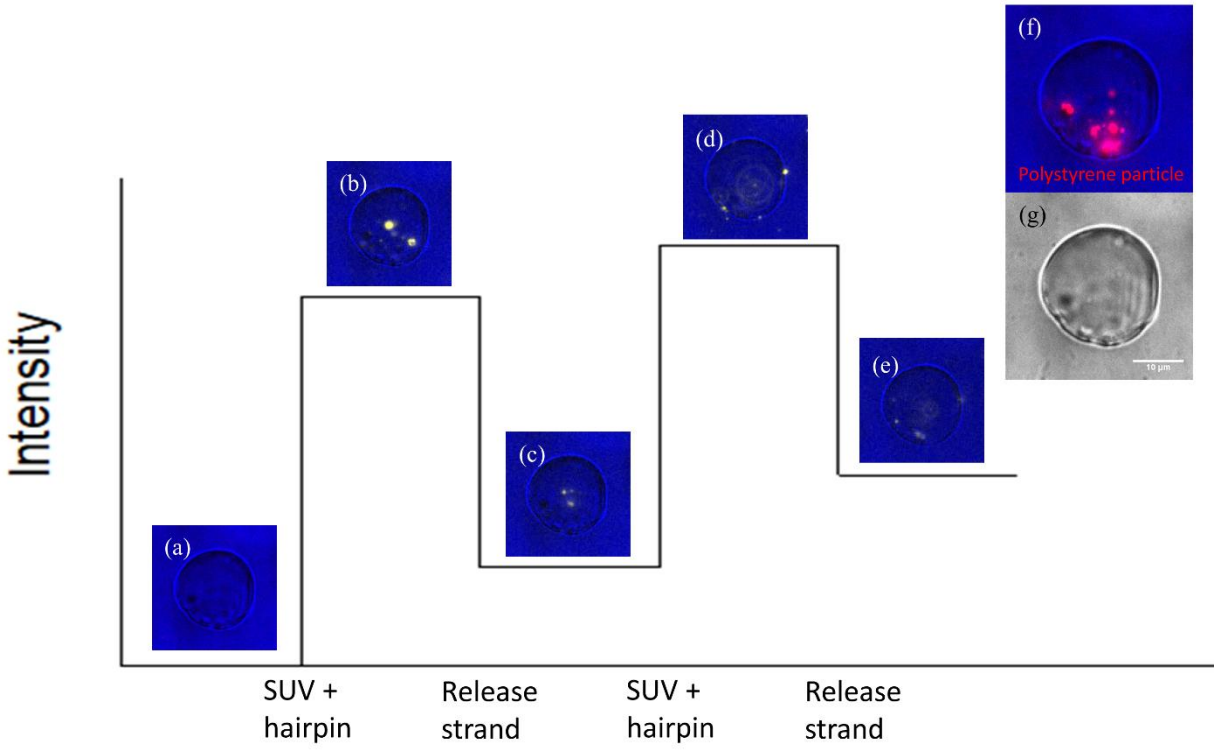

Figure 6.11. Locally reversible liposome aggregate and release controlled by addition of DNA signals. (a)-(e): A large liposome with DNA origami pore inserted and Exo III coated nanoparticle encapsulated is immobilized in a microfluidic channel. With the addition of hairpin DNA signals and small liposomes, linker DNA will be generated through hybridization of hairpin strand by Exo III, and small liposomes will bind to the large liposome through DNA hybridization to increase fluorescence ((b), (d)). Once the release DNA strand is added into the solution, it is fully complementary to linker strand so the linking between large liposomes and small liposomes will break. The small liposome fluorescence will then drop as (c), (e) show. (f) indicates the encapsulation of polystyrene particles inside the targeted liposome. (g) is the bright field image of the large liposome. Scale bar is 10 μm.

6.5 Conclusion

In this chapter, we introduce DNA signals into the artificial cell system for reversible cell aggregation and release control. With the establishment of DNA signal ability from previous several chapters, DNA signals have been modified and optimized for interacting with liposome system. The interaction between DNA signals and liposomes indicates a possibly method for future artificial cell aggregation control and research. In addition, real cell studies may also benefit from this system. This system may further contribute to *in vitro* and *in vivo* study of cell behaviors. Building on that, additional functions could also be added into this system, including ON/OFF control and molecular screening by modifications on DNA origami pores and more possibilities.

7 CONCLUSION AND FUTURE WORK

7.1 Conclusion

In this thesis, DNA is deeply studied with its applications including DNA origami platform, cancer cell anti-proliferation, dynamic motor protein system, and artificial cell system. Mechanisms and kinetics of DNA interaction with these systems have been studied. With the help of DNA signals, it is possible to introduce a new type of control method into the systems.

In DNA origami platform, DNA strands achieve molecular capture and release function by DNA signals from base-pairing properties. DNA logic gate is also created, analog as the electrical circuit logic gate, generating corresponding output with certain input added. The interactions between DNA and small molecules, proteins, and nanoparticles also indicates the possibility of manipulating other molecules with DNA strands.

In cancer cell anti-proliferation, DNA signals are used as the anti-cancer drug for cancer therapy purpose based on their secondary structure. The AS1411 DNA drug has been proven to inhibit cancer cell growth. To have a controllable release of DNA drugs, a DNAzyme based DNA walker is also introduced into the system. By linking the AS1411 segment onto the fuel strands for DNA walking, DNA drug can be released while DNA walks. The drug release speed is proportional to magnesium concentration as it controls DNA walking speed. Thus, a cation concentration-controlled drug release system is created.

In motor protein system, DNA is used based on its mechanical property to pull microtubules in order to change their moving directions. With the help of immobilized polystyrene particle and biotin-streptavidin conjugate, DNA strands can attach microtubules and redirect them. As the major redirection force, double-stranded DNA dissociation force is analyzed along with the physical model of microtubule direction change in this study.

In the artificial cell system, DNA signals are proven to trigger reversible liposome aggregation and release. DNA has been used for the combination of all its properties including liposome linking

and releasing, Exo III digestion and DNA origami pore construction. With the demonstration of using DNA signals to control the artificial cell systems, it may also be possible to use DNA strands to control real cells.

Overall, DNA material has been explored as an engineering, far beyond its traditional genetic carrier function. In fact, building on the fundamental DNA base pairing property, DNA nanotechnology has evolved dramatically. Starting from the very simple DNA structure formed by several single-strands DNA, till now that complex 2-D or 3-D structures have been constructed from DNA and these structures could even achieve extraordinary functions by interacting with different systems. DNA nanotechnology has impacted a wide range of research area. As the research work keeps progressing forward, it will be closer and closer for using DNA signals, either synthesized or natural to interact with live systems for better understanding and control.

7.2 Future Work

Current research on DNA associated liposome research is quite limited. The majority is putting DNA strands on the surface of liposomes and perform functions like liposome linking or fusion. However, the complex DNA structure like DNA origami pore involved liposome research is not a lot. As the research projects of artificial cells improve further, they will certainly become more complex. A powerful DNA nanostructure will be needed for artificial cell study. Thus, improving the existing DNA origami pore system will be necessary. With the current DNA origami pore system, ON/OFF function can and should be added, with not only controlled by DNA signals but also involving other external signals including light, pH, heat and more. In addition, modifications can also be done on DNA origami. As the channel of artificial cell, molecules have to pass through origami pore to get in and out, so if one molecular screening moiety is attached inside DNA origami channel, artificial cell function can also be improved. Other improvements of DNA origami pore are also necessary including optimized pore size, mechanism of DNA origami pore integration into liposome membrane, and number of DNA origami pores per liposome.

Furthermore, the actual application of DNA controlled liposome should also be explored. It is important to see if these DNA controlled liposomes could be integrated with cell systems. This

includes the study of liposome interaction with live cells, DNA signal-based liposome-cell interaction, and control of real cells with synthesized DNA signals.

REFERENCES

1 Seeman, N. C. & Sleiman, H. F. DNA nanotechnology. *Nature Reviews Materials* **3**, 17068 (2017).

2 Chen, Y.-J., Groves, B., Muscat, R. A. & Seelig, G. DNA nanotechnology from the test tube to the cell. *Nature nanotechnology* **10**, 748-760 (2015).

3 Kallenbach, N. R., Ma, R.-I. & Seeman, N. C. An immobile nucleic acid junction constructed from oligonucleotides. *Nature* **305**, 829-831 (1983).

4 Winfree, E., Liu, F., Wenzler, L. A. & Seeman, N. C. Design and self-assembly of two-dimensional DNA crystals. *Nature* **394**, 539-544 (1998).

5 Seeman, N. C. DNA in a material world. *Nature* **421**, 427-431 (2003).

6 He, Y., Ye, T., Su, M., Zhang, C., Ribbe, A. E., Jiang, W. & Mao, C. Hierarchical self-assembly of DNA into symmetric supramolecular polyhedra. *Nature* **452**, 198-201 (2008).

7 Rothemund, P. W. Folding DNA to create nanoscale shapes and patterns. *Nature* **440**, 297-302 (2006).

8 Voigt, N. V., Tørring, T., Rotaru, A., Jacobsen, M. F., Ravnsbæk, J. B., Subramani, R., Mamdouh, W., Kjems, J., Mokhir, A. & Besenbacher, F. Single-molecule chemical reactions on DNA origami. *Nature nanotechnology* **5**, 200-203 (2010).

9 Ding, B., Deng, Z., Yan, H., Cabrini, S., Zuckermann, R. N. & Bokor, J. Gold nanoparticle self-similar chain structure organized by DNA origami. *Journal of the American Chemical Society* **132**, 3248-3249 (2010).

10 Helmig, S., Rotaru, A., Arian, D., Kovbasyuk, L., Arnbjerg, J., Ogilby, P. R., Kjems, J., Mokhir, A., Besenbacher, F. & Gothelf, K. V. Single molecule atomic force microscopy studies of photosensitized singlet oxygen behavior on a DNA origami template. *ACS nano* **4**, 7475-7480 (2010).

11 Jin, Z., Sun, W., Ke, Y., Shih, C.-J., Paulus, G. L., Wang, Q. H., Mu, B., Yin, P. & Strano, M. S. Metallized DNA nanolithography for encoding and transferring spatial information for graphene patterning. *Nature communications* **4**, 1663 (2013).

12 Marras, A. E., Zhou, L., Su, H.-J. & Castro, C. E. Programmable motion of DNA origami mechanisms. *Proceedings of the National Academy of Sciences* **112**, 713-718 (2015).

13 Chen, H., Li, R., Li, S., Andréasson, J. & Choi, J. H. Conformational effects of UV light on DNA origami. *Journal of the American Chemical Society* **139**, 1380-1383 (2017).

14 Zhang, D. Y. & Seelig, G. Dynamic DNA nanotechnology using strand-displacement reactions. *Nature chemistry* **3**, 103-113 (2011).

15 Qian, L. & Winfree, E. Scaling up digital circuit computation with DNA strand displacement cascades. *Science* **332**, 1196-1201 (2011).

16 Yoshida, W. & Yokobayashi, Y. Photonic Boolean logic gates based on DNA aptamers. *Chemical communications*, 195-197 (2007).

17 Douglas, S. M., Bachelet, I. & Church, G. M. A logic-gated nanorobot for targeted transport of molecular payloads. *Science* **335**, 831-834 (2012).

18 Zhang, D. Y. & Winfree, E. Control of DNA strand displacement kinetics using toehold exchange. *Journal of the American Chemical Society* **131**, 17303-17314 (2009).

19 Srinivas, N., Ouldridge, T. E., Šulc, P., Schaeffer, J. M., Yurke, B., Louis, A. A., Doye, J. P. & Winfree, E. On the biophysics and kinetics of toehold-mediated DNA strand displacement. *Nucleic acids research* **41**, 10641-10658 (2013).

20 Yurke, B., Turberfield, A. J., Mills Jr, A. P., Simmel, F. C. & Neumann, J. L. A DNA-fuelled molecular machine made of DNA. *Nature* **406**, 605-608 (2000).

21 Kelly, T. R. Molecular Motors: Synthetic DNA-Based Walkers Inspired by Kinesin. *Angewandte Chemie International Edition* **44**, 4124-4127 (2005).

22 Shin, J.-S. & Pierce, N. A. A synthetic DNA walker for molecular transport. *Journal of the American Chemical Society* **126**, 10834-10835 (2004).

23 Tian, Y., He, Y., Chen, Y., Yin, P. & Mao, C. A DNAzyme that walks processively and autonomously along a one-dimensional track. *Angewandte Chemie International Edition* **44**, 4355-4358 (2005).

24 Joyce, G. F. RNA cleavage by the 10-23 DNA enzyme. *Methods in enzymology* **341**, 503-517 (2001).

25 Shin, J.-S. & Pierce, N. A., *Nanoscale Molecular Transport by Synthetic DNA Machines*, in *Nanotechnology: Science and Computation*. 2006, Springer. p. 175-188.

26 Thubagere, A. J., Li, W., Johnson, R. F., Chen, Z., Doroudi, S., Lee, Y. L., Izatt, G., Wittman, S., Srinivas, N. & Woods, D. A cargo-sorting DNA robot. *Science* **357**, eaan6558 (2017).

27 He, Y. & Liu, D. R. Autonomous multistep organic synthesis in a single isothermal solution mediated by a DNA walker. *Nature nanotechnology* **5**, 778-782 (2010).

28 Mallik, R. & Gross, S. P. Molecular motors: strategies to get along. *Current Biology* **14**, R971-R982 (2004).

29 Molloy, J. E. & Veigel, C. Myosin motors walk the walk. *Science* **300**, 2045-2046 (2003).

30 Gennerich, A. & Vale, R. D. Walking the walk: how kinesin and dynein coordinate their steps. *Current opinion in cell biology* **21**, 59-67 (2009).

31 Orozco, J. T., Wedaman, K. P., Signor, D., Brown, H., Rose, L. & Scholey, J. M. Movement of motor and cargo along cilia. *Nature* **398**, 674 (1999).

32 Wang, F., Good, J. A., Rath, O., Kaan, H. Y. K., Sutcliffe, O. B., Mackay, S. P. & Kozielski, F. Triphenylbutanamines: kinesin spindle protein inhibitors with in vivo antitumor activity. *Journal of medicinal chemistry* **55**, 1511-1525 (2012).

33 Sanhaji, M., Friel, C. T., Wordeman, L., Louwen, F. & Yuan, J. Mitotic centromere-associated kinesin (MCAK): a potential cancer drug target. *Oncotarget* **2**, 935-947 (2011).

34 Svoboda, K. & Block, S. M. Force and velocity measured for single kinesin molecules. *Cell* **77**, 773-784 (1994).

35 Sheetz, M. P., Chasan, R. & Spudich, J. A. ATP-dependent movement of myosin in vitro: characterization of a quantitative assay. *The Journal of cell biology* **99**, 1867-1871 (1984).

36 Kodera, N. & Ando, T. The path to visualization of walking myosin V by high-speed atomic force microscopy. *Biophysical reviews* **6**, 237-260 (2014).

37 Böhm, K. J., Stracke, R., Baum, M., Zieren, M. & Unger, E. Effect of temperature on kinesin-driven microtubule gliding and kinesin ATPase activity. *FEBS letters* **466**, 59-62 (2000).

38 Gearhart, D. A., Sickles, D. W., Buccafusco, J. J., Prendergast, M. A. & Terry Jr, A. V. Chlorpyrifos, chlorpyrifos-oxon, and diisopropylfluorophosphate inhibit kinesin-dependent microtubule motility. *Toxicology and applied pharmacology* **218**, 20-29 (2007).

39 Miyazono, Y., Hayashi, M., Karagiannis, P., Harada, Y. & Tadakuma, H. Strain through the neck linker ensures processive runs: a DNA-kinesin hybrid nanomachine study. *The EMBO journal* **29**, 93-106 (2010).

40 Hariadi, R., Sommese, R., Adhikari, A., Taylor, R., Sutton, S., Spudich, J. & Sivaramakrishnan, S. Mechanical coordination in motor ensembles revealed using engineered artificial myosin filaments. *Nature nanotechnology* **10**, 696-700 (2015).

41 Brunner, C., Wahnes, C. & Vogel, V. Cargo pick-up from engineered loading stations by kinesin driven molecular shuttles. *Lab on a Chip* **7**, 1263-1271 (2007).

42 Schmidt, C. & Vogel, V. Molecular shuttles powered by motor proteins: loading and unloading stations for nanocargo integrated into one device. *Lab on a Chip* **10**, 2195-2198 (2010).

43 Taira, S., Du, Y. Z., Hiratsuka, Y., Konishi, K., Kubo, T., Uyeda, T. Q., Yumoto, N. & Kodaka, M. Selective detection and transport of fully matched DNA by DNA-loaded microtubule and kinesin motor protein. *Biotechnology and bioengineering* **95**, 533-538 (2006).

44 Keya, J. J., Suzuki, R., Kabir, A. M. R., Inoue, D., Asanuma, H., Sada, K., Hess, H., Kuzuya, A. & Kakugo, A. DNA-assisted swarm control in a biomolecular motor system. *Nature communications* **9**, 453 (2018).

45 Isozaki, N., Shintaku, H., Kotera, H., Hawkins, T. L., Ross, J. L. & Yokokawa, R. Control of molecular shuttles by designing electrical and mechanical properties of microtubules. *Science Robotics* **2**, eaan4882 (2017).

46 Chang, T. M. S., *Artificial cells*, in *Biomaterials Science (Third Edition)*. 2013, Elsevier. p. 811-827.

47 Chang, T. (1957 Research Report for Physiology 43b for partial fulfillment of honors B. Sc. in Physiology McGill, 1957).

48 Xu, C., Hu, S. & Chen, X. Artificial cells: from basic science to applications. *Materials Today* **19**, 516-532 (2016).

49 Bozzuto, G. & Molinari, A. Liposomes as nanomedical devices. *International journal of nanomedicine* **10**, 975-999 (2015).

50 Ding, Y., Wu, F. & Tan, C. Synthetic biology: A bridge between artificial and natural cells. *Life* **4**, 1092-1116 (2014).

51 Sunamoto, J. & Iwamoto, K. Protein-coated and polysaccharide-coated liposomes as drug carriers. *Critical reviews in therapeutic drug carrier systems* **2**, 117-136 (1986).

52 Kurihara, K., Tamura, M., Shohda, K.-i., Toyota, T., Suzuki, K. & Sugawara, T. Self-reproduction of supramolecular giant vesicles combined with the amplification of encapsulated DNA. *Nature chemistry* **3**, 775-781 (2011).

53 Al-Jamal, W. T. & Kostarelos, K. Liposomes: from a clinically established drug delivery system to a nanoparticle platform for theranostic nanomedicine. *Accounts of chemical research* **44**, 1094-1104 (2011).

54 Zhao, J., Jedlicka, S. S., Lannu, J. D., Bhunia, A. K. & Rickus, J. L. Liposome-Doped Nanocomposites as Artificial-Cell-Based Biosensors: Detection of Listeriolysin O. *Biotechnology progress* **22**, 32-37 (2006).

55 Deamer, D. A giant step towards artificial life? *Trends in biotechnology* **23**, 336-338 (2005).

56 Keber, F. C., Loiseau, E., Sanchez, T., DeCamp, S. J., Giomi, L., Bowick, M. J., Marchetti, M. C., Dogic, Z. & Bausch, A. R. Topology and dynamics of active nematic vesicles. *Science* **345**, 1135-1139 (2014).

57 Sato, Y., Hiratsuka, Y., Kawamata, I., Murata, S. & Shin-ichiro, M. N. Micrometer-sized molecular robot changes its shape in response to signal molecules. *Science Robotics* **2**, eaal3735 (2017).

58 Göpfrich, K., Li, C.-Y., Ricci, M., Bhamidimarri, S. P., Yoo, J., Gyenes, B., Ohmann, A., Winterhalter, M., Aksimentiev, A. & Keyser, U. F. Large-conductance transmembrane porin made from DNA origami. *ACS nano* **10**, 8207-8214 (2016).

59 Burns, J. R., Stulz, E. & Howorka, S. Self-assembled DNA nanopores that span lipid bilayers. *Nano letters* **13**, 2351-2356 (2013).

60 Burns, J. R., Seifert, A., Fertig, N. & Howorka, S. A biomimetic DNA-based channel for the ligand-controlled transport of charged molecular cargo across a biological membrane. *Nature nanotechnology* **11**, 152-156 (2016).

61 Langecker, M., Arnaut, V., Martin, T. G., List, J., Renner, S., Mayer, M., Dietz, H. & Simmel, F. C. Synthetic lipid membrane channels formed by designed DNA nanostructures. *Science* **338**, 932-936 (2012).

62 Hernández-Ainsa, S., Bell, N. A., Thacker, V. V., Gopfrich, K., Misiunas, K., Fuentes-Perez, M. E., Moreno-Herrero, F. & Keyser, U. F. DNA origami nanopores for controlling DNA translocation. *ACS nano* **7**, 6024-6030 (2013).

63 Krishnan, S., Ziegler, D., Arnaut, V., Martin, T. G., Kapsner, K., Henneberg, K., Bausch, A. R., Dietz, H. & Simmel, F. C. Molecular transport through large-diameter DNA nanopores. *Nature communications* **7**, 12787 (2016).

64 Deng, Z., Samanta, A., Nangreave, J., Yan, H. & Liu, Y. Robust DNA-functionalized core/shell quantum dots with fluorescent emission spanning from UV–vis to near-IR and compatible with DNA-directed self-assembly. *Journal of the American Chemical Society* **134**, 17424-17427 (2012).

65 Samanta, A., Deng, Z. & Liu, Y. Aqueous synthesis of glutathione-capped CdTe/CdS/ZnS and CdTe/CdSe/ZnS core/shell/shell nanocrystal heterostructures. *Langmuir* **28**, 8205-8215 (2012).

66 Ma, N., Sargent, E. H. & Kelley, S. O. One-step DNA-programmed growth of luminescent and biofunctionalized nanocrystals. *Nature nanotechnology* **4**, 121-125 (2009).

67 Cha, T.-G., Baker, B. A., Sauffer, M. D., Salgado, J., Jaroch, D., Rickus, J. L., Porterfield, D. M. & Choi, J. H. Optical nanosensor architecture for cell-signaling molecules using DNA aptamer-coated carbon nanotubes. *ACS nano* **5**, 4236-4244 (2011).

68 Jeng, E. S., Barone, P. W., Nelson, J. D. & Strano, M. S. Hybridization Kinetics and Thermodynamics of DNA Adsorbed to Individually Dispersed Single-Walled Carbon Nanotubes. *Small* **3**, 1602-1609 (2007).

69 Chiba, M., Miyazaki, M. & Ishiwata, S. i. Quantitative analysis of the lamellarity of giant liposomes prepared by the inverted emulsion method. *Biophysical journal* **107**, 346-354 (2014).

70 Pautot, S., Frisken, B. J. & Weitz, D. Production of unilamellar vesicles using an inverted emulsion. *Langmuir* **19**, 2870-2879 (2003).

71 Nalluri, S. K. M., Voskuhl, J., Bultema, J. B., Boekema, E. J. & Ravoo, B. J. Light-responsive capture and release of DNA in a ternary supramolecular complex. *Angewandte Chemie International Edition* **50**, 9747-9751 (2011).

72 Katz, E., Pingarron, J. M., Mailloux, S., Guz, N., Gamella, M., Melman, G. & Melman, A. Substance release triggered by biomolecular signals in bioelectronic systems. *The journal of physical chemistry letters* **6**, 1340-1347 (2015).

73 Zhao, W., Cui, C. H., Bose, S., Guo, D., Shen, C., Wong, W. P., Halvorsen, K., Farokhzad, O. C., Teo, G. S. L. & Phillips, J. A. Bioinspired multivalent DNA network for capture and release of cells. *Proceedings of the National Academy of Sciences* **109**, 19626-19631 (2012).

74 Richards, J. L., Seward, G. K., Wang, Y. H. & Dmochowski, I. J. Turning the 10–23 DNAzyme on and off with light. *ChemBioChem* **11**, 320-324 (2010).

75 Elbaz, J., Wang, Z.-G., Orbach, R. & Willner, I. pH-stimulated concurrent mechanical activation of two DNA "tweezers". A "SET− RESET" logic gate system. *Nano letters* **9**, 4510-4514 (2009).

76 Lo, P. K., Karam, P., Aldaye, F. A., McLaughlin, C. K., Hamblin, G. D., Cosa, G. & Sleiman, H. F. Loading and selective release of cargo in DNA nanotubes with longitudinal variation. *Nature chemistry* **2**, 319-328 (2010).

77 Wei, B., Cheng, I., Luo, K. Q. & Mi, Y. Capture and Release of Protein by a Reversible DNA-Induced Sol–Gel Transition System. *Angewandte Chemie International Edition* **47**, 331-333 (2008).

78 Dittmer, W. U., Reuter, A. & Simmel, F. C. A DNA-based machine that can cyclically bind and release thrombin. *Angewandte Chemie International Edition* **43**, 3550-3553 (2004).

79 Genot, A. J., Bath, J. & Turberfield, A. J. Reversible logic circuits made of DNA. *Journal of the American Chemical Society* **133**, 20080-20083 (2011).

80 Stojanovic, M., Stefanovic, D., LeBean, T. & Yan, H. (Wiley-VCH, Weinheim, 2005).

81 Mailloux, S., Gerasimova, Y. V., Guz, N., Kolpashchikov, D. M. & Katz, E. Bridging the two worlds: a universal interface between enzymatic and DNA computing systems. *Angewandte Chemie International Edition* **54**, 6562-6566 (2015).

82 Yin, P., Choi, H. M., Calvert, C. R. & Pierce, N. A. Programming biomolecular self-assembly pathways. *Nature* **451**, 318-322 (2008).

83 Katz, E., *Biomolecular information processing: from logic systems to smart sensors and actuators*. 2013: John Wiley & Sons.

84 Seelig, G., Soloveichik, D., Zhang, D. Y. & Winfree, E. Enzyme-free nucleic acid logic circuits. *science* **314**, 1585-1588 (2006).

85 Zhu, J., Zhang, L., Li, T., Dong, S. & Wang, E. Enzyme-Free Unlabeled DNA Logic Circuits Based on Toehold-Mediated Strand Displacement and Split G-Quadruplex Enhanced Fluorescence. *Advanced Materials* **25**, 2440-2444 (2013).

86 Santoro, S. W. & Joyce, G. F. A general purpose RNA-cleaving DNA enzyme. *Proceedings of the National Academy of Sciences* **94**, 4262-4266 (1997).

87 Medintz, I. L., Pons, T., Trammell, S. A., Grimes, A. F., English, D. S., Blanco-Canosa, J. B., Dawson, P. E. & Mattoussi, H. Interactions between redox complexes and semiconductor quantum dots coupled via a peptide bridge. *Journal of the American Chemical Society* **130**, 16745-16756 (2008).

88 Santoro, S. W. & Joyce, G. F. Mechanism and utility of an RNA-cleaving DNA enzyme. *Biochemistry* **37**, 13330-13342 (1998).

89 Zadeh, J. N., Steenberg, C. D., Bois, J. S., Wolfe, B. R., Pierce, M. B., Khan, A. R., Dirks, R. M. & Pierce, N. A. NUPACK: analysis and design of nucleic acid systems. *Journal of computational chemistry* **32**, 170-173 (2011).

90 Chen, H. Mechanics and Dynamic Behaviors of DNA Origami. (2017).

91 Proudnikov, D. & Mirzabekov, A. Chemical methods of DNA and RNA fluorescent labeling. *Nucleic acids research* **24**, 4535-4542 (1996).

92 Chen, Y., Liu, H., Ye, T., Kim, J. & Mao, C. DNA-directed assembly of single-wall carbon nanotubes. *Journal of the American Chemical Society* **129**, 8696-8697 (2007).

93 Chen, H., Cha, T.-G., Pan, J. & Choi, J. H. Hierarchically assembled DNA origami tubules with reconfigurable chirality. *Nanotechnology* **24**, 435601 (2013).

94 Degen, S. J. F. & Davie, E. W. Nucleotide sequence of the gene for human prothrombin. *Biochemistry* **26**, 6165-6177 (1987).

95 Barton, J. K., Danishefsky, A. & Goldberg, J. Tris (phenanthroline) ruthenium (II): stereoselectivity in binding to DNA. *Journal of the American Chemical Society* **106**, 2172-2176 (1984).

96 Brummel, K. E., Paradis, S. G., Butenas, S. & Mann, K. G. Thrombin functions during tissue factor–induced blood coagulation. *Blood* **100**, 148-152 (2002).

97 Macaya, R. F., Schultze, P., Smith, F. W., Roe, J. A. & Feigon, J. Thrombin-binding DNA aptamer forms a unimolecular quadruplex structure in solution. *Proceedings of the National Academy of Sciences* **90**, 3745-3749 (1993).

98 Huang, Y., Chen, J., Zhao, S., Shi, M., Chen, Z.-F. & Liang, H. Label-free colorimetric aptasensor based on nicking enzyme assisted signal amplification and DNAzyme amplification for highly sensitive detection of protein. *Analytical chemistry* **85**, 4423-4430 (2013).

99 Tian, Y. & Mao, C. DNAzyme amplification of molecular beacon signal. *Talanta* **67**, 532-537 (2005).

100 Bath, J. & Turberfield, A. J. DNA nanomachines. *Nature nanotechnology* **2**, 275-284 (2007).

101 Pan, J., Li, F., Cha, T.-G., Chen, H. & Choi, J. H. Recent progress on DNA based walkers. *Current opinion in biotechnology* **34**, 56-64 (2015).

102 Simmel, F. C. Processive motion of bipedal DNA walkers. *ChemPhysChem* **10**, 2593-2597 (2009).

103 Omabegho, T., Sha, R. & Seeman, N. C. A bipedal DNA Brownian motor with coordinated legs. *Science* **324**, 67-71 (2009).

104 Wang, C., Tao, Y., Song, G., Ren, J. & Qu, X. Speeding up a bidirectional DNA walking device. *Langmuir* **28**, 14829-14837 (2012).

105 Bath, J., Green, S. J. & Turberfield, A. J. A free-running DNA motor powered by a nicking enzyme. *Angewandte Chemie* **117**, 4432-4435 (2005).

106 Yin, P., Yan, H., Daniell, X. G., Turberfield, A. J. & Reif, J. H. A unidirectional DNA walker that moves autonomously along a track. *Angewandte Chemie International Edition* **43**, 4906-4911 (2004).

107 Qian, L., Winfree, E. & Bruck, J. Neural network computation with DNA strand displacement cascades. *Nature* **475**, 368-372 (2011).

108 Gu, H., Chao, J., Xiao, S.-J. & Seeman, N. C. A proximity-based programmable DNA nanoscale assembly line. *Nature* **465**, 202-205 (2010).

109 Li, W., Wang, L. & Jiang, W. A catalytic assembled enzyme-free three-dimensional DNA walker and its sensing application. *Chemical Communications* **53**, 5527-5530 (2017).

110 Mason, S. D., Tang, Y., Li, Y., Xie, X. & Li, F. Emerging bioanalytical applications of DNA walkers. *TrAC Trends in Analytical Chemistry* **107**, 212-221 (2018).

111 Cha, T.-G., Pan, J., Chen, H., Salgado, J., Li, X., Mao, C. & Choi, J. H. A synthetic DNA motor that transports nanoparticles along carbon nanotubes. *Nature nanotechnology* **9**, 39-43 (2014).

112 Pan, J., Cha, T.-G., Li, F., Chen, H., Bragg, N. A. & Choi, J. H. Visible/near-infrared subdiffraction imaging reveals the stochastic nature of DNA walkers. *Science advances* **3**, e1601600 (2017).

113 Cha, T.-G., Pan, J., Chen, H., Robinson, H. N., Li, X., Mao, C. & Choi, J. H. Design principles of DNA enzyme-based walkers: Translocation kinetics and photoregulation. *Journal of the American Chemical Society* **137**, 9429-9437 (2015).

114 Bates, P. J., Laber, D. A., Miller, D. M., Thomas, S. D. & Trent, J. O. Discovery and development of the G-rich oligonucleotide AS1411 as a novel treatment for cancer. *Experimental and molecular pathology* **86**, 151-164 (2009).

115 Otake, Y., Soundararajan, S., Sengupta, T. K., Kio, E. A., Smith, J. C., Pineda-Roman, M., Stuart, R. K., Spicer, E. K. & Fernandes, D. J. Overexpression of nucleolin in chronic lymphocytic leukemia cells induces stabilization of bcl2 mRNA. *Blood* **109**, 3069-3075 (2007).

116 Soundararajan, S., Chen, W., Spicer, E. K., Courtenay-Luck, N. & Fernandes, D. J. The nucleolin targeting aptamer AS1411 destabilizes Bcl-2 messenger RNA in human breast cancer cells. *Cancer research* **68**, 2358-2365 (2008).

117 Wu, J., Song, C., Jiang, C., Shen, X., Qiao, Q. & Hu, Y. Nucleolin targeting AS1411 modified protein nanoparticle for antitumor drugs delivery. *Molecular pharmaceutics* **10**, 3555-3563 (2013).

118 Uhrich, K. E., Cannizzaro, S. M., Langer, R. S. & Shakesheff, K. M. Polymeric systems for controlled drug release. *Chemical reviews* **99**, 3181-3198 (1999).

119 Wong, P. T. & Choi, S. K. Mechanisms of drug release in nanotherapeutic delivery systems. *Chemical reviews* **115**, 3388-3432 (2015).

120 Seawright, A., Ozcelikkale, A., Dutton, C. & Han, B. Role of Cells in Freezing-Induced Cell-Fluid-Matrix Interactions Within Engineered Tissues. *Journal of biomechanical engineering* **135**, 091001 (2013).

121 Wang, C.-L., Teo, K. Y. & Han, B. An amino acidic adjuvant to augment cryoinjury of MCF-7 breast cancer cells. *Cryobiology* **57**, 52-59 (2008).

122 Ireson, C. R. & Kelland, L. R. Discovery and development of anticancer aptamers. *Molecular cancer therapeutics* **5**, 2957-2962 (2006).

123 Xu, X., Hamhouyia, F., Thomas, S. D., Burke, T. J., Girvan, A. C., McGregor, W. G., Trent, J. O., Miller, D. M. & Bates, P. J. Inhibition of DNA replication and induction of S phase cell cycle arrest by G-rich oligonucleotides. *Journal of Biological Chemistry* **276**, 43221-43230 (2001).

124 Pulskamp, K., Diabaté, S. & Krug, H. F. Carbon nanotubes show no sign of acute toxicity but induce intracellular reactive oxygen species in dependence on contaminants. *Toxicology letters* **168**, 58-74 (2007).

125 Schipper, M. L., Nakayama-Ratchford, N., Davis, C. R., Kam, N. W. S., Chu, P., Liu, Z., Sun, X., Dai, H. & Gambhir, S. S. A pilot toxicology study of single-walled carbon nanotubes in a small sample of mice. *Nature nanotechnology* **3**, 216-221 (2008).

126 Liu, Y., Zhao, Y., Sun, B. & Chen, C. Understanding the toxicity of carbon nanotubes. *Accounts of Chemical Research* **46**, 702-713 (2012).

127 Liu, Z., Davis, C., Cai, W., He, L., Chen, X. & Dai, H. Circulation and long-term fate of functionalized, biocompatible single-walled carbon nanotubes in mice probed by Raman spectroscopy. *Proceedings of the National Academy of Sciences* **105**, 1410-1415 (2008).

128 Sun, H., Zhu, X., Lu, P. Y., Rosato, R. R., Tan, W. & Zu, Y. Oligonucleotide aptamers: New tools for targeted cancer therapy. *Molecular Therapy—Nucleic Acids* **3**, e182 (2014).

129 Dennis, J. R., Howard, J. & Vogel, V. Molecular shuttles: directed motion of microtubules along nanoscale kinesin tracks. *Nanotechnology* **10**, 232-236 (1999).

130 Hutchins, B. M., Platt, M., Hancock, W. O. & Williams, M. E. Directing transport of CoFe2O4-functionalized microtubules with magnetic fields. *small* **3**, 126-131 (2007).

131 Kumar, K. S., Amrutha, A. S. & Tamaoki, N. Spatiotemporal control of kinesin motor protein by photoswitches enabling selective single microtubule regulations. *Lab on a Chip* **16**, 4702-4709 (2016).

132 Jeppesen, G. M. & Hoerber, J. H. (Portland Press Limited, 2012).

133 Martin, D. S., Yu, L. & Van Hoozen, B. L. Flexural Rigidity Measurements of Biopolymers Using Gliding Assays. *Journal of visualized experiments: JoVE* (2012).

134 Verma, V., Hancock, W. O. & Catchmark, J. M. The role of casein in supporting the operation of surface bound kinesin. *Journal of biological engineering* **2**, 14 (2008).

135 Agarwal, A. & Hess, H. Biomolecular motors at the intersection of nanotechnology and polymer science. *Progress in Polymer Science* **35**, 252-277 (2010).

136 Hess, H. & Ross, J. L. Non-equilibrium assembly of microtubules: from molecules to autonomous chemical robots. *Chemical Society Reviews* **46**, 5570-5587 (2017).

137 Fischer, T., Agarwal, A. & Hess, H. A smart dust biosensor powered by kinesin motors. *Nature nanotechnology* **4**, 162-166 (2009).

138 Raab, M. & Hancock, W. O. Transport and detection of unlabeled nucleotide targets by microtubules functionalized with molecular beacons. *Biotechnology and bioengineering* **99**, 764-773 (2008).

139 Parimalam, S. S., Tarhan, M. C., Karsten, S. L., Fujita, H., Shintaku, H., Kotera, H. & Yokokawa, R. On-chip microtubule gliding assay for parallel measurement of tau protein species. *Lab on a Chip* **16**, 1691-1697 (2016).

140 Korten, T., Månsson, A. & Diez, S. Towards the application of cytoskeletal motor proteins in molecular detection and diagnostic devices. *Current opinion in biotechnology* **21**, 477-488 (2010).

141 Hess, H. Engineering applications of biomolecular motors. *Annual review of biomedical engineering* **13**, 429-450 (2011).

142 Korten, T. & Diez, S. Setting up roadblocks for kinesin-1: mechanism for the selective speed control of cargo carrying microtubules. *Lab on a Chip* **8**, 1441-1447 (2008).

143 Kawaguchi, K. & Ishiwata, S. i. Thermal activation of single kinesin molecules with temperature pulse microscopy. *Cytoskeleton* **49**, 41-47 (2001).

144 Dujovne, I., van den Heuvel, M., Shen, Y., de Graaff, M. & Dekker, C. Velocity modulation of microtubules in electric fields. *Nano letters* **8**, 4217-4220 (2008).

145 Kumar, K. S., Kamei, T., Fukaminato, T. & Tamaoki, N. Complete ON/OFF photoswitching of the motility of a nanobiomolecular machine. *ACS nano* **8**, 4157-4165 (2014).

146 Amrutha, A. S., Kumar, K. S., Kikukawa, T. & Tamaoki, N. Targeted Activation of Molecular Transportation by Visible Light. *ACS nano* **11**, 12292-12301 (2017).

147 Rahim, M. A., Fukaminato, T., Kamei, T. & Tamaoki, N. Dynamic photocontrol of the gliding motility of a microtubule driven by kinesin on a photoisomerizable monolayer surface. *Langmuir* **27**, 10347-10350 (2011).

148 Böhm, K., Stracke, R. & Unger, E. Speeding up kinesin-driven microtubule gliding in vitro by variation of cofactor composition and physicochemical parameters. *Cell biology international* **24**, 335-341 (2000).

149 Hiratsuka, Y., Tada, T., Oiwa, K., Kanayama, T. & Uyeda, T. Q. Controlling the direction of kinesin-driven microtubule movements along microlithographic tracks. *Biophysical Journal* **81**, 1555-1561 (2001).

150 Clemmens, J., Hess, H., Lipscomb, R., Hanein, Y., Böhringer, K. F., Matzke, C. M., Bachand, G. D., Bunker, B. C. & Vogel, V. Mechanisms of microtubule guiding on microfabricated kinesin-coated surfaces: Chemical and topographic surface patterns. *Langmuir* **19**, 10967-10974 (2003).

151 Cheng, L. J., Kao, M. T., Meyhöfer, E. & Guo, L. J. Highly efficient guiding of microtubule transport with imprinted CYTOP nanotracks. *Small* **1**, 409-414 (2005).

152 Reuther, C., Mittasch, M. u., Naganathan, S. R., Grill, S. W. & Diez, S. Highly-Efficient Guiding of Motile Microtubules on Non-Topographical Motor Patterns. *Nano letters* **17**, 5699-5705 (2017).

153 Kim, T., Kao, M.-T., Hasselbrink, E. F. & Meyhöfer, E. Active alignment of microtubules with electric fields. *Nano Letters* **7**, 211-217 (2007).

154 Van den Heuvel, M. G., De Graaff, M. P. & Dekker, C. Molecular sorting by electrical steering of microtubules in kinesin-coated channels. *Science* **312**, 910-914 (2006).

155 Stracke, R., Böhm, K. J., Burgold, J., Schacht, H.-J. & Unger, E. Physical and technical parameters determining the functioning of a kinesin-based cell-free motor system. *Nanotechnology* **11**, 52-56 (2000).

156 Yokokawa, R., Murakami, T., Sugie, T. & Kon, T. Polarity orientation of microtubules utilizing a dynein-based gliding assay. *Nanotechnology* **19**, 125505 (2008).

157 Agayan, R. R., Tucker, R., Nitta, T., Ruhnow, F., Walter, W. J., Diez, S. & Hess, H. Optimization of isopolar microtubule arrays. *Langmuir* **29**, 2265-2272 (2013).

158 Van den Heuvel, M., De Graaff, M. & Dekker, C. Microtubule curvatures under perpendicular electric forces reveal a low persistence length. *Proceedings of the National Academy of Sciences* **105**, 7941-7946 (2008).

159 Hoffmann, C., Mazari, E., Lallet, S., Le Borgne, R., Marchi, V., Gosse, C. & Gueroui, Z. Spatiotemporal control of microtubule nucleation and assembly using magnetic nanoparticles. *Nature nanotechnology* **8**, 199-205 (2013).

160 Platt, M., Muthukrishnan, G., Hancock, W. O. & Williams, M. E. Millimeter scale alignment of magnetic nanoparticle functionalized microtubules in magnetic fields. *Journal of the American Chemical Society* **127**, 15686-15687 (2005).

161 Hutchins, B. M., Hancock, W. O. & Williams, M. E. Magnet assisted fabrication of microtubule arrays. *Physical Chemistry Chemical Physics* **8**, 3507-3509 (2006).

162 Hiyama, S., Gojo, R., Shima, T., Takeuchi, S. & Sutoh, K. Biomolecular-motor-based nano-or microscale particle translocations on DNA microarrays. *Nano Letters* **9**, 2407-2413 (2009).

163 Muthukrishnan, G., Roberts, C. A., Chen, Y.-C., Zahn, J. D. & Hancock, W. O. Patterning surface-bound microtubules through reversible DNA hybridization. *Nano Letters* **4**, 2127-2132 (2004).

164 Hiyama, S., Isogawa, Y., Suda, T., Moritani, Y. & Sutoh, K. A design of an autonomous molecule loading/transporting/unloading system using DNA hybridization and biomolecular linear motors. *arXiv preprint arXiv:0708.1839* (2007).

165 Wollman, A. J., Sanchez-Cano, C., Carstairs, H. M., Cross, R. A. & Turberfield, A. J. Transport and self-organization across different length scales powered by motor proteins and programmed by DNA. *Nature nanotechnology* **9**, 44-47 (2014).

166 Diez, S., Reuther, C., Dinu, C., Seidel, R., Mertig, M., Pompe, W. & Howard, J. Stretching and transporting DNA molecules using motor proteins. *Nano Letters* **3**, 1251-1254 (2003).

167 Kim, T., Kao, M.-T., Meyhöfer, E. & Hasselbrink, E. F. Biomolecular motor-driven microtubule translocation in the presence of shear flow: analysis of redirection behaviours. *Nanotechnology* **18**, 025101 (2006).

168 Yokokawa, R., Takeuchi, S., Kon, T., Nishiura, M., Sutoh, K. & Fujita, H. Unidirectional transport of kinesin-coated beads on microtubules oriented in a microfluidic device. *Nano Letters* **4**, 2265-2270 (2004).

169 Wang, Y., Wang, Y., Zheng, X., Ducrot, É., Yodh, J. S., Weck, M. & Pine, D. J. Crystallization of DNA-coated colloids. *Nature communications* **6**, 7253 (2015).

170 Meyhöfer, E. & Howard, J. The force generated by a single kinesin molecule against an elastic load. *Proceedings of the National Academy of Sciences* **92**, 574-578 (1995).

171 Visscher, K., Schnitzer, M. J. & Block, S. M. Single kinesin molecules studied with a molecular force clamp. *Nature* **400**, 184-189 (1999).

172 Pincet, F. & Husson, J. The solution to the streptavidin-biotin paradox: the influence of history on the strength of single molecular bonds. *Biophysical journal* **89**, 4374-4381 (2005).

173 Wong, J., Chilkoti, A. & Moy, V. T. Direct force measurements of the streptavidin–biotin interaction. *Biomolecular engineering* **16**, 45-55 (1999).

174 Bockelmann, U., Thomen, P., Essevaz-Roulet, B., Viasnoff, V. & Heslot, F. Unzipping DNA with optical tweezers: high sequence sensitivity and force flips. *Biophysical journal* **82**, 1537-1553 (2002).

175 Cocco, S., Monasson, R. & Marko, J. F. Force and kinetic barriers to unzipping of the DNA double helix. *Proceedings of the National Academy of Sciences* **98**, 8608-8613 (2001).

176 AMOS, L. A. & Klug, A. Arrangement of subunits in flagellar microtubules. *Journal of cell science* **14**, 523-549 (1974).

177 Neish, C. S., Martin, I. L., Henderson, R. M. & Edwardson, J. M. Direct visualization of ligand-protein interactions using atomic force microscopy. *British journal of pharmacology* **135**, 1943-1950 (2002).

178 Zoeteweij, M., Van der Donck, J. & Versluis, R. Particle removal in linear shear flow: model prediction and experimental validation. *Journal of adhesion science and technology* **23**, 899-911 (2009).

179 Di Carlo, D. Inertial microfluidics. *Lab on a Chip* **9**, 3038-3046 (2009).

180 Bruus, H. Governing Equations in Microfluidics. (2014).

181 Pan, L. & Arratia, P. E. A high-shear, low Reynolds number microfluidic rheometer. *Microfluidics and nanofluidics* **14**, 885-894 (2013).

182 Leith, D. Drag on nonspherical objects. *Aerosol science and technology* **6**, 153-161 (1987).

183 Palacci, H., Idan, O., Armstrong, M. J., Agarwal, A., Nitta, T. & Hess, H. Velocity fluctuations in kinesin-1 gliding motility assays originate in motor attachment geometry variations. *Langmuir* **32**, 7943-7950 (2016).

184 Stewart, R. J., Thaler, J. P. & Goldstein, L. Direction of microtubule movement is an intrinsic property of the motor domains of kinesin heavy chain and Drosophila ncd protein. *Proceedings of the National Academy of Sciences* **90**, 5209-5213 (1993).

185 Gibbons, F., Chauwin, J.-F., Despósito, M. & José, J. V. A dynamical model of kinesin-microtubule motility assays. *Biophysical journal* **80**, 2515-2526 (2001).

186 Eckford, A. W., Farsad, N., Hiyama, S. & Moritani, Y. in *Nanotechnology (IEEE-NANO), 2010 10th IEEE Conference on.* 854-858 (IEEE).

187 Lilliefors, H. W. On the Kolmogorov-Smirnov test for normality with mean and variance unknown. *Journal of the American statistical Association* **62**, 399-402 (1967).

188 Massey Jr, F. J. The Kolmogorov-Smirnov test for goodness of fit. *Journal of the American statistical Association* **46**, 68-78 (1951).

189 Saltzman, W. M. & Kyriakides, T. R., *Cell interactions with polymers*, in *Principles of tissue engineering*. 2014, Elsevier. p. 385-406.

190 Yoshimoto, M., Tamura, R. & Natsume, T. Liposome clusters with shear stress-induced membrane permeability. *Chemistry and physics of lipids* **174**, 8-16 (2013).

191 Yoshimoto, M., Sakakida, Y., Tamura, R., Natsume, T. & Ikeda, T. Clusters of Phospholipid Vesicles as Platforms for Glucose Oxidase-Catalyzed Reaction in a Bubble-Column Bioreactor. *Chemical Engineering & Technology* **39**, 1130-1136 (2016).

VITA

Feiran Li obtained a bachelor's degree in Biomedical Engineering from Tsinghua University in China. His Ph.D. study is in the School of Mechanical Engineering at Purdue University with Prof. Jong Hyun Choi. His research focuses on DNA nanotechnology and artificial cell.

PUBLICATIONS

Journal Papers

1. Pan, J., Du, Y., Qiu, H., Upton, L. R., Li, F., & Choi, J. H. (2019). Mimicking Chemotactic Cell Migration with DNA Programmable Synthetic Vesicles. Nano letters, 19(12), 9138-9144.
2. Li, F., Pan, J., & Choi, J. H. (2019). Local direction change of surface gliding microtubules. Biotechnology and bioengineering, 116(5), 1128-1138.
3. Zhang, H. T., Zuo, F., Li, F., Chan, H., Wu, Q., Zhang, Z., Narayanan, B., Ramadoss, K., Chakraborty, I., Saha, G., Kamath, G., Roy, K., Zhou, H., Chubykin, A. A., Sankaranarayanan, S., Choi, J. H., & Ramanathan S. (2019). Perovskite nickelates as bio-electronic interfaces. Nature communications, 10(1), 1651.
4. Pan, J., Cha, T. G., Li, F., Chen, H., Bragg, N. A., & Choi, J. H. (2017). Visible/near-infrared subdiffraction imaging reveals the stochastic nature of DNA walkers. *Science advances*, *3*(1), e1601600.
5. Pan, J., Li, F., & Choi, J. H. (2017). Single-walled carbon nanotubes as optical probes for bio-sensing and imaging. *Journal of Materials Chemistry B*, *5*(32), 6511-6522.
6. Li, F., Cha, T. G., Pan, J., Ozcelikkale, A., Han, B., & Choi, J. H. (2016). DNA Walker-Regulated Cancer Cell Growth Inhibition. *ChemBioChem*, *17*(12), 1138-1141.
7. Li, F., Chen, H., Pan, J., Cha, T. G., Medintz, I. L., & Choi, J. H. (2016). A DNAzyme-mediated logic gate for programming molecular capture and release on DNA origami. *Chemical Communications*, *52*(54), 8369-8372.
8. Choi, J., Chen, H., Li, F., Yang, L., Kim, S. S., Naik, R. R., Ye, P.D. and Choi, J.H. (2015). Nanomanufacturing of 2D Transition Metal Dichalcogenide Materials Using Self-Assembled DNA Nanotubes. *Small*, *11*(41), 5520-5527.
9. Pan, J., Li, F., Cha, T. G., Chen, H., & Choi, J. H. (2015). Recent progress on DNA based walkers. *Current opinion in biotechnology*, *34*, 56-64.

Book Chapters

1. Pan, J., Cha, T. G., Chen, H., Li, F., & Choi, J. H. (2017). DNA Walkers as Transport Vehicles of Nanoparticles Along a Carbon Nanotube Track. In *3D DNA Nanostructure* (pp. 269-280). Humana Press, New York, NY.
2. Chen, H., Li, F., Pan, J., & Choi, J. H. (2015). DNA Origami as Programmable Nanomanufacturing Tools, edited by B. Bhushan in Encyclopedia of Nanotechnology, Springer.